Check for updates

NMR in Biomedicine

WILEY

NMR IN BIOMEDICINE

REVIEW ARTICLE OPEN ACCESS

Synthetic Data in MR Spectroscopy: Current Practices, Applications, and Considerations

John T. LaMaster[1,2] | Aaron T. Gudmundson[3] | Alireza Abaei[4] | Seyma Alcicek[5,6,7] | Arturo Alvarado[8] | Ovidiu Andronesi[9] | Tiffany Bell[10,11,12] | Wolfgang Bogner[13,14,15] | Hanna Bugler[10,11,12,16] | Alexander R. Craven[17,18] | Cristina Cudalbu[19,20] | Alma Davidson[21] | Christopher W. Davies-Jenkins[22] | Dinesh Deelchand[23,24] | Richard Edden[22] | Morteza Esmaeili[25] | Candace C. Fleischer[26,27] | Abdelrahman Gad[22] | Guglielmo Genovese[28] | Saumya Gurbani[26] | Ashley D. Harris[10,11,12] | Pierre-Gilles Henry[23,24] | Kay Chioma Igwe[21] | Ajin Joy[29] | Margarida Julià-Sapé[30,31,32] | Hyeonjin Kim[33,34] | Roland Kreis[35,36] | Fan Lam[37,38] | Karl Landheer[39] | Bernard Lanz[19,20] | Chu-Yu Lee[40] | Clémence Ligneul[41] | Julian P. Merkofer[42] | Jack J. Miller[43,44] | Jessie Mosso[19,45,46] | Stanislav Motyka[13,14,15] | Eloïse Mougel[47] | Paul G. Mullins[48] | Saipavitra Murali-Manohar[22] | Chloé Najac[49] | Shinichiro Nakajima[50,51] | Georg Oeltzschner[22] | İpek Özdemir[22] | Esin Ozturk-Isik[52] | Marco Palombo[53,54] | Ulrich Pilatus[55] | Justyna Platek[56,57,58] | Esau Poblador Rodriguez[59] | Xiaobo Qu[60,61,62] | Rudy Rizzo[63] | Christopher T. Rodgers[64] | Yeison Rodriguez[65] | Manoj K. Sammi[66] | Manoj Kumar Sarma[67] | Francesca Saviola[68] | Anouk Schrantee[69] | Amirmohammad Shamaei[70,71] | Dunja Simicic[22] | Brian J. Soher[72] | Nico Sollmann[73,74,75,76] | Yulu Song[22] | Jeffrey A. Stanley[77] | Bernhard Strasser[13] | Antonia Susnjar[78] | Kelley M. Swanberg[79,80] | M. Albert Thomas[29,81] | Ivan Tkáč[23] | Zhangren Tu[60,61,62] | Dennis M. J. van de Sande[82] | Emma Van Praagh[21] | Paul J. Weiser[9,13] | Mark Widmaier[19,20,83] | Martin Wilson[84] | Christopher J. Wu[21,85] | Lijing Xin[86] | Helge J. Zöllner[22] | MRS Synthetic Data Working Group | Antonia Kaiser[86]

Correspondence: Antonia Kaiser (antonia.kaiser@epfl.ch)

Received: 5 March 2026 | **Revised:** 7 September 2026 | **Accepted:** 21 September 2026

Keywords: artificial intelligence | clinical application | diffusion MRS | fMRS | MR spectroscopy | MRSI | preclinical application | synthetic data | X-nuclei

ABSTRACT

Synthetic data generation has become an increasingly important component of methodological development in magnetic resonance spectroscopy (MRS), particularly in contexts where ground-truth in vivo measurements are limited, noisy, or inaccessible. This review provides a structured overview of current practices in synthetic MRS data generation, with emphasis on the physical, biochemical, and computational assumptions that underpin commonly used models. A decomposition of synthetic MRS data is presented in terms of core building blocks, including basis sets, signal formation models, and

Abbreviations: AI, Artificial intelligence; Ace, Acetate; Ala, Alanine; Asc, Ascorbate; Asp, Aspartate; bHB, β-Hydroxybutyrate; BOLD, Blood Oxygen Level-Dependent; Cho, Choline; Cr, Creatine; CSF, Cerebrospinal Fluid; DL, Deep Learning; dMRS, diffusion-weighted Magnetic Resonance Spectroscopy; EPSI, Echo-Planar Spectroscopic Imaging; fMRS, functional Magnetic Resonance Spectroscopy; GABA, γ-Aminobutyric Acid; GAN, Generative Adversarial Network; Glc, Glucose; Gln, Glutamine; Glu, Glutamate; Gly, Glycine; Glyc, Glycerol; GM, Gray Matter; GPC, Glycerophosphocholine; GSH, Glutathione; IU, Institutional Units; Lac, Lactate; LCM, Linear Combination Model(ing); ML, Machine Learning; mI, Myo-inositol; MM, Macromolecules; MRS, Magnetic Resonance Spectroscopy; MRSI, Magnetic Resonance Spectroscopic Imaging; NAA, *N*-Acetyl-Aspartate; NAAG, *N*-Acetyl-Aspartyl-Glutamate; NSA, Number of Signal Averages (Transients); ISMRM, International Society for Magnetic Resonance in Medicine; PCh, Phosphocholine; PCr, Phosphocreatine; PE, Phosphoethanolamine; PRESS, Point-Resolved Spectroscopy; RF, Radio frequency; sI, Scyllo-inositol; sLASER, Semi-Localized by Adiabatic Selective Refocusing; SNR, Signal-to-Noise Ratio; STEAM, Stimulated Echo Acquisition Mode; Tau, Taurine; TE, Echo Time; tCr, Total Creatine (Creatine + Phosphocreatine); tCho, Total Choline (Glycerophosphocholine + Phosphocholine + Choline); tNAA, Total *N*-Acetyl-Aspartate (*N*-Acetyl-Aspartate + *N*-Acetyl-Aspartyl-Glutamate); TR, Repetition Time; WM, White Matter; VAE, Variational Autoencoder; 2-HG, 2-hydroxyglutarate.

John T. LaMaster, Aaron T. Gudmundson, and Antonia Kaiser made equal contributions.

John T. LaMaster and Aaron T. Gudmundson Shared first authorship.

For affiliations refer to page 29.

This is an open access article under the terms of the Creative Commons Attribution License, which permits use, distribution and reproduction in any medium, provided the original work is properly cited.

© 2026 The Author(s). *NMR in Biomedicine* published by John Wiley & Sons Ltd.

metabolite parameter distributions such as concentration and relaxation properties. This framework is extended to advanced components required for realistic data synthesis, including baseline and nuisance signals, spatial encoding effects such as coil sensitivities and field inhomogeneities, k-space sampling and gradient imperfections, as well as sample-specific and temporal dynamics. Beyond single-voxel modeling, synthetic data generation across multiple MRS modalities is discussed, including functional MRS, diffusion-weighted MRS, and spectroscopic imaging, with emphasis on modality-specific challenges such as physiological variability, motion, and confounding signal contributions. The role of synthetic data in clinical and preclinical research, acquisition optimization, software validation, and emerging artificial intelligence applications is further examined, with particular attention to domain shift and representational realism. Current practices in validation, reporting standards, and data accessibility are also reviewed, and key gaps limiting reproducibility and interoperability across studies are identified. Overall, this work provides a unified conceptual framework for synthetic MRS data generation, clarifies underlying assumptions across modeling choices, and outlines open challenges toward improving realism, standardization, and utility in both methodological and translational applications. Conducted by the MRS Synthetic Data Working Group under the Code & Data Sharing Committee of the MRS Study Group of the International Society for Magnetic Resonance in Medicine (ISMRM), this review encompasses the existing literature, supplemented by the collective experience and in-house methodologies of its contributors, providing a community perspective that extends beyond the published record.

1 | Introduction

Magnetic resonance spectroscopy (MRS) is a non-invasive technique that enables the measurement of tissue metabolite levels, providing critical insights into metabolic and biochemical changes associated with various diseases [1–3]. Its applications span both clinical and preclinical research, supporting advancements in neuroscience, oncology, and other medical disciplines.

Despite its utility, MRS faces several challenges that limit its broader adoption and application. Variability in data acquisition methods, limited availability of large datasets, and difficulties in replicating experiments across different sites and scanners hinder the validation and standardization of methods [4]. These challenges slow the progress of the field and delay the development of robust algorithms and reproducible workflows. Addressing these challenges requires not only methodological advances but also improved practices in data sharing, reporting, and standardization that support reproducible research and align with broader open science principles.

One promising approach to address these limitations is the use of **synthetic MRS data**, which involves generating realistic simulated MRS data under controlled conditions. By employing synthetic datasets, researchers can conduct extensive analyses and validations without the ethical or logistical constraints of human or animal experiments. Synthetic data offers a practical and scalable alternative to in vivo datasets, overcoming key obstacles related to data acquisition, variability, and accessibility.

Synthetic data provide various critical advantages for MRS research and development. They enable controlled ground truths by allowing precise specification of parameters such as metabolite concentrations, which facilitates rigorous validation of algorithms and models against known values. Additionally, synthetic data is scalable and permits great diversity, as large datasets can be generated economically and computationally efficiently. This scalability supports the optimization of acquisition methods, training of machine learning and deep learning pipelines, and systematic pipeline testing. Synthetic data also supports the study of pathological cases by using ground truth metabolic profiles derived from rare or extreme in vivo conditions to generate data across a wide range of acquisition settings. This approach enables systematic evaluation and optimization of measurement protocols and analysis methods under conditions that are difficult to sample empirically. Furthermore, synthetic datasets are valuable for teaching MRS techniques and validating methods under well-defined conditions, providing clear benchmarks for reproducibility. Finally, in clinical settings where data availability is limited and inter-subject variability is high, synthetic datasets allow controlled testing of algorithm performance under clinically relevant variability, supporting assessment of stability, bias, and transferability across heterogeneous populations. By addressing these needs, synthetic data play an indispensable role in overcoming the challenges associated with MRS research and applications.

While synthetic data is capable of closing many gaps in MRS research, the field is still in the early days of development of generation methodologies. For many researchers, simulating a realistic MRS dataset can be an overwhelming task with no clear starting point. For the field at large, the definition of what is "realistic" and appropriate is ambiguous and unregulated. Such definitions change depending on the targeted application and evolve with the development of new methodologies and empirical findings.

To provide clarity and guidance for the field, this article outlines existing works on generating, using, and leveraging synthetic MRS data. We begin by detailing the **core components** necessary for constructing the essentials and foundation of synthetic spectra. Next, the **advanced components** are presented in an in-depth overview of the next level of features that allow researchers to simulate specialized or nonstandard scenarios. We then expand to **modality-specific considerations**, highlighting how synthetic data can be adapted for different MRS techniques and nuclei. Subsequently, we describe **application contexts**, illustrating how synthetic datasets can support a wide range of research questions, tool development, and methodological benchmarking. Finally, we present current **validation approaches** for assessing synthetic data quality and realism, i.e., in vivo-likeness, and propose **standardized file formats and general reporting guidelines** to promote reproducibility,

10991492, 2026, 12, Downloaded from https://analyticalsciencejournals.onlinelibrary.wiley.com/doi/10.1002/nbm.70427, Wiley Online Library on [17/11/2026]. See the Terms and Conditions (https://onlinelibrary.wiley.com/terms-and-conditions) on Wiley Online Library for rules of use; OA articles are governed by the applicable Creative Commons License

interoperability, **transparency, and data reusability**, in line with open science principles, within the MRS community.

This review, conducted by the MRS Synthetic Data Working Group from the Code & Data Sharing Committee of the MRS Study Group of the International Society for Magnetic Resonance in Medicine (ISMRM), includes insights from the literature and contributions from active researchers (please find a list of publications in Table S1 Master Table). By identifying gaps and opportunities, this work aims to guide researchers in using synthetic data effectively to advance MRS research and applications. The preparation of this manuscript has also provided an important opportunity to develop considerations and highlight where differences lie.

In each section of this manuscript, we begin by outlining the "Considerations" necessary for robust synthetic MRS data generation and applications (please find a summary of these in Table S2), followed by a detailed discussion of current practices. A comprehensive master table of publications (Table S1 Master Table) employing synthetic data in these contexts accompanies this manuscript and will remain a living document that can be updated by the community as new contributions emerge.

The "Considerations" in this work are **not prescriptive requirements**, but rather useful suggestions. There are many choices to make when simulating synthetic MRS data, and these choices merit careful consideration and discussion in future publications. Our working group acknowledges that deviation from these suggestions *can be appropriate* in various scenarios, but we believe that justification should always be provided.

2 | Core Components for Synthetic MRS Data

2.1 | Basis Sets

Considerations:
General:

- *Synthetic data should be derived from a defined basis set (broadly including simulated or experimentally acquired basis functions). The basis set should be provided alongside the synthetic dataset.*
- *Essential acquisition parameters (field strength, sequence type, echo time [TE], spectral width [SW], and number of data points [Ns]) should be documented in full.*
- *J-coupling evolution and accurate metabolite basis functions should be incorporated into the signal model.*

^{1}H MRS:

- *Signal models should reflect common* in vivo *scenarios relevant to the tissue under investigation (e.g., human brain).*
- *For echo times below approximately 80 ms, inclusion of macromolecular (MM) signals is strongly encouraged.*

Basis sets are a foundational component in MRS data simulation and analysis, enabling the deconvolution of complex spectral data into meaningful biochemical information. These sets mathematically represent individual metabolite signals and are essential for linear combination modeling (LC modeling) of MR spectra. While the development and validation of basis sets have been extensively reviewed in prior works [5, 6], some essential points must be reiterated due to their critical importance in synthetic data simulations.

The quality and compatibility of a basis set with the experimental setup directly impact the accuracy of MRS quantification. Basis sets are typically generated under specific acquisition parameters, such as for a given field strength, specific pulse sequence, echo time (TE), spectral width (SW), and the number of data points, using simulations or experimental data thereof. These parameters capture the nuances of metabolite behavior, including chemical shifts and coupling patterns, which are crucial for realistic synthetic MRS data. Basis set composition is a critical determinant of fitting performance when analyzing experimentally acquired spectra that closely resemble the intended acquisition protocol. In a synthetic data context, careful consideration is required, as the selected metabolite and macromolecular components define the model space and may bias validation or benchmarking outcomes. Several studies have systematically investigated how basis set composition affects quantification accuracy and robustness [7–10]. Although a comprehensive evaluation of basis set optimization is beyond the scope of this manuscript, readers interested in detailed metabolite-specific physical properties can consult the living MRS-Sim database, which compiles moiety-specific spin definitions and relevant simulation parameters; MRS-Sim GitHub repository [11].

Metabolite basis sets are often derived from:

- **Mathematical models** (elaborated on below);
- Phantom experiments;
- **Density-matrix simulations,** which account for chemical shifts and couplings under specific pulse sequence conditions [12].

Various dedicated software packages can generate these basis sets, including (see a detailed table in Table S2):

- **FID-A** (MATLAB): Comprehensive and open-source [13];
- **GAMMA/PyGAMMA** (C++; Python): Offers high flexibility for quantum mechanical simulations [14];
- **MARSS** (MATLAB): User-friendly, fast, and optimized for typical MRS studies [15];
- **MRSCloud** (Web-based): Accessible to users with limited local resources [16];
- **NMRScopeB** (Java; Python): Seamlessly integrates advanced NMR analysis [17];
- **Vespa** (Python): Flexible and well-documented for advanced users [18].

These packages provide predefined metabolite spin-system definitions, common pulse sequences, and adjustable parameters, ensuring compatibility with various experimental setups. Additionally, presimulated basis sets can be found on several publicly accessible databases (https://mrshub.org/datasets_basissets/).

10991492, 2026, 12, Downloaded from https://analyticalsciencejournals.onlinelibrary.wiley.com/doi/10.1002/nbm.70427, Wiley Online Library on [17/11/2026]. See the Terms and Conditions (https://onlinelibrary.wiley.com/terms-and-conditions) on Wiley Online Library for rules of use; OA articles are governed by the applicable Creative Commons License

2.1.1 | Macromolecular Basis Sets

Macromolecular (MM) signals, representing broad resonances in MR spectra, are typically modeled using (Supplementary Table S3 contains a more comprehensive list of literature):

- Parameterized mathematical functions (e.g., Gaussian or Voigt lineshape resonances);
- Basis functions derived from in vivo experiments, such as metabolite-nulled spectra matched for field strength and TE [19].

Some synthetic datasets [20–22] include sequence-specific MM basis functions, either as raw experimental data or as cleaned, noise-free models [23]. Resources like MRSHub (https://mrshub.org/datasets_mm/) provide growing libraries of MM experimental data for broader use.

2.1.2 | X-Nuclei Basis Sets

For X-nuclei MRS (e.g., ^{31}P, ^{13}C, ^{23}Na), basis sets often rely on individual lineshape functions constrained by prior knowledge of parameters like chemical shifts and coupling constants. Tools such as AMARES [24, 25], OXSA [26], and jMRUI [27] facilitate the creation and simulation of these datasets. Additionally, packages like LCModel [28], FSL-MRS [29], and MARSS [30] support simulation of X-nuclei basis sets for both research and clinical applications.

While some ^{31}P datasets include field-specific parameters for metabolites like NAD$^+$/NADH [31, 32], other nuclei such as ^{23}Na and ^{13}C remain underexplored in synthetic simulations, presenting opportunities for future development. For ^{2}H MRS, spin system parameters are largely unchanged when *J*-couplings are scaled by the respective gyromagnetic ratios and the simulation program can properly accommodate spin1 nuclear evolution [30]. Spin definitions for ^{31}P [31, 33] and ^{13}C [34] metabolites have been published. However, most other nuclei have sufficiently sparse resonances that researchers instead rely on peak fitting instead of linear combination modeling, bypassing the need for basis functions.

2.2 | Signal Model Components

Considerations:

- ***Noise:*** *Simulated datasets should span coil-combined signal-to-noise ratios (SNRs) representative of typical* in vivo *acquisitions (approximately 5–75), while allowing extension beyond this range when required for specific benchmarking applications.*
- **Line broadening:** *Both Lorentzian and non-Lorentzian broadening mechanisms should be implemented to approximate realistic* in vivo *spectral lineshapes.*
- ***Phase and frequency Shifts:*** *Global phase and frequency shifts should be incorporated into the final synthetic spectrum to enhance realism. Small metabolite-specific frequency shifts may be included where appropriate.*
- ***Macromolecular, lipid****, and* ***baseline*** *components should be modeled where relevant to the intended in vivo scenario.*

Similar to linear combination-based modeling approaches, synthetic data apply a signal model to a set of metabolite basis functions. This involves modifying several free parameters to adjust the basis functions, which are then combined into a plausible approximation of an acquired spectrum. At minimum, a signal model should include amplitude and lineshape adjustments to integrate the basis set into a single spectrum. However, additional signal components would need to be implemented to better mimic in vivo data and their artifacts [35]. A general overview of a simulation workflow is shown in Figure 1.

The basic signal model of a spectrum is shown here in Equation (1). This model includes the set of metabolites $n \in N$ where M is the amplitude, or metabolite scaling factor, representing the concentration, φ is the quantum mechanically simulated basis function, t is the time vector, d is the Lorentzian lineshape broadening term, g is the Gaussian lineshape broadening term, Δf is the frequency shift, ϕ_0 is the zero-order phase term, ϕ_1 is the first-order phase term, and σ is the standard deviation of the noise to achieve a specific SNR. The sum of all modulated metabolites produces the FID, and the Fourier transform then yields the spectrum in the frequency domain.

$$s(\omega) = \mathcal{F}\left(\sum_n^N M_n * \varphi_n e^{-d_n t - g_n t^2} e^{-i\Delta f_n t} e^{i(\phi_0 + \phi_1 t)} + N(0,\sigma)\right) \tag{1}$$

2.2.1 | Amplitude

Metabolite-specific amplitude parameters are used to linearly scale basis functions. These values are often derived from distributions informed by large datasets or population-specific priors [20–22, 36, 37]. Simulators can extend this by incorporating tissue-specific distributions [20, 22, 36, 37], or dynamic changes, such as those in T_2 series [22] or task-related fMRS experiments [38]. Recent simulation frameworks, such as MRS-Sim, have introduced modular approaches that allow for the flexible integration of these amplitude parameter definitions and sampling strategies, enhancing the realism and adaptability of synthetic MRS data generation [11].

These amplitudes represent the metabolite concentrations in the simulations. Metabolite concentrations in the literature are reported in various units [37], including ratios relative to water or reference metabolites (commonly tCr), "absolute" units such as mol/kg or mol/L, and institutional units (IU). "Absolute" quantification requires correction for relaxation effects and appropriate signal scaling relative to a known reference (e.g., internal water, external phantom, or electronic reference methods) [5], synthetic MRS studies often adopt whichever reporting convention aligns with their simulation strategy. Transparency about the chosen units and how they map onto simulated amplitudes is essential, as this determines how concentration ranges are interpreted during synthetic data construction.

2.2.2 | Phase

Zero- and first-order phase shifts applied to the final synthetic spectrum are typically drawn from zero-centered distributions

10991492, 2026, 12, Downloaded from https://analyticalsciencejournals.onlinelibrary.wiley.com/doi/10.1002/nbm.70427, Wiley Online Library on [17/11/2026]. See the Terms and Conditions (https://onlinelibrary.wiley.com/terms-and-conditions) on Wiley Online Library for rules of use; OA articles are governed by the applicable Creative Commons License

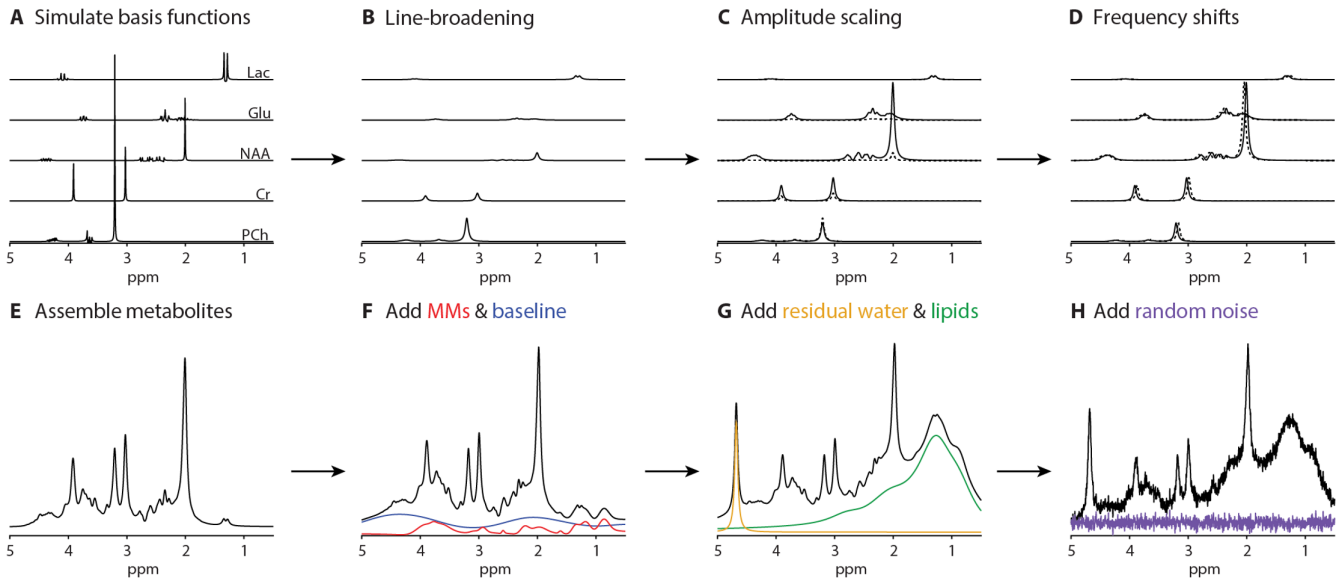


FIGURE 1 | Illustrative workflow for generating an in vivo–like synthetic MRS spectrum. Schematic overview of the steps involved in constructing a realistic synthetic spectrum: (A) simulation of a metabolite basis set with the desired pulse sequence; (B–D) application of line broadening, amplitude scaling, and frequency shifts; (E) summation of metabolite components; (F–H) addition of macromolecular signal, baseline distortions, residual water/lipid contributions, and random noise to approximate in vivo spectral characteristics.

to reflect in vivo variability [11, 20, 22, 35, 36, 39, 40]. While common, their inclusion is not universal [38, 41].

2.2.3 | Frequency Shift

Global frequency shifts can be applied to the final synthetic spectrum to simulate experimental B_0 changes caused by thermal drift, subject motion, etc. Small metabolite-specific frequency shifts are applied to account for factors like temperature and pH variations and spin-system inaccuracies. These shifts are often drawn from random distributions [11, 20, 22, 35, 36, 39, 40] or obtained from measured in vivo B_0 maps [42].

2.2.4 | Lineshape

2.2.4.1 | Lorentzian. Most, but not all [41], simulators apply global [23], metabolite-specific [20–22, 36, 38, 39], or even moiety-specific [36, 40] Lorentzian line broadening to mimic the effects of T_2 relaxation times on the lineshape. When available and applicable, tissue-specific T_2 literature or measured values are used [20, 22, 40] to account for tissue-specific relaxation, but also other processes such as dipolar interactions that may be relevant for certain nuclei. They may also be modulated across a time series of spectra to simulate BOLD effects in fMRS experiments [38], as elaborated on in the fMRS section.

2.2.4.2 | Non-Lorentzian. Non-Lorentzian line broadening arises from local B_0 inhomogeneities, e.g., local field susceptibility and imperfect shimming. Gaussian lineshapes can be used to describe the effect of normally distributed intra-voxel field inhomogeneities [11, 22, 23, 36, 38–40]. More complex definable lineshape convolution kernels or simulations including measured B_0 maps [42] can be used to describe non-normality of B_0 within the voxel, and while this can be used in simulations, to date, it has only been used in spectral fitting routines [20, 28, 43]. Both are usually applied equally to all basis functions, although some simulators differentiate between MMs and metabolites [11, 44], and one added a per-metabolite jitter [36].

The lineshape of MM peaks can be challenging to model. The consensus paper [19] explained that MM peaks represent a collection of amino acids with different T_2 relaxation values and different *J*-couplings. The strong spectral overlap sums these lineshapes into the observed spectral peaks. Because of this, modeling T_2 relaxation and B_0 inhomogeneities alone does not sufficiently account for the observed lineshapes of MM peaks. Therefore, they are sometimes given an extra Gaussian term during fitting and simulations.

2.2.4.3 | Voigt. The Voigt function describes a signal decay resulting from the multiplication of exponential, i.e., Lorentzian, and Gaussian decays in the time domain; in the frequency domain, this corresponds to a convolution of Lorentzian and Gaussian lineshapes. It represents the combined effects of homogeneous broadening (e.g., relaxation-related exponential decay processes contributing to T_2^*) and inhomogeneous broadening arising from normally distributed intra-voxel magnetic field variations. The Voigt profile is the common lineshape encountered in in vivo data [45, 46].

2.2.5 | Noise

Most simulators and synthetic datasets include uncorrelated Gaussian noise along with the final metabolite spectrum [20–23,

10991492, 2026, 12, Downloaded from https://analyticalsciencejournals.onlinelibrary.wiley.com/doi/10.1002/nbm.70427, Wiley Online Library on [17/11/2026]. See the Terms and Conditions (https://onlinelibrary.wiley.com/terms-and-conditions) on Wiley Online Library for rules of use; OA articles are governed by the applicable Creative Commons License

35, 36, 39, 40, 47, 48]; some can add noise correlations between transients or coils [11, 20, 22]. To simulate realistic acquisition conditions, the noise is often sampled independently in the real and imaginary parts and scaled to achieve a desired signal-to-noise ratio (SNR). Definitions of target SNR are generally well defined within a given work, but the definitions can vary considerably and therefore are difficult to compare across studies.

2.2.6 | X-Nuclei

Synthetic data generation for X-nuclei MRS differs from ^{1}H MRS. Notably, water contamination or suppression, lipid contamination, and MM contributions are mostly unnecessary to model, as these components do not dominate the spectra of most X-nuclei. Because the gyromagnetic ratio of X-nuclei is lower than that of ^{1}H, both their linewidths (from B_0 inhomogeneity) and their signal amplitudes are reduced. Simulations should scale these parameters accordingly, even for voxel sizes bigger than those of ^{1}H acquisitions. Furthermore, the spectral profile of a typical in vivo X-nuclei MRS spectrum can vary dramatically across field strength due to the dipolar broadening effect being more prominent at lower field strengths [49], acquiring data with or without ^{1}H-decoupling at low fields [50], and the pre-acquisition delay time [51]. For ^{31}P-MRS specifically, synthetic data should account for: frequency shifts arising from variations in intracellular pH and magnesium (Mg^{2+}) concentrations [52, 53]; homonuclear *J*-coupling, particularly in ATP, to reproduce the characteristic multiplet structures [31, 54]; and effects of magnetization transfer in dynamic studies that result from enzymatic activity [55–57]. These factors play a critical role in the estimation of the membrane phospholipid and high-energy phosphate metabolite levels. It is also essential to understand that most X-nuclear MRS is dynamic in nature (e.g., ^{2}H [58, 59], ^{31}P [60, 61], ^{13}C [62, 63]), which plays a critical role for realistic synthesis (see Section 3.4).

2.3 | Metabolites

Considerations:

- ***Type:*** *The simulation framework should explicitly state whether parameters are defined as fixed single values or sampled from a distribution.*
- ***References:*** *All parameter ranges should be justified and supported by appropriate literature references or empirical data.*
- ***Choice:*** *Parameter ranges should be selected according to the intended purpose of the simulation. For software validation and benchmarking, ranges should be sufficiently broad to challenge fitting stability, robustness, and sensitivity. For simulations designed to reflect clinical scenarios, parameter limits should prioritize physiological plausibility and expected patient variability.*
- ***Implementation:*** *It should be explicitly acknowledged that metabolite concentrations and spectral amplitudes are not equivalent quantities. The relationship between concentration and signal amplitude (including sequence timing, relaxation effects, and scaling factors) should be clearly defined within the simulation model.*

Metabolite concentration ranges in synthetic MRS data refer to the minimum and maximum values used to define a distribution of metabolite concentration levels and relaxation rates, corresponding to signal amplitudes and lineshapes, respectively. Accurate metabolite ranges are essential when generating synthetic MRS data, as the development of software packages for processing and quantification relies upon synthetic data serving as a ground truth reference and being representative of the in vivo target data. Therefore, it is desirable to use ranges that are consistent with those present in biological tissue and also consider that these values are greatly influenced by organ, anatomical brain regions [64], tissue type [65], age [66, 67], sex/gender, metabolic state (e.g., fasting vs. post-prandial), hormonal status (e.g., menstrual cycle, menopause) [68–71], and of course pathology. Additionally, nonbiological factors such as scanner vendor [72, 73] and acquisition sequence [74–76] have been shown to influence quantified metabolite values and may need to be reflected when defining synthetic ranges for specific use cases.

2.3.1 | Concentrations

Metabolite concentration ranges for generating synthetic MRS data can be determined through employing meta-analytic methods across a collection of in vivo research literature, performing single study-specific or hypothesis-driven experiments, or a combination of both. Literature-derived values provide broad coverage of typical metabolite levels across tissues, conditions, and populations, enabling researchers to define general realistic ranges [37]. Experimental measurements, on the other hand, offer flexibility for targeting specific research questions or simulating conditions that are underrepresented or insufficiently characterized in the literature. Together, these approaches allow concentration ranges to be tailored to the intended biological context of the synthetic dataset.

To examine how synthetic MRS data are typically constructed, we conducted a focused literature review of metabolite concentration values used in simulations. A total of 24 studies employing synthetic MRS data were identified (see Supporting Information S1: Section 3). Comparability across studies was limited by a mixture of reporting units and heterogeneous levels of methodological detail. Eight studies reported concentrations in millimolar (mM), the most common unit among the surveyed literature, and these were therefore used for aggregated visualization. Figure 2 shows the mean and range of each metabolite based on the mM values reported.

Across these studies, the concentration ranges expressed in mM were relatively consistent and generally reflected values typical of healthy brain tissue, unsurprising given that synthetic datasets are most frequently used for algorithm or pipeline validation [78–80] (see also Section 5.3). When comparing these simulation-derived ranges to values reported in recent meta-analyses [37], the central tendency aligns reasonably well (e.g., Glx $\approx 11.5 \pm 4.2$ mM in the meta-analysis). However, the reported ranges used in the simulations tended to be narrower. This likely reflects both the limited number of simulation studies ($N = 8$ reporting in mM) and the fact that most simulations

10991492, 2026, 12, Downloaded from https://analyticalsciencejournals.onlinelibrary.wiley.com/doi/10.1002/nbm.70427, Wiley Online Library on [17/11/2026]. See the Terms and Conditions (https://onlinelibrary.wiley.com/terms-and-conditions) on Wiley Online Library for rules of use; OA articles are governed by the applicable Creative Commons License

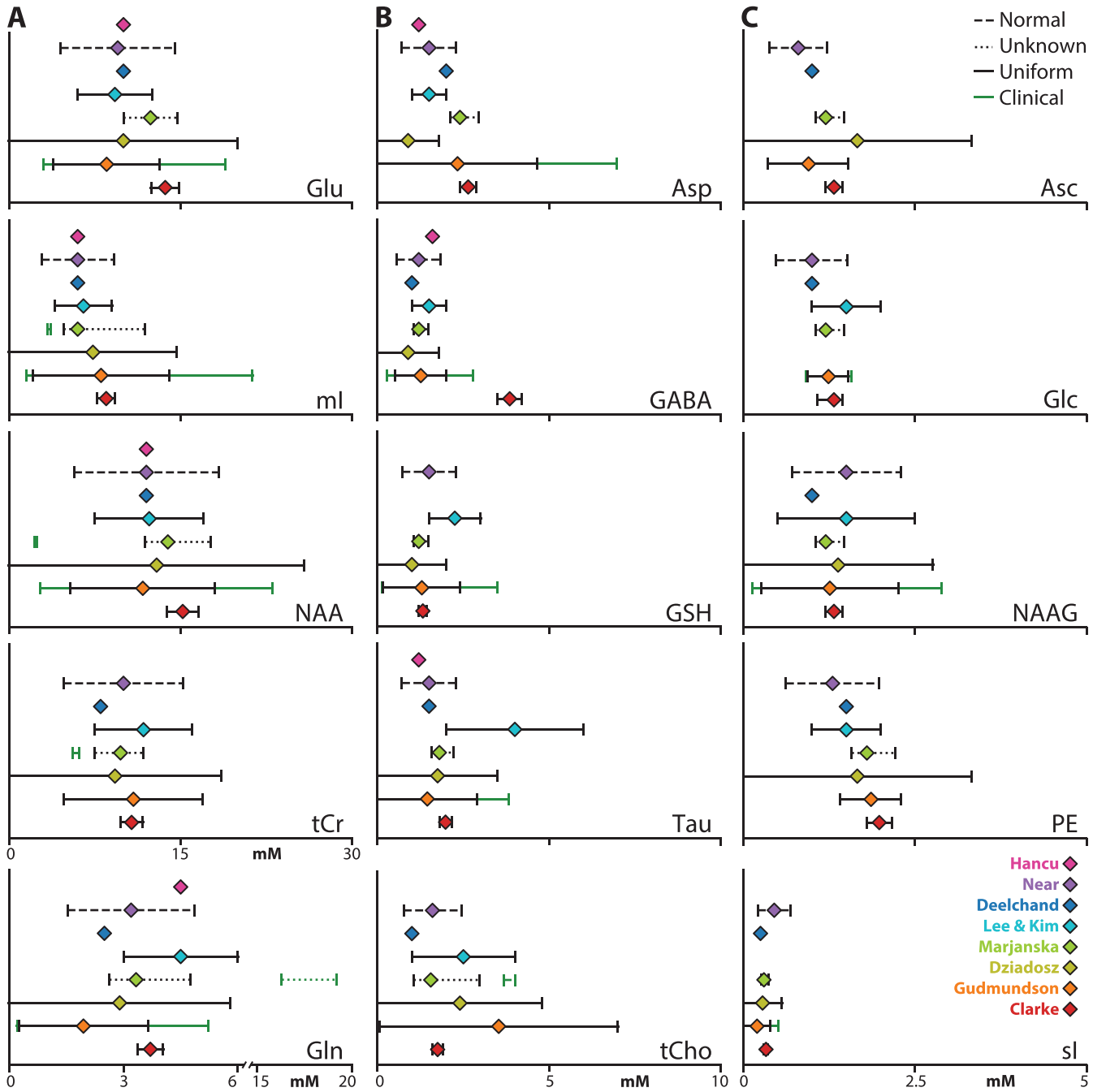


FIGURE 2 | Concentrations for (A) high (0–30 mM), (B) medium (0–10 mM), and (C) low (0–5 mM) concentrated metabolites used in synthetic MRS data. Diamond markers indicate the mean concentration value. The statistical distribution can be seen as a dashed line for normal, solid line for uniform, dotted line for unknown distributions when a range was provided. Green lines were given to datasets that provided an additional clinical range with the exception of [77] whose values for healthy and clinical populations could not be separated.

target "typical healthy" concentrations rather than attempting to represent the full variability reported in the literature, including values from larger samples or heterogeneous clinical populations.

These observations highlight the importance of clearly defining and justifying the intended physiological scope of synthetic metabolite concentration ranges, whether they are meant to represent typical healthy values, narrower application-specific ranges, or broader variability for algorithm stress-testing.

2.3.1.1 | **Amplitudes From Concentrations.** Metabolite concentrations are used to determine the amplitude coefficients that scale each basis function during synthetic spectrum generation. In practice, most simulation frameworks do not attempt to model the full physical signal scaling that would link in vivo concentrations to measured signal amplitudes. Such a mapping would require explicit simulation of the unsuppressed water reference signal, together with assumptions about tissue composition, relaxation properties, and water visibility [5]. Instead, synthetic MRS studies typically use concentration ratios to

10991492, 2026, 12, Downloaded from https://analyticalsciencejournals.onlinelibrary.wiley.com/doi/10.1002/nbm.70427, Wiley Online Library on [17/11/2026]. See the Terms and Conditions (https://onlinelibrary.wiley.com/terms-and-conditions) on Wiley Online Library for rules of use; OA articles are governed by the applicable Creative Commons License

specify relative amplitudes. This is commonly implemented in one of two ways.

The first approach selects a reference metabolite, historically tCr, and normalizes all basis functions using this reference, and then applies literature-derived relative concentration ratios to determine their relative amplitudes [78–80]. This method preserves realistic metabolite relationships without requiring 'absolute' quantification, by setting the reference metabolite's concentration to 1.0 and defining the remaining concentrations with respect to the reference. The second approach assumes that each basis function corresponds to the signal produced by a 1.0 mM solution of that metabolite, which allows millimolar literature concentrations to be used directly as amplitude scaling factors [18, 29]. In both cases, the resulting amplitude coefficients represent relative signal levels rather than "absolute" concentrations, a behavior reflected in several modern simulation and analysis toolboxes [20, 81].

Transparent reporting of how amplitudes were derived, including the assumed relationship between concentration values and basis function scaling, is essential. Clear documentation ensures that synthetic data can be reproduced, interpreted correctly, and compared across studies, and it provides necessary context for downstream quantification or algorithm validation.

2.3.2 | Relaxation

Relaxation properties contribute critically to the appearance of synthetic MRS data because they influence both signal amplitude and lineshape. Although the studies reviewed were relatively consistent in their stated choices of metabolite concentrations, there were notable differences in how relaxation was implemented. The equations for the different types of relaxation are shown in Table 1. Some studies applied metabolite-specific relaxation constants, using measured or literature-derived T_1 and T_2 values for individual metabolites or metabolite moieties (e.g., [84–86]). Others scaled all metabolite amplitudes by a fixed relaxation factor relative to water, which simplifies implementation but does not capture differences in relaxation across metabolites (e.g., [29, 76]). A smaller number of studies applied no relaxation-based modulation of amplitude or linewidth, producing spectra that may not reflect realistic in vivo characteristics. The models for relaxation are shown below.

TABLE 1 | Relaxation Mechanisms.

Relaxation Mechanism	Equations
Longitudinal relaxation T_1	$M_0\left(1-e^{-\frac{TR}{T_1}}\right)$
Apparent (steady-state) longitudinal relaxation T_1* [82, 83]	$M_0 \times \frac{1-e^{-\frac{TR}{T_1}}}{1-cos(\alpha)\, e^{-\frac{TR}{T_1}}} \times sin\, \alpha$
Transverse relaxation T_2	$M_0 e^{-\frac{TE}{T_2}}$
Apparent transverse relaxation T_2*	$M_0\, e^{-\frac{TE}{T_2^*}}$

Implementations for incorporating relaxation fall into a few main approaches. First, they can be incorporated into the density matrix simulations for the basis functions, such as MARSS [15], which fixes the values for the entire dataset. Greater flexibility is achieved by applying relaxation during the spectral simulations instead of the basis function simulations. For greater variability, they can be applied per metabolite or per moiety if the moieties in the basis functions are stored separately. Of the reviewed literature, when relaxation was included in data simulations, it was always limited to T_2 relaxation. So far, T_1 relaxation has not been included in simulations. These different implementations can result in synthetic spectra with markedly different appearances. T_1 relaxation determines longitudinal recovery during the acquisition sequence and has a substantial effect on signal amplitude, particularly in short TR experiments. T_2* relaxation governs transverse decay and contributes to Lorentzian broadening, thereby influencing spectral resolution and the practical visibility of J-resolved multiplet structures. Because metabolite T_1 and T_2 values vary across field strength, tissue type, and acquisition parameters [87–89], the choice of relaxation model should reflect the intended simulation context.

2.4 | Challenges and Next Steps

2.4.1 | Basis Sets

The development and application of basis sets are central to generating realistic synthetic MRS data. Advances in tools, improvements to spin system definitions, and the incorporation of real pulse and gradient shapes that reflect the sequence used on the scanner have substantially increased the fidelity of simulated basis sets. Despite these advances, several challenges remain.

Variability in sequence parameters, particularly pulse timings, and the widespread use of ideal radiofrequency pulses during basis set simulation remain persistent sources of discrepancy. Many real-world sequences rely on proprietary or undocumented pulse shapes, making it difficult to simulate them with perfect fidelity. Sequence imperfections, including those arising from hardware limitations such as gradient nonlinearity or B_1 inhomogeneity, are also frequently overlooked.

Macromolecule, lipid, and baseline signal simulations vary considerably across synthetic data generators, and these differences can meaningfully affect linear-combination modeling results. Since the impact of broad signal modeling on quantitative fitting is well documented [19, 90], careful evaluation is needed to determine whether particular simulation frameworks unintentionally favor certain modeling algorithms.

A promising idea to increase flexibility is to oversample the temporal sampling grid during basis set simulation, which allows a single high-resolution simulation to be downsampled to multiple commonly used spectral widths by subsampling the time points [36]. Further exploration of this approach may reduce the need to regenerate basis sets when acquisition parameters vary within typical ranges [36].

10991492, 2026, 12, Downloaded from https://analyticalsciencejournals.onlinelibrary.wiley.com/doi/10.1002/nbm.70427, Wiley Online Library on [17/11/2026]. See the Terms and Conditions (https://onlinelibrary.wiley.com/terms-and-conditions) on Wiley Online Library for rules of use; OA articles are governed by the applicable Creative Commons License

2.4.2 | Signal Models

Synthetic data generators vary widely in how they implement key components (e.g., metabolite and noise) of the signal model. Without sufficient methodological detail, this variability limits the ability to compare synthetic datasets and complicates reproducibility across platforms (see Section 3).

Even basic definitions can differ. For example, the consensus definition of SNR from the Terminology Consensus [91] is not consistently adopted across existing tools. This variation reflects differences in the intended complexity of simulation frameworks, which range from simple weighted combinations of ideal basis functions to detailed reproductions of pulse sequence physics in spatially varying geometries with accurate timing information. Adoption of the consensus guidelines for defining SNR is strongly encouraged to facilitate comparison, reproducibility, and transparency.

A significant next step is the ability to synthesize a corresponding unsuppressed water reference signal [92]. Generating an unsuppressed water signal would support several goals. First, it would allow metabolite- and water-specific T_1 and T_2 relaxation times and diffusion properties to be incorporated into amplitude and linewidth modeling consistently. Second, it would align synthetic datasets more closely with in vivo quantification workflows, which typically rely on water scaling for amplitude normalization. Third, it would enable systematic assessment of fitting accuracy in "absolute" quantification pipelines, thereby bridging a long-standing gap in validation efforts.

In parallel, incorporating realistic tissue fraction data are essential because metabolite concentrations and relaxation rates may differ across gray matter, white matter, and cerebrospinal fluid. Accounting for tissue composition and effective water visibility (i.e., compartment- and relaxation-dependent differences in observable water signal across GM, WM, CSF, and vascular contributions) improves the physiological realism of synthetic spectra, particularly when generating synthetic unsuppressed water references.

2.4.3 | Metabolite Parameter Ranges

Defining metabolite concentration ranges that are suitable for all use cases remains challenging. Users must remain aware that narrowly chosen ranges may not capture the variability observed across different acquisition methods, anatomical regions, age groups, field strengths, and scanner vendors. Broader literature sources or meta-analyses, such as [37], may provide appropriate guidance when natural variability is substantial. Conversely, when simulating specific scenarios, for example, particular brain regions or clinical cohorts, ranges should be tailored to reflect the relevant physiological context.

A major next step involves clarifying not only the choice of ranges but also the distributions from which synthetic concentrations are drawn. Specifying minimum and maximum values often leads users to apply a uniform distribution by default, which may not reflect the true variability of metabolite concentrations in vivo. More appropriate alternatives may include normal distributions, skewed Gaussian distributions, or Poisson-like distributions, depending on the metabolite and target population. Clear recommendations regarding distribution shape would help users generate synthetic datasets that more accurately represent underlying biological variability.

Our review did not evaluate macromolecule and lipid concentrations because their amplitudes are sparsely reported and span broad ranges. These resonances are frequently modeled separately from metabolites, creating uncertainty in their relative amplitude scaling. As macromolecular signals significantly influence quantification, improved guidance for MM and lipid amplitude modeling is warranted.

Finally, until simulations routinely incorporate synthetic unsuppressed water references, bridging the gap between metabolite concentrations and the amplitude values used in simulations remains an open challenge. Detailed reporting of the choices made, including the selection of concentration ranges, the type of distribution applied, and the strategy for mapping concentration to amplitude is essential for reproducibility and accurate interpretation.

3 | Advanced Components for Synthetic MRS Data

While core components establish the bare minimum for synthetic MRS data (see *previous section*), advanced components are essential for maximal realism. This section reviews features included in the simulation of synthetic datasets that go beyond minimum considerations, incorporating additional signal components to better reflect real-world MRS data.

Advanced components address the intricate interplay between spectral features and experimental conditions. For instance, the spectral dimension for simulated metabolites and macromolecules must account for chemical shifts, *J*-coupling, and their interactions with water and lipid-suppression modules, RF pulses, B_1^+ field inhomogeneities, B_0-field variations, and T_1 and T_2 relaxation times. But simulating these complex interactions is computationally intensive, which has historically limited their incorporation in synthetic data models. Most existing simulations simplify these factors, focusing only on chemical shifts, *J*-coupling, or singlet resonances. However, as computational resources and modeling techniques advance, integrating these sophisticated interactions becomes increasingly feasible, offering more accurate and application-relevant synthetic datasets.

3.1 | Spectral Components

Considerations:

- ***^{1}H:***
  - ***Macromolecular*** *signals should be included with tissue-specific scaling appropriate to the simulated anatomical or physiological context.*
  - ***Baseline*** *contributions should be modeled using flexible approaches such as cubic splines, Voigt lines, or polynomial functions, depending on the intended* in vivo *scenario and fitting strategy being evaluated.*
  - *Common* ***nuisance*** *signals, including residual water, lipids, and echo artifacts, should be incorporated where relevant to the acquisition type and study objective.*

10991492, 2026, 12, Downloaded from https://analyticalsciencejournals.onlinelibrary.wiley.com/doi/10.1002/nbm.70427, Wiley Online Library on [17/11/2026]. See the Terms and Conditions (https://onlinelibrary.wiley.com/terms-and-conditions) on Wiley Online Library for rules of use; OA articles are governed by the applicable Creative Commons License

3.1.1 | Baseline

According to recent terminology consensus [91], "baseline" describes broad nuisance signals underlying the metabolite spectra of interest (e.g., from poor water suppression), but not MM. Some (but not all [23, 40]) synthetic data generators add broad signals to achieve this, but while their parameterization varies, many choose to generate baselines using the same methods they use for modeling them. Cubic splines are a common choice [20–22, 35, 39], as are very broad Voigt line shape signals [48] and Gaussian peaks [93]. However, some work has explored unconventional approaches, such as constructing the baseline from in vivo fit residuals [38] or using a model-agnostic smoothed, pseudo-random walk algorithm [11].

3.1.2 | Nuisance Signals

In vivo spectra further contain partially suppressed water, lipids, and out-of-voxel or "ghost" signals. These nuisance signals are challenging to parametrize and therefore less commonly included in synthetic data and usually included when they are the specific focus.

3.1.2.1 | Residual Water. Water artifacts from partially suppressed water are simulated either by considering sequence parameters, relaxation weighting and variable water suppression due to off-resonance and flip angle errors or simply by adding Lorentzian lines of variable amplitude but fixed chemical shift. Some simulators describe residual water with a single simulated peak [23] (with varying lineshape, frequency, width, phase, and amplitude) or multiple peaks [36] to mimic the resemblance of imperfect in vivo water suppression, while another used a smoothed pseudo-random walk algorithm to generate random signal fluctuations for the residual water region [11].

3.1.2.2 | Lipids. Artifacts from extracranial lipids may be modeled randomly or based on in vivo MRSI data to consider natural variability of lipid amplitudes and patterns or by simulating singlets at known chemical shifts. Lipid contamination is incorporated in some simulators by optionally adding one or more Voigt lines with defined center frequencies, widths, and amplitude distributions [20, 22, 35, 40] or extracted from high-lipid in vivo data [23, 94]. An alternative modeling approach is the use of, e.g., cubic basis splines [93].

3.1.2.3 | Spurious Echoes. Some simulators have explicit models of spurious echoes [36], a troublesome artifact that has consistently remained an issue for the field. These spurious signals most often arise from unsuppressed water signals from outside the voxel of interest. A robust model of these artifacts has yet to be defined. Approaches thus far have paramete, rized the spurious echo as a complex time-domain exponential-form signal with features that define a center time point, frequency, phase, and amplitude [35, 36]. Since spurious echoes arise from unwanted coherence pathways, a more physically grounded approach could be to model these pathways directly. The coherence-pathway origin of spurious signals and their sequence-dependent behavior are discussed in [18].

3.2 | Spatial Components

Considerations:

- ***Coil-Specific Factors****: Array coil data should be simulated with realistic noise correlations, receive sensitivity profiles, and head-position variability to approximate* in vivo *acquisition conditions.*
- ***Spatial Field Variations****: Spatial inhomogeneities in B_0 and B_1 fields, as well as spatially varying metabolite distributions, should be incorporated into the simulation framework. This is particularly important for MRSI datasets, where voxel-specific variations should reflect realistic* in vivo *patterns.*
- ***k-Space Sampling****: Realistic k-space encoding schemes should be implemented, including conventional phase encoding and alternative trajectory-based spatial–spectral encoding techniques. Gradient imperfections and system-related distortions should be modeled where feasible to improve the accuracy of the simulated spatial response function.*

Synthetic MRS data can be made substantially more realistic by incorporating spatially dependent factors that influence the measured signal in vivo. These include coil-specific receive profiles, spatial variations in the B_0 and B_1^+ fields, spatially nonuniform metabolite distributions, and realistic k-space encoding. While these spatial components are essential for generating advanced MRSI or multi-voxel synthetic datasets, they remain underrepresented across existing simulation tools.

3.2.1 | Phased-Array Receiver Coils

Realistic simulation of phased-array multi-coil acquisitions requires modeling spatially varying B_1^- (receive) fields, coil sensitivity profiles, and inter-coil noise correlations. These factors determine how signal amplitude, phase, and noise vary across space and with different head positions inside the coil. Such variability is critical for replicating the acquisition characteristics of multichannel MRSI data. Although these parameters can be simulated by assigning coil sensitivity maps, coil loading factors, and noise correlation matrices, only two studies to date have explicitly incorporated these coil-specific effects into synthetic MRS data [95, 96]. Wider adoption of array-coil modeling would specifically enable more realistic benchmarking of reconstruction, the ability to develop denoising methodologies, and facilitate work investigating channel combination strategies.

3.2.2 | Effects of B_0 and B_1^+ Inhomogeneities

Spatial inhomogeneities in the static magnetic field (B_0) and transmit field (B_1^+) strongly affect MRSI signals. In earlier sections (Section 2.2), line broadening, signal decay, and frequency shifts were discussed independently. However, spatially resolved modeling of B_0 inhomogeneities provides a unified and physically grounded way to simulate all three effects simultaneously.

10991492, 2026, 12, Downloaded from https://analyticalsciencejournals.onlinelibrary.wiley.com/doi/10.1002/nbm.70427, Wiley Online Library on [17/11/2026]. See the Terms and Conditions (https://onlinelibrary.wiley.com/terms-and-conditions) on Wiley Online Library for rules of use; OA articles are governed by the applicable Creative Commons License

B_0 field maps may be obtained from large MRI repositories, measured per scan, or measured once and fitted using smooth spatial basis functions such as polynomials. Several modern simulators implement B_0 inhomogeneity by over-discretizing the MRS voxel into many sub-voxels. For example, MRS-Sim simulates a three-dimensional voxel subdivided into a high-resolution grid and modulates each basis function with the complex exponential corresponding to the local B_0 offset, summing over the volume to produce the final line shape. This approach captures realistic intra-voxel dephasing beyond simple Gaussian broadening models.

Other tools, such as Osprey, do not explicitly model spatial B_0 distributions; instead, they optimize relaxation and line shape parameters that implicitly capture the effects of inhomogeneity. Additional simulation methods have been proposed for realistic B_0 modeling using high-resolution in vivo field maps or synthetic 3D fields [11, 97, 98]. Ideally, these approaches should also incorporate the true, non-ideal VOI selection profile and, in MRSI, the spatial response function (SRF, see Section 3.2.3) to achieve accurate spatial contamination patterns.

B_1^+ inhomogeneities, although less frequently modeled, can be incorporated similarly by scaling simulated signals according to transmit field variations across space, which is particularly relevant at high field strengths.

3.2.3 | K-Space Sampling and Gradient Imperfections

MRSI data acquisition uses spatial encoding: the specific k-space trajectory and the imperfections of gradient hardware determine the spatial response function. The SRF governs how signals originating from one location spread into adjacent or distant voxels, which is especially consequential when strong nuisance signals, for example extracranial lipids, contaminate the measurement.

To simulate realistic MRSI data, the high-resolution spatial metabolite distribution can be transformed into low-resolution k-space using simulated gradient trajectories that incorporate temporal delays, amplitude errors, and trajectory distortions. This produces an SRF that matches in vivo behavior more closely than idealized phase encoding.

Despite its importance, only two publications have simulated nonphase-encoded trajectories, such as spiral or rosette readouts, while nearly all others have relied solely on idealized phase encoding [99, 100]. Incorporating realistic k-space paths, especially those affected by gradient nonlinearities or eddy-current-induced distortions, remains an important next step for synthetic MRSI development [95, 97, 98, 101–104].

Taken together, current simulation tools vary widely in their ability to incorporate spatially dependent effects. Some support voxel over-discretization or field-map-based modeling, while others rely on simplified parameter adjustments that do not capture true spatial heterogeneity. To help guide tool selection and future development, here are some of the existing simulators, detailing which spatial components they implement and identifying key challenges, including coil modeling, realistic B_0/B_1^+ fields, and non-ideal k-space trajectories [105–109].

3.3 | Sample-Specific Components

Sample-specific components capture biological and experimental characteristics that differ across species, developmental stages, tissue types, and pathological conditions. Incorporating these elements enables synthetic MRS data to support a wide range of experimental, clinical, and methodological applications. These factors become particularly important for the modality-specific use cases discussed in Section 4.1 Functional MRS (fMRS), Section 4.2 Diffusion MRS (dMRS), and Section 4.3 Magnetic Resonance Spectroscopic Imaging (MRSI), as well as the application contexts described in Section 5.1 Clinical Applications and Section 5.2 Preclinical Applications. Although many of these components are well characterized in vivo, only a limited number of synthetic data generators currently incorporate them.

Human and nonhuman species differ in linewidths, chemical shifts, macromolecular content, and metabolite concentrations, particularly at high field strengths [110]. Gray matter, white matter, and other tissue types exhibit distinct relaxation properties and susceptibility profiles that influence spectral appearance. Incorporating region-specific relaxation or partial-volume effects improves realism, especially for spatially resolved approaches. Metabolite levels and relaxation times change across development, aging, and disease. Temperature, pH, susceptibility gradients, and preparation conditions alter resonance frequency, relaxation, and linewidth, particularly in preclinical or ex vivo studies. Spatial variations in B_0 and B_1^+ fields influence linewidth, frequency offsets, and signal scaling.

3.4 | Dynamic Aspects

Dynamic aspects in MRS reflect any process that causes the spectrum to change over time, and synthetic data frameworks must capture these changes to reproduce realistic experimental conditions. Such temporal variation can arise from biological mechanisms that are of primary interest, from experimental manipulations designed to elicit a measurable response, or from unwanted instabilities originating in the scanner, the subject, or the acquisition itself. Importantly, these processes unfold across different timescales, and the dominant timescale observed depends on both the physiology under study and the experimental paradigm applied. This distinction is relevant for within-session paradigms such as functional MRS (fMRS), isotopic labeling studies, hyperpolarized experiments, magnetization/saturation transfer investigations, and diffusion-weighted acquisitions, as well as for between-session, or longitudinal, measurements in which inter-session variance plays a different and often larger role [111–117].

Biological or metabolically driven temporal changes are those that synthetic datasets are typically designed to emulate. In fMRS, for example, neural activation can lead to task-related

10991492, 2026, 12, Downloaded from https://analyticalsciencejournals.onlinelibrary.wiley.com/doi/10.1002/nbm.70427, Wiley Online Library on [17/11/2026]. See the Terms and Conditions (https://onlinelibrary.wiley.com/terms-and-conditions) on Wiley Online Library for rules of use; OA articles are governed by the applicable Creative Commons License

changes in metabolite levels, accompanied by small BOLD-related linewidth or frequency modulations (Section 4.1). Isotopic labeling studies similarly require modeling of concentration trajectories governed by chemical exchange and metabolic flux, while hyperpolarized MRS produces rapid, large-amplitude decays dictated by the short T_1 relaxation times of the hyperpolarized substrate. These mechanisms generate interpretable temporal structure and represent the "desired" component of temporal dynamics.

A second category of temporal variation arises from the experimental design rather than biology. Block-design and event-related fMRS paradigms, inversion-recovery sequences for T_1 mapping, or diffusion-weighted MRS protocols with systematically varied gradient strengths (Section 4.2) all impose predictable temporal patterns on the acquired data. Multichannel acquisitions may further introduce slow changes in relative coil phase or SNR due to coil loading differences or subtle shifts in head position. Dynamic MRSI protocols extend these effects spatially, producing metabolite maps whose temporal evolution reflects both physiology and the specifics of the acquisition strategy. These elements represent deliberate, experimenter-controlled variability that synthetic data must represent when used to test analysis methods under realistic conditions.

In contrast, several forms of temporal variation are unwanted and act as noise sources that obscure the biological effects of interest. Scanner-related instabilities include both rapid, within-echo fluctuations and slow, session-level drifts. Almost all instabilities are predominantly driven by eddy currents generated by rapidly switching gradients, producing phase evolution or lineshape distortions that can be approximated using one- or two-parameter models [13, 23, 38] or through irregular lineshape convolutions [20, 22]. Slow timescale changes arise from gradual heating of gradient coils and passive B_0 shim components, leading to magnetic field drift across the experiment. These effects can be simulated by sampling frequency offsets across successive transients, as implemented in MRS-Sim [11]. Physiological fluctuations further modulate phase, frequency, and amplitude on timescales corresponding to respiration, cardiac pulsation, or motion, and become increasingly prominent at high magnetic fields [118] or with specifically susceptible pulse sequences [119]. Incorporating these instabilities into synthetic datasets enables systematic testing of correction strategies and is essential for evaluating the robustness of preprocessing and quantification pipelines.

Real experiments often exhibit combinations of the above mechanisms, and several recent approaches therefore emphasize multidimensional modeling. Rather than simulating the time dimension independently across spectral components, these methods jointly model chemical kinetics, relaxation processes, and temporal covariance across spectra, allowing time-resolved fitting algorithms to exploit structured relationships in the data [120]. As synthetic MRS frameworks continue to evolve, the ability to reproduce these interacting processes, both the desired biological effects and the accompanying unwanted instabilities, will be critical for generating datasets. These will serve as realistic, discriminative test sets for emerging analytical methods.

3.5 | Challenges and Next Steps

Despite considerable progress in synthetic MRS data generation, several challenges remain, particularly when attempting to capture domain-specific nuances with sufficient accuracy. One unresolved issue concerns the scaling and characterization of macromolecular and lipid signals, which vary across brain regions, field strengths, and acquisition methods, yet remain insufficiently standardized for simulation purposes. Similarly, dynamic responses such as functional changes, diffusion sensitivity, and metabolic turnover are only partially represented in current frameworks, even though these effects are essential for the modality-specific applications described in Section 4.1 Functional MRS, Section 4.2 Diffusion MRS, and Section 4.3 MRSI.

A second set of challenges relates to spatial heterogeneity. Spatial variation in metabolite levels, relaxation parameters, and macromolecular content is still not fully understood, limiting the ability of synthetic data generators to accurately model regional specificity. While vendor differences and sequence-specific features can be accounted for in basis set simulation and signal modeling [72, 76], reproducing voxel-level variation requires incorporating B_0 and B_1 fields, coil sensitivity profiles, and partial-volume effects. These components are particularly important for the 2D and 3D MRSI applications discussed in Section 4.3, where realistic spatial contamination patterns and metabolite distributions are critical.

Multi-spectrum data generation represents another frontier. Many emerging techniques, including functional MRS, diffusion-weighted MRS, metabolic kinetics, relaxometry, and spectral fingerprinting, require large sets of related transients with controlled variability. Advances in computing resources, algorithmic efficiency, and understanding of in vivo variability will be necessary to support the creation of such comprehensive, multi-transient datasets.

Several physical effects also remain insufficiently characterized for reliable simulation. Baseline contributions result from a combination of macromolecular, lipid, and sequence-dependent effects and are not yet fully understood. Metabolite distributions are typically known only at coarse spatial resolution, which complicates efforts to generate realistic high-resolution MRSI datasets. Simulating difficult-to-quantify metabolites such as GABA or lactate adds another layer of uncertainty. Furthermore, the creation of realistic MRSI data often requires large intermediate data structures, posing computational and storage challenges for practical simulation workflows.

Future efforts should prioritize the development and sharing of standardized synthetic datasets and include underrepresented modalities such as hyperpolarized MRS or X-nuclei spectroscopy. Improving reproducibility across studies will require harmonizing simulation parameters, reporting standards, and methodological choices. The next major step involves integrating the diverse effects described across Sections 3.1–3.4 into unified simulation frameworks that incorporate scanner imperfections, frequency drifts, spatial heterogeneity, and temporal dynamics within a single model. Hard-to-characterize

10991492, 2026, 12, Downloaded from https://analyticalsciencejournals.onlinelibrary.wiley.com/doi/10.1002/nbm.70427, Wiley Online Library on [17/11/2026]. See the Terms and Conditions (https://onlinelibrary.wiley.com/terms-and-conditions) on Wiley Online Library for rules of use; OA articles are governed by the applicable Creative Commons License

components such as baseline contributions and macromolecular variability also require further investigation to enhance realism.

Ultimately, progress will depend on broad collaboration across research domains, improved understanding of metabolic spatial and temporal dynamics, and the integration of advanced computational and analytical tools. These developments will collectively enable more realistic synthetic data, improve benchmarking of analysis pipelines, and support the expanding clinical and preclinical applications described in Sections 5.1 and 5.2.

4 | Modalities in MRS

Synthetic data have become an essential resource across multiple MRS modalities, enabling optimization of acquisition strategies, validation and benchmarking of analysis pipelines, and the development of data-driven models, including AI-based approaches. This section examines how synthetic data are applied within three major contexts: functional MRS (fMRS), diffusion MRS (dMRS), and MR spectroscopic imaging (MRSI). For each modality, we summarize how synthetic datasets are generated, their advantages and limitations, and the roles they play in advancing methodological development. We also outline the key challenges and future directions specific to each application, identifying gaps in current simulation frameworks and opportunities for improvement.

4.1 | Functional MRS (fMRS)

Considerations:

- ***Dynamic Changes in Concentrations and MR Visibility:*** *Time-resolved simulations should account for metabolite fluctuations arising from metabolic flux and/or compartmental shifts. These processes may occur on timescales ranging from subseconds to minutes and should be modeled according to the intended experimental paradigm (*e.g.*, functional MRS, metabolic tracing, or hyperpolarized studies). Changes in MR visibility should be distinguished from true concentration changes where relevant.*
- ***Dynamic Linewidth and Relaxation Changes:*** *Time-dependent alterations in linewidth and relaxation parameters should be incorporated where appropriate. For example, BOLD-related effects may induce transient linewidth narrowing, which should be reflected in realistic functional simulations.*
- ***Confounding Effects due to long Acquisition Time:*** *For prolonged acquisitions, simulations should include potential confounding effects such as gradual concentration drift, lineshape variability, frequency shifts, and phase instability. These effects may arise from subject motion, physiological fluctuations, or scanner instability and should be modeled when robustness to such perturbations is being evaluated.*

Functional MRS (fMRS) measures changes in metabolite levels over time (as shown in Figure 3), i.e., the temporal dynamics of metabolites in response to functional tasks, pharmacological interventions, or changes in physiology (see reviews [121–123]). Although many of these experiments operate on short timescales within a single scanning session, fMRS does not capture the ms timescale of neurotransmission directly. The concept more broadly encompasses any paradigm in which metabolite dynamics are interpreted relative to an experimental condition or state change typically over seconds to minutes. This also distinguishes fMRS from longitudinal studies, where inter-session differences and longer-term variance dominate, even though both approaches examine metabolite responses to interventions or physiology. While fMRS is most commonly applied using ^{1}H MRS, for example, lactate and glutamate levels that change in response to pain and visual stimulation [115, 116, 124, 125], dynamic MRS(I) has also been used with other nuclei such as ^{31}P, ^{2}H, and ^{13}C [58–60, 126, 127]. Although some principles carry over, additional complexities, like pH-related peak shifts (^{31}P) or polarization dynamics (^{13}C), come into play. We acknowledge these X-nuclei approaches but focus here on ^{1}H MRS, as no publicly available synthetic datasets are currently available for the other nuclei.

Synthetic data are playing an increasingly valuable role in fMRS and can be used to: (1) test hypotheses about the origins of neurometabolite fluctuations and their response functions, (2) assess the accuracy of both traditional and novel fitting methods in quantifying dynamic changes, (3) examine the impact of nuisance parameters (e.g., BOLD-induced linewidth fluctuations) on these measurements, and (4) explore the limits of temporal and spatial resolution in ^{1}H fMRS acquisitions [120, 128, 129].

The key distinction between synthetic functional MRS and static MRS data lies in modeling neurometabolite fluctuations over extended acquisition times, along with associated confounding factors. While fMRS may be used to evaluate dynamics across longer timescales (days) by comparing metabolite levels across multiple acquisition sessions, we focus here on the more typical scenario, involving a time course of conventional or edited spectra in which one or more metabolites exhibit concentration changes within the scan duration. Key considerations in such simulations include the magnitude of the response (e.g., percentage concentration change) and its temporal characteristics (e.g., onset, peak, and decay profile). Commonly studied metabolites, such as lactate (Lac) and glutamate (Glu), have expected concentration changes in response to various functional stimuli that can be informed by findings summarized in recent meta-analyses [117, 130]. While some studies suggest both shifts in metabolic flux and compartmental redistribution alter MR visibility, the exact mechanisms driving these changes remain unclear and controversial. Importantly, metabolite dynamics appear to reflect processes operating on different timescales, and the timescale observed depends on the experimental paradigm. For example, rapid glutamate changes have been reported to peak within approximately 0.5 s [111, 117], whereas slower, sustained changes may reach a maximum around 120 s [112, 115].

10991492, 2026, 12, Downloaded from https://analyticalsciencejournals.onlinelibrary.wiley.com/doi/10.1002/nbm.70427, Wiley Online Library on [17/11/2026]. See the Terms and Conditions (https://onlinelibrary.wiley.com/terms-and-conditions) on Wiley Online Library for rules of use; OA articles are governed by the applicable Creative Commons License

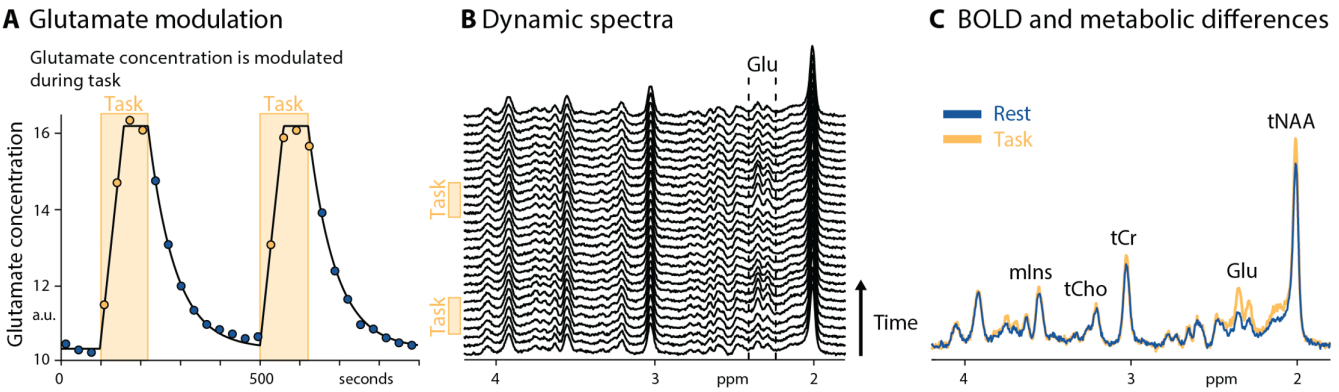


FIGURE 3 | Synthetic fMRS block-design experiment illustrating dynamic glutamate modulation and potential BOLD-related confounds. Rest periods are shown in blue and task periods in yellow. (A) The simulated ground-truth glutamate concentration increases during two task blocks before gradually returning toward baseline. Concentrations are expressed in arbitrary units. (B) Stacked spectra acquired over time illustrate the corresponding dynamic changes in the glutamate spectral region during the task blocks. (C) Simulated mean spectra during rest and task. In addition to the genuine increase in glutamate concentration, BOLD-related line narrowing produces changes in spectral peak height and shape across multiple metabolites. Consequently, the apparent task-related increases in tNAA, tCr, tCho, and myo-inositol do not reflect changes in their simulated concentrations but arise from the linewidth change. This example illustrates why linewidth effects must be modeled or corrected when estimating task-related metabolite changes in fMRS.

An important consideration in synthetic fMRS is the inclusion of task-related linewidth changes resulting from BOLD-induced alterations in T_2*. While BOLD effects do not directly affect metabolite concentrations, they can influence spectral lineshapes in ways that can be misinterpreted as changes in concentration [131] (Figure 3C—tNAA changes only due to linewidth changes). Consequently, these effects may often require explicit modeling or correction during fMRS analysis to avoid bias in estimates of task-related metabolite changes. Several early fMRS studies have reported indicative ranges for these linewidth fluctuations (e.g., [112, 115, 116, 132]), although their exact characteristics remain poorly defined [133]. Motion presents another source of variability, introducing shifts in tissue composition within the voxel, changes in B_1^+ field homogeneity, and fluctuations in overall signal intensity over time. Additionally, scanner-related instabilities may cause gradual frequency drifts and imperfect water or lipid suppression that can accumulate over longer acquisitions. These gradual signal changes are particularly problematic for long block-design (> 1 min) fMRS, where slow glutamate and lactate changes associated with prolonged stimuli can be difficult to distinguish from scanner drift and progressive head motion.

Advances in fMRS analysis methods have increasingly relied on synthetic data to evaluate and refine their performance under controlled conditions [128]. Traditionally, fMRS studies grouped transients by block or event type and applied conventional spectral fitting methods, such as LCModel, to each group independently. However, newer approaches, such as 2D fitting techniques [41, 120, 134–136] and direct linear modeling in the temporal domain [137] (Figure 3B), offer improved precision by jointly modeling spectral and temporal dimensions. These methods help disentangle true metabolite responses from nuisance factors like baseline shifts, linewidth changes, or motion-related artifacts. Simulation studies have shown that 2D fitting can substantially increase precision, particularly in the presence of overlapping peaks, while also reducing the uncertainty of estimated response amplitudes [120, 136]. These gains arise from jointly fitting multiple noisy spectra within a unified model, allowing shared parameters and explicit modeling of metabolite dynamics across time. This reduces noise-driven variance but may introduce bias if the assumed temporal model is violated. Similarly, regularization of fitting parameters, while proven effective in static MRS, has yet to be systematically explored in the context of fMRS [138]. Synthetic datasets provide a powerful platform to test such strategies and define optimal analysis pipelines tailored to dynamic MRS data.

4.2 | Diffusion MRS (dMRS)

Considerations:

- *When generating synthetic diffusion-resolved MRS (dMRS) spectra,* ***artifacts specific to diffusion*** *acquisitions should be incorporated. These include phase and frequency drifts, signal intensity outliers, and other instabilities expected under* in vivo *diffusion-weighted conditions.*
- *To evaluate a processing pipeline and/or optimize an acquisition protocol, quantum-mechanical (QM) simulation of both the spectral and* ***diffusion dimensions*** *should be performed using the specific MRS sequence and an appropriate forward analytical signal model.*
- *When the objective is to assess sensitivity of the acquisition framework to a specific biophysical parameter (*e.g., *soma radius), generation of full synthetic dMRS spectra may not be necessary. In such cases, Monte Carlo simulations of metabolite diffusion within synthetic cellular geometries may be sufficient and more computationally efficient.*

^{1}H diffusion-weighted MRS (dMRS) uniquely combines the properties of ^{1}H MRS (spectral/chemical shift) and

10991492, 2026, 12, Downloaded from https://analyticalsciencejournals.onlinelibrary.wiley.com/doi/10.1002/nbm.70427, Wiley Online Library on [17/11/2026]. See the Terms and Conditions (https://onlinelibrary.wiley.com/terms-and-conditions) on Wiley Online Library for rules of use; OA articles are governed by the applicable Creative Commons License

diffusion-weighting acquisitions (*b*-value, diffusion time) to measure the diffusion properties of mostly intracellular metabolites and, as such, informs on the cell-type-specific microstructure. For an overview of dMRS, refer to the consensus and recommendations paper [139] and dMRS reviews [140, 141], as well as resources on MRSHub (https://forum.mrshub.org/c/study-experiment-design/everything-about-diffusion-weighted-mrs/36). dMRS simulations are pivotal to further our understanding of the complex relationship between tissue microstructure at the cellular scale and the encoded dMRS signal. In addition to the chemical shift and quantum interactions specific to MRS (with related artifacts and challenges), stochastic dynamics (e.g., diffusion and relaxation) encoded with specific RF and gradient schemes should be included in simulation frameworks.

To the best of our knowledge, Table S1 compiles the references using synthetic dMRS data and available repositories with open-source simulation materials. These references can be separated into two categories: (i) the ones in which an analytical biophysical diffusion model is applied to each metabolite signal simulated with a (d)MRS sequence [142, 47, 120, 143, 144] (Table S1), and (ii) the ones creating numerical simulations of metabolites' molecular diffusion in substrates mimicking neural cells [139, 145, 146] (Table S1). An overview of simulation strategies for dMRS data is shown in Figure 4.

Pipelines from (i) aim at evaluating protocols and processing/fitting approaches for typical in vivo dMRS acquisitions. Synthetic dMRS was used to highlight the benefits of 2D simultaneous fitting (of the spectral and diffusion dimensions) over 1D sequential fitting, the former increasing precision and accuracy of diffusion estimates and artifact corrections (Table S1: [120, 142, 144]), and compare phase/frequency shift correction methods (Table S5: [143]). Additionally, synthetic data are key to developing and validating denoising algorithms, especially for low-SNR modalities such as dMRS. Principal component analysis (PCA) denoising was tested on simulated dMRS spectra and showed mixed results. While it improved the precision of diffusion estimates within a cohort, it also showed a deleterious homogenization of diffusion properties across metabolites, dependent on the inclusion of artifacts (Table S1: [47, 110]).

Pipelines from (**ii**) aim at evaluating modeling approaches, typically to understand which features of the complex cellular morphology can be estimated using the diffusion of intracellular metabolites. Synthetic data are often generated by simulating how metabolites diffuse within realistic cellular environments. A common approach is to create digital cellular structures that reflect morphometric features observed in microscopy data and then run Monte Carlo simulations of metabolite random walks within these structures using a specified dMRS protocol and a range of diffusivities. The resulting signal decays provide a controlled set of diffusion-sensitive metabolite-specific signal intensities. These synthetic datasets can then be used to train machine-learning models to learn the inverse mapping, enabling the estimation of microstructural features, such as branching order, projection length, or soma size, from the measured dMRS amplitude decays. (Table S1: [139, 145, 146]). These pipelines have so far been used without generating synthetic MR spectra.

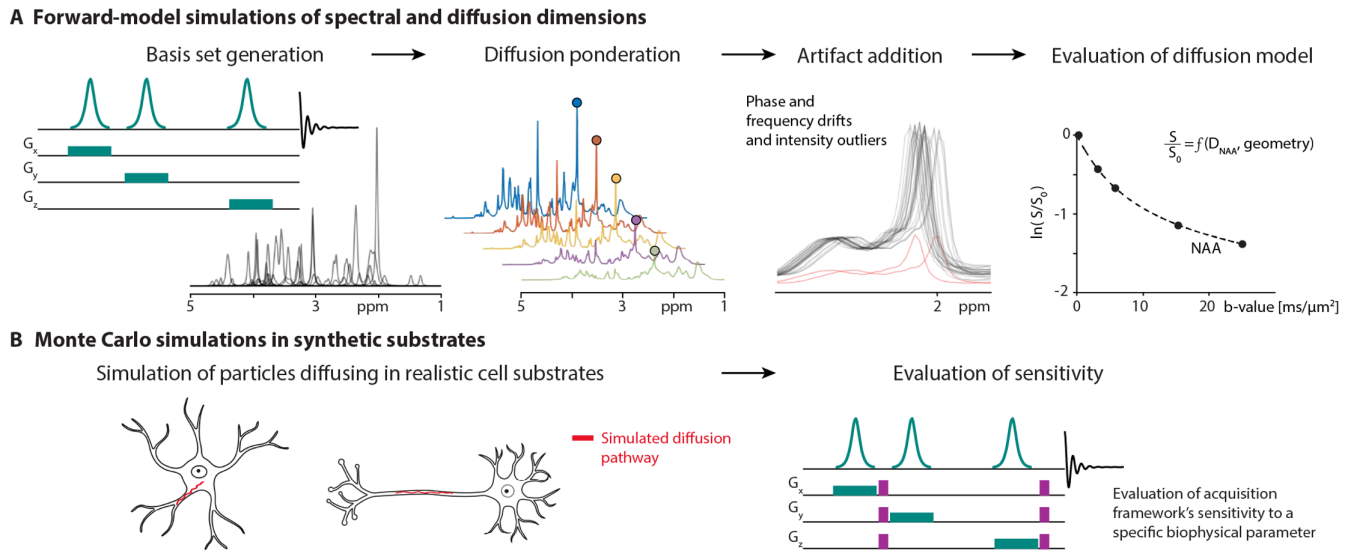


FIGURE 4 | Overview of simulation strategies used so far for diffusion-weighted MR spectroscopy (dMRS). **A:** Forward-model simulations combine spectral and diffusion dimensions. (1) A basis set is first generated for the chosen (d)MRS sequence, followed by (2) diffusion weighting according to a geometric diffusion model (e.g., metabolite-specific signal attenuation as a function of *b*-value). (3) Realistic artifacts, including frequency and phase drifts and intensity outliers, are then added to emulate single-shot experimental variability. (4) This framework enables evaluation of how well a given acquisition protocol or processing pipeline can recover diffusion-related geometric features. Note that in (2), we assume no interaction between quantum interactions (basis set simulation accounting for J-coupling and multiple coherence pathways) and diffusion effects such that their ponderations can be applied sequentially, which is also assumed when simulating basis sets for non-diffusionweighted MRS sequences. **B:** Monte Carlo simulations in synthetic cellular substrates, where (1) particles diffuse within realistic neuron- or glia-like geometries, are used to identify which microstructural features are accessible with a (2) given protocol and/or which best explain experimental dMRS data.

10991492, 2026, 12, Downloaded from https://analyticalsciencejournals.onlinelibrary.wiley.com/doi/10.1002/nbm.70427, Wiley Online Library on [17/11/2026]. See the Terms and Conditions (https://onlinelibrary.wiley.com/terms-and-conditions) on Wiley Online Library for rules of use; OA articles are governed by the applicable Creative Commons License

4.3 | MR Spectroscopic Imaging (MRSI)

Considerations:

- ***Spatial variation*** *of metabolite concentrations should be anatomically meaningful and consistent with reported literature values for the tissue type and field strength under investigation.*
- *Field-strength–dependent spatial variations in magnetic fields (**B_0 and B_1**) should be modeled to reflect their influence on spectral appearance, including linewidth, frequency offsets, and signal amplitude heterogeneity.*
- ***Lipid and residual water*** *artifacts should be simulated with realistic spatial propagation characteristics. In particular, the spatial response function (sometimes referred to as point-spread function, PSF) of the acquisition should be taken into account to ensure that contamination patterns reflect* in vivo *behavior rather than voxel-wise independent additions.*

Robust, high-quality MRSI processing methods that enable accurate and repeatable mapping of metabolite levels or concentrations are essential for clinical applications. To identify the best among the many proposed approaches, they must be compared using identical datasets with known ground truth. Openly available synthetic data provide a practical solution to this dilemma and would accelerate scientific exchange and the development of MRSI processing methods.

Most physical effects present in MRSI are also inherent to single-voxel MRS and are discussed in Section 2.2 Signal Models and Section 3 Advanced Components. These include chemical shift, *J*-coupling, T_1 and T_2 relaxation, B_0 inhomogeneities, B_1^+ and B_1^- field variations (e.g., in array coils), residual water and lipid signals, and physiological or scanner-related instabilities. However, only a subset of these, primarily *J*-coupling and relaxation behavior, can be simulated in a manner similar to single-voxel MRS. Other effects must be modeled differently in MRSI because of the typically larger encoded volume, the spatial subdivision into many voxels, and the stronger spatial variability across the field of view.

In addition, MRSI requires explicit modeling of k-space sampling and spatial distributions, as described in Section 3.2 Spatial Components, which contrasts with single-voxel MRS that can be treated entirely in the time or frequency domain and has sharply defined spatial boundaries. While a single voxel can often be optimized for B_0 and B_1 field homogeneity before acquisition, even well-optimized MRSI acquisitions commonly exhibit substantial spatial variation in these fields across a slice or volume. These spatial dependencies must therefore be incorporated into synthetic data generation to achieve realistic simulations.

To date, the majority of publications on MRSI simulations have accounted for the spatial in vivo-*like* distribution of metabolite concentrations [42, 101, 104, 118, 147–150], but simpler assumptions have also been used [99, 102, 151]. However, in terms of spatial encoding, all aspects of realistic k-space encoding have typically been neglected with the exception of exploring nonphase-encoded k-space trajectories [99, 100].

Regarding non-MRSI-specific effects, most publications incorporated spectral effects such as chemical shift, T_2 or T_2* decay, and *J*-coupling. However, some simulations were limited to singlet Lorentzian peaks. Seven publications modeled water nuisance signals [95, 97, 100, 104, 106, 108, 118], typically as a single Lorentzian singlet, without scaling to account for spatial variations in water-suppression efficiency. Some considered variable water suppression due to off-resonance and flip angle errors or simply by adding Lorentzian lines of variable amplitude but with fixed chemical shift. Lipid signals were simulated in only five publications [42, 97, 98, 100, 108].

Eleven studies considered B_0 inhomogeneities [42, 95, 97, 98, 102, 104, 118, 149], but just two simulated B_1^+ inhomogeneities [97, 98] and another two addressed B_1^- inhomogeneities [95, 152]. Notably, only one publication so far has investigated the effects of subject motion [153].

The spatial nature of MRSI adds complexity that SVS does not need to address. These additional considerations make simulating MRSI datasets more challenging. Figure 5 highlights the spatial nature of MRSI and illustrates additional considerations that differentiate MRSI from SVS. The following aspects are fundamental in MRSI:

4.3.1 | Prescans and Prior MRI Data

Many MRSI processing steps rely on information obtained from MRI acquisitions performed in the same session, including anatomical images for tissue segmentation and partial-volume correction, B_0 maps for frequency correction, B_1^+ maps for transmit field correction, and coil sensitivity maps for signal combination and reconstruction. Thus, it is important to also simulate prescan data (e.g., T_1w-MRI, B_0, B_1^+, coil sensitivities) with a typical range of errors along with the synthetic MRSI data. This point has been partially addressed [95, 97] but is sometimes replaced by using actual, measured in vivo data.

4.3.2 | Motion and Breathing Artifacts/Physiological Instabilities

Voluntary motion and breathing are major sources of instabilities, which cause smearing of nuisance signals, even to distant voxels [154]. This makes an appropriate simulation of motion a favorable feature for a range of applications. High-temporal-resolution in vivo data, e.g., using optical tracking or EPI-navigator data, provide realistic motion patterns. Ideally, this also includes changes in B_0^- and B_1^+-fields that are caused by participant motion. Only one abstract simulated this effect for MRSI [153].

4.3.3 | Spatial Metabolic Distributions

For realistic MRSI data, it is essential to reflect the variability over a range of in vivo human metabolite concentrations and anatomical properties and account for population differences (e.g., age, sex, and pathologies). Most of the publications simulated spatial metabolic distributions (e.g., GM/WM/CSF contributions or virtual phantoms) in some form.

10991492, 2026, 12, Downloaded from https://analyticalsciencejournals.onlinelibrary.wiley.com/doi/10.1002/nbm.70427, Wiley Online Library on [17/11/2026]. See the Terms and Conditions (https://onlinelibrary.wiley.com/terms-and-conditions) on Wiley Online Library for rules of use; OA articles are governed by the applicable Creative Commons License

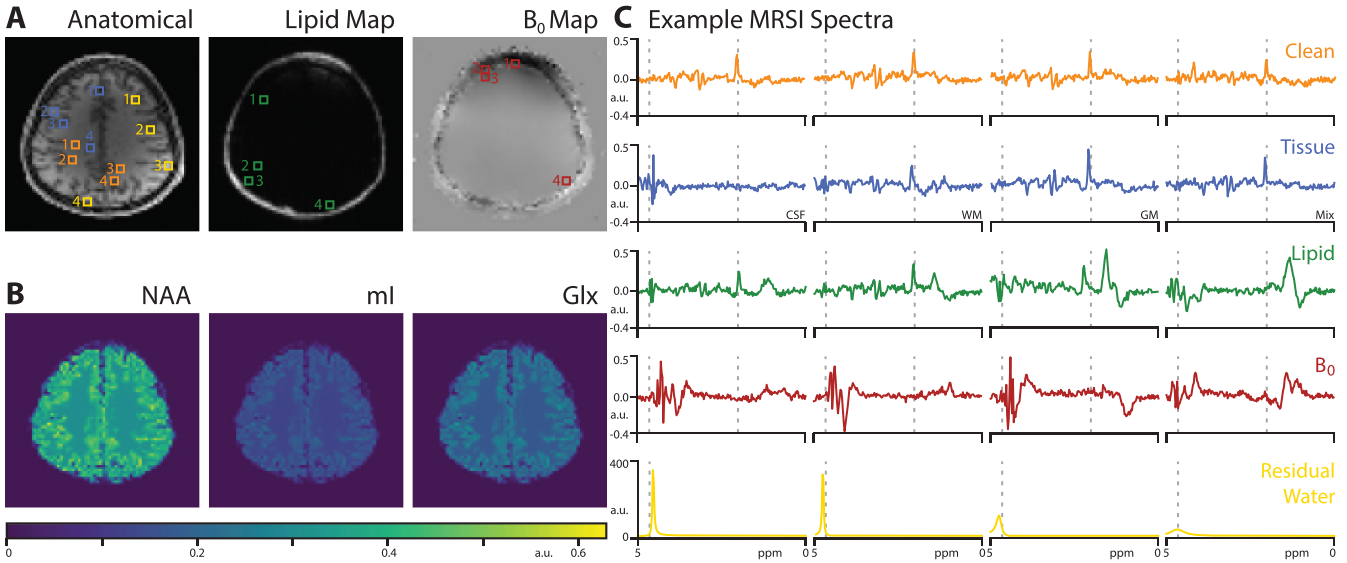


FIGURE 5 | Illustration of MRSI data simulation using the MRSI Data Processing Challenge from the ISMRM Workshop on MR Spectroscopy, 2024. (A) The anatomical, B_0 map, and lipid map. (B) Metabolite maps for NAA, mI, and Glx. (C) Example spectra from 20 voxels were produced by isolating the residual water using HSVD, isolating the lipid to downscale by a factor of 100× by removing residual water from the combined nuisance signal, and finally subtracting the nuisance from the full signal, correcting the phase, and combining with updated lipid signal. These spectra demonstrate clean (**orange**), differing tissue types (**blue**), variability in lipid artifacts (**green**) and field homogeneity (**red**), and the scale and shape of the residual water (**yellow**). The spectra are ordered from left to right as they appear in the brain maps from top to bottom shown in A.

4.4 | Challenges and Next Steps

4.4.1 | fMRS

For functional MRS, three key areas of uncertainty were identified in the modeling of dynamic metabolite changes:

4.4.1.1 | **The Metabolite Response Function.** Akin to the hemodynamic response function in fMRI, the metabolite response function in fMRS (as shown in Figure 3A) aims to map the temporal dynamics of a metabolite given a cognitive process [117]. While early findings provide some indications, the precise nature of dynamic responses, particularly for key metabolites such as Glu, remains speculative [117]. For many other metabolites, this response is even less well defined. Since meaningful simulations of transient-to-transient metabolite fluctuations depend on an accurate response function, refining our understanding in this area is a critical topic of ongoing research. Meanwhile, any synthetic data modeling tools should remain adaptable to accommodate future advancements in response function characterization.

4.4.1.2 | **BOLD-Related Effects on Spectra.** While the BOLD effect follows the well-characterized hemodynamic response from fMRI studies, typically peaking around 5 s [155], its influence on metabolite spectra is more complex. The BOLD effect introduces changes in MRS signal characteristics, particularly metabolite lineshape, which in turn may impact the fitting process and, consequently, the derived metabolite concentration estimates. Many studies assume that these effects result in a simple, global Lorentzian broadening. However, a combination of Lorentzian and Gaussian broadening, along with potential higher-order asymmetries, may be more accurate [156]. Additionally, hypothesized compartmental shifts and other physiological changes could lead to metabolite-specific lineshape alterations that are independent of the BOLD effect itself.

4.4.1.3 | **Confounding Factors.** Both subject motion and scanner instabilities have the potential to introduce unwanted spectral variance and, therefore, errors in metabolite estimates. At best, these errors will mask the genuine metabolite dynamics, reducing the sensitivity of fMRS. At worst, these artifacts may be coincident with anticipated metabolite changes, resulting in spuriously elevated estimates of metabolite level changes. For example, a strong pain stimulus may introduce involuntary movement, and therefore coincident spectral variance, which may be mistaken for a metabolic change.

Given that lineshape changes induced by BOLD fluctuations can mimic spurious metabolite changes [155], improved susceptibility contrast in high-field MRS necessitates a more detailed characterization of these effects. To improve the realism of synthetic fMRS datasets, future simulation frameworks should incorporate more flexibility in modeling lineshape variations, including the ability to selectively apply different broadening mechanisms to distinct spectral signal models.

Beyond these issues, other dynamic confounds, such as subject motion, B_0 drift, and lipid and water instability, are rarely accounted for in existing synthetic fMRS datasets. Incorporating these factors will enhance the realism of simulations and provide more reliable testing grounds for modeling approaches.

Finally, we emphasize the importance of sharing experimentally acquired fMRS datasets to refine synthetic data accuracy. The impact of BOLD and other physiological confounds is likely to depend on multiple factors, including field strength, behavioral paradigms, and acquisition parameters. Thus, pooling data

10991492, 2026, 12, Downloaded from https://analyticalsciencejournals.onlinelibrary.wiley.com/doi/10.1002/nbm.70427, Wiley Online Library on [17/11/2026]. See the Terms and Conditions (https://onlinelibrary.wiley.com/terms-and-conditions) on Wiley Online Library for rules of use; OA articles are governed by the applicable Creative Commons License

across multiple studies may be necessary to generate sufficient evidence to support or refute specific models.

4.4.2 | dMRS

The complexity and heterogeneity of dMRS simulations are highlighted by the references in Table S1. The inclusion of artifacts in synthetic dMRS data appears necessary for an accurate evaluation of processing pipelines (Table S1: [143, 144]). Such artifacts should be made *b*-value-dependent when this is expected in vivo (e.g., stronger phase drifts and more motion-corrupted shots at high *b*-values) [157], and their subsequent influence on processing and fitting results should be evaluated.

Future applications of synthetic dMRS data include evaluating the interplay between diffusion and relaxation and quantum properties, optimizing thresholds for outlier removal, and fine-tuning acquisition parameters. For example, selecting the optimal *b*-value range or SNR to maximize sensitivity to a specific model feature under experimental constraints such as fixed scan time, maximum gradient amplitude, slew rate, or peripheral nerve stimulation limits. It should be noted that although analytical models of diffusion are useful to test processing pipelines with synthetic data, degeneracies and often invalid assumptions, such as the short gradient pulse approximation, may bias the inference of cellular microstructure from dMRS signals. Numerical simulations of dMRS signals in neural cell substrates can also guide the design of sequences and inversion algorithms and help generate more reliable datasets to train machine learning models (Table S1: [139, 145, 146]).

Overall, a more unified dMRS simulator (including analytical modeling and Monte Carlo simulation approaches) is needed because the synthetic data resources found in literature so far are mostly application-specific. Inspiration for such a unified simulator can be found in the MRI (MRzero [158]) and diffusion MRI literature (DISIMPY [159], MCMRSimulator.jl [160]) and should be adapted to address the challenges specific to dMRS.

4.4.3 | MRSI

MRSI faces significant challenges in achieving robust and high-quality processing methods essential for clinical applications, as objective comparison across methods requires standardized data with known ground truths. Synthetic MRSI data offer a potential solution by enabling fair and reproducible benchmarking. They can also support the development of machine learning models, which can reduce the time and computational cost associated with processing large MRSI datasets, but only when extensive representative training and validation data are available.

As discussed in Section 4.3, several studies have incorporated specific physical effects, such as B_0 and B_1^+ inhomogeneities, into synthetic MRSI data generation. However, these implementations remain incomplete. The majority of studies reviewed in Section 4.3 overlook complex physical effects such as gradient imperfections, array coil simulations, non-Cartesian encoding, subject motion, and frequency drifts. Moreover, the interdependence of effects like chemical shift, B_0-inhomogeneity, and RF pulses has largely been neglected.

To address these limitations, the next step should involve integrating the various effects considered in prior studies into a comprehensive simulation. This should include incorporating well-understood factors like system imperfections and the interdependence of multiple effects. So far, no publication has addressed scanner instabilities such as frequency drifts, eddy currents, or other gradient imperfections in simulations. Complex interdependencies have also been largely overlooked, including factors such as water- or lipid-suppression efficiencies influenced by B_0- and B_1-inhomogeneities through pulse profiles, the effects of water and lipid suppression on metabolites, or the interaction between T_1-weighting of metabolites and B_1-inhomogeneities, which results in varying T_1-weighting for different B_1 values.

Simulations should also account for impacts such as k-space trajectory, filtering, and point-spread functions. Further investigation is needed on contributions to spectral baselines along with MM and lipid signals. These components remain poorly understood and consequently cannot be adequately simulated.

Another unresolved challenge is the need for high-resolution metabolic maps over the entire brain, especially for low-concentration metabolites that could serve as a foundation for realistic simulations. Initial efforts should focus on generating 2D MRSI data to provide more control over physics-based data creation. The optimization process should be incremental, beginning with these factors and later expanding to include spatially correlated B_0, B_1, and eddy current imperfections. These steps should facilitate the transition to generating 3D MRSI data.

In summary, synthetic MRSI data has supported the development of advanced spectroscopic imaging techniques and validated complex pipelines, for example: Simulating spatial distributions of metabolites and B_0/B_1 inhomogeneities has been critical for evaluating quantification algorithms [22]. Incorporating gradient imperfections and physiological instabilities into MRSI synthetic datasets ensures realistic k-space reconstructions. Also, modeling coil-specific receive profiles and noise correlations has improved accuracy in array coil setups [96]. Future work should focus on sharing standardized synthetic MRSI datasets.

5 | Applications

5.1 | Clinical Applications

Considerations:

- *Metabolite concentrations, relaxation parameters, and metabolite ratios should be tailored to reflect* ***physiology- or pathology-specific*** *metabolic profiles relevant to the intended simulation scenario.*
- *When simulating data for specific pathologies, parameter inputs should be derived from* ***well-powered, representative*** *datasets to ensure that simulated alterations reflect realistic population variability rather than anecdotal or underpowered findings.*

10991492, 2026, 12, Downloaded from https://analyticalsciencejournals.onlinelibrary.wiley.com/doi/10.1002/nbm.70427, Wiley Online Library on [17/11/2026]. See the Terms and Conditions (https://onlinelibrary.wiley.com/terms-and-conditions) on Wiley Online Library for rules of use; OA articles are governed by the applicable Creative Commons License

In clinical settings, synthetic data have two primary use cases. The first is validating software packages, such as spectral fitting methods, which use a priori assumptions to constrain the problem space. In such cases, soft or hard constraints may be violated by different pathologies, causing the methods to fail. The second is supplementing pathological datasets to develop and validate machine learning and deep learning models. In both cases, the synthetic data must be representative of the targeted pathologies. So far, synthetic data have been employed to model pathological metabolite profiles associated with neurodegenerative diseases, psychiatric conditions, and tumors, with notable examples including:

- **AGNOSTIC Dataset:** Synthetic data representing over 20 clinical profiles, including neurodegenerative, psychiatric, and trauma-related conditions [36].
- **Oncometabolites:** Tumor spectra were simulated by adding contributions from 2HG and Cystat, increasing contributions from tCho, mI, Lac, lip09, and lip20, while decreasing contributions from tNAA and Glu [7].
- **Idealized Setting:** Metabolite concentrations were sampled independently and uniformly between 0 and twice the reference average concentration for a normal, healthy brain, but tCho was extended to [0 mM, 5 mM], where elevated values above twice the reference average concentration represents tumor tissues [40].
- **Tumor Modeling:** Machine learning-generated synthetic data for healthy tissue, low-grade, and high-grade brain tumors [161].
- **2016 ISMRM Fitting Challenge:** Synthetic tumor datasets were generated in addition to healthy datasets by adding varying amounts of lipids and acetate [23].

Despite these advancements, the use of synthetic data in clinical settings remains limited, particularly for rare diseases and complex clinical scenarios. For instance, biological variability in brain tumors complicates synthetic data modeling, as overlapping peaks between classes and varying necrotic lipid contributions, particularly in glioblastoma, can obscure clear differentiation [162]. Additionally, strong heterogeneity is often observed within individual patients and between patients with the same pathology [163]. Only a few studies have generated synthetic MRS data tailored to clinical scenarios [36, 164, 165]. Using data from the INTERPRET project, a synthetic dataset with 24 metabolites, including citrate and 2-HG, was developed to differentiate metastatic brain tumors from glioblastoma [164]. However, key necrotic lipid contributions were omitted, and some simulated metabolites like bHB which are less relevant in this context [163] were included. Another approach utilized the INTERPRET SV short-TE dataset (20–32 ms) with Bayesian non-negative matrix factorization (NMF) to generate synthetic data [166]. Here, one representative case from each of four brain tumor classes was expanded into 50 instances per class using two types of randomly generated mixing matrices (20% and 35% variability). This synthetic dataset was designed not to replicate the empirical population but to validate the ideal number of sources for Bayesian NMF extraction. Another approach was used in a doctoral dissertation, where a hill-climbing algorithm was employed to construct a Bayesian belief network from a small Alzheimer's disease sample, and forward sampling was used to generate 1000 synthetic examples, resulting in improved classification performance within that dataset [167]. Finally, synthetic SV MRS data at short-TE (30 ms) have been used for three-class brain tumor classification (healthy tissue, low-grade, and high-grade brain tumors) employing generative adversarial networks, deep convolutional GANs, and pairwise mixture models [161]. Accuracy values were above 90% except for the Deep Convolutional Generative Adversarial Network (DCGAN), although few details are provided about the numbers of generated spectra.

5.2 | Preclinical Applications

Considerations:

- ***^{1}H:***
  - ***B_0 and Gradient Strength:*** *B_0 field strength and gradient performance should reflect the high-field systems and strong gradients typically used in preclinical MRS acquisitions.*
  - ***SNR Scaling:*** *Signal-to-noise characteristics should account for the inherently lower SNR per transient associated with smaller voxel sizes commonly used in small-animal studies.*
  - ***Spectral Resolution and Linewidth:*** *Linewidth and spectral resolution parameters should be adjusted to reflect the higher spectral dispersion and field-dependent effects observed at preclinical field strengths.*
  - ***Macromolecules and Baseline:*** *Macromolecular contributions and baseline characteristics should be modeled according to preclinical acquisition conditions and field strength.*
- ***General:***
  - ***RF Pulse and TE Constraints:*** *Sequence simulations should account for short RF pulses and very short echo times (TEs) that are frequently used in preclinical implementations.*
  - ***X-nuclei Considerations:*** *Realistic signal behavior should be implemented for non-^{1}H nuclei commonly used in preclinical research, such as ^{13}C, ^{2}H and ^{31}P, including appropriate relaxation properties and spectral characteristics.*
  - ***Noise and Motion Effects:*** *Physiological noise sources and motion-related distortions specific to small-animal experiments should be modeled where relevant to the simulation objective.*

Similar to human studies, proton and X-nuclei synthetic data have been generated and used in preclinical settings for research in mice, rats, and other animal models [47, 48, 118, 168–170]. However, preclinical MRS operates with higher B_0 field strengths, stronger gradients, shorter RF pulses, very short TEs, and smaller volumes of interest, among other differences from their human counterparts. As a result, acquired MR spectra will exhibit distinct SNRs, spectral resolutions, linewidths, and artifacts when compared to human data. Each of these features needs to be identified and considered in the preclinical context when using synthetic data.

10991492, 2026, 12, Downloaded from https://analyticalsciencejournals.onlinelibrary.wiley.com/doi/10.1002/nbm.70427, Wiley Online Library on [17/11/2026]. See the Terms and Conditions (https://onlinelibrary.wiley.com/terms-and-conditions) on Wiley Online Library for rules of use; OA articles are governed by the applicable Creative Commons License

While preclinical synthetic data must account for many differences from clinical data, they have been similarly used for tasks such as validation of new acquisition protocols, testing processing algorithms, and emerging quantification methods, all of which need comprehensive evaluations. For newly developed acquisition protocols, preclinical synthetic data have been used to assess signal loss due to J-modulation under different sequences and conditions [171, 172]. Due to the small size of the rodent brain, preclinical ^{1}H MRS suffers from reduced SNR, which, by design, becomes particularly problematic in lower-SNR techniques such as MRSI and dMRS, creating a greater interest in synthetic data for testing denoising algorithms [47, 118]. Nevertheless, recent advances in rodent MRS have demonstrated sub-microliter voxel localization at 11.7 T, allowing for reliable quantification of 19 distinct metabolites in the mouse cortex [173]. While the overall neurochemical profile is similar between rodents and humans, there are some notable differences, reflecting differences in metabolism, osmoregulation, and tissue composition. The most pronounced difference is in Tau, which reaches concentrations of approximately 5–12 mM in the healthy rodent brain [174, 175] compared with ~2 mM in the adult human brain [36], consistent with its greater role in osmoregulation. In addition, tCho concentrations are generally lower in rodents (0.5–1.5 mM) [174, 175] than in humans (1–2.5 mM) [64, 176]. Rodents also tend to have higher Gln and, in some brain regions, Glu concentrations [174, 175]. Differences in most other metabolites are less consistent and largely depend on the brain region examined.

Such empirical data provide an invaluable benchmark for synthetic MRS frameworks that aim to capture the high-spatial-resolution conditions seen in preclinical neuroimaging. For model fitting, synthetic data have been used to compare acquired versus simulated basis sets [168] as well as to assess the impact of using full versus parameterized modeling of experimentally acquired MM spectra and of the degree of baseline freedom on metabolite quantification [48, 177]. In addition to proton MRS, X-nuclei synthetic data have been more commonly used for preclinical work, including hyperpolarized MRSI [178], which also uses the underlying signal models more generally [179], novel reconstruction algorithms [180], advanced Proton-Observed Carbon-Edited pulse sequence design [181, 182], and evaluating the necessity of proton decoupling for ^{13}C MRS [183].

Described briefly in the AI Section (Section 5.4), preclinical synthetic data have also been used in the development of machine learning and deep learning approaches for the quantification of extracellular pH [184] and targeted quantification of overlapping metabolites [169]. A more detailed description of these works can be found in Table S1. Furthermore, synthetic data have been extensively used to validate acquisition and quantification methods in preclinical models, such as:

- **High-field models:** Basis sets derived from 9.4 T rodent brain spectra have been used to simulate metabolic and relaxation dynamics [23].
- **X-nuclei spectroscopy:** Simulations have validated techniques for tracking metabolic changes using [^{13}C]-labeled compounds [114].
- **Physiological modeling:** Synthetic datasets incorporating motion artifacts and field instabilities have improved the robustness of preclinical imaging pipelines [118].

Despite their success so far, preclinical synthetic data still lack standardization and comprehensive models for species-specific nuances and experimental paradigms. Lanz et al. [185] provides a detailed overview and expert recommendations regarding rodent models, the effects of anesthesia, and data acquisition protocols that should inform the simulations of synthetic preclinical MRS data.

5.3 | Software Validation Methods

Considerations:

- *Synthetic datasets should be recognized as essential for definitive validation of MRS methodologies, as they provide a* ***known ground truth*** *and eliminate uncontrolled biases and noise sources inherent to experimental data.*
- *The design and characteristics of synthetic validation datasets should be tailored to the specific application under investigation. To ensure* ***reproducibility and comparability across studies****, transparent data sharing and adherence to reporting standards are strongly recommended.*
- ***Large,* in vivo*–like synthetic datasets*** *should be developed as accessible community resources for benchmarking emerging methods. Such datasets should be derived from generative models of sufficient biophysical and acquisition complexity to ensure realistic variability. The development of a widely adopted reference synthetic dataset for benchmarking new software would represent a valuable addition to the existing MRS methodological infrastructure.*

The field of MRS is rich with methodological development, particularly in the arenas of data processing and modeling. While the end goal of this research is application to in vivo spectra, researchers cannot fully evaluate the accuracy and precision of their new methods without a known ground truth with which to compare. Synthetic spectra provide such a ground truth, allowing researchers to uncover potential biases inadvertently introduced by their methods.

As a result, synthetic data have been deployed in a diverse array of applications for validating new software tools. New data processing methods often leverage this approach to validate their accuracy, for example, in correcting shot-to-shot frequency and phase drift [41, 186, 187], residual water removal. [188], and denoising [93, 134], to name just a few. Likewise, the complex interplay of individual linear combination modeling (LCM) components necessitates stringent testing of new methods. These have included the optimization of the baseline definition and basis set composition [134], optimal model parameter regularization [138], and even the establishment of entirely new LCMs [20, 22, 39, 120, 189]. Indeed, the latter is a particular concern for the MRS community, with different

10991492, 2026, 12, Downloaded from https://analyticalsciencejournals.onlinelibrary.wiley.com/doi/10.1002/nbm.70427, Wiley Online Library on [17/11/2026]. See the Terms and Conditions (https://onlinelibrary.wiley.com/terms-and-conditions) on Wiley Online Library for rules of use; OA articles are governed by the applicable Creative Commons License

LCMs producing distinct metabolite amplitude estimates [190]. Synthetic data have also been used to validate more specific modeling assumptions or conceptual approaches, such as the separation of choline-containing compounds (PCh and GPC) from total choline signals [191].

The need for validation and benchmarking has prompted community-driven efforts such as the MRS fitting challenges [23, 192]. While these and other validation datasets cover spectra with various features, the datasets themselves are limited in size [193]. This restricts the conclusions that can be drawn from them as benchmarking datasets, particularly for data-hungry AI applications (Section 5.3). The scale and sheer diversity of the validation data needed might be met by other methods [36, 37, 40, 194], but it is crucial that the specific approach taken by researchers must be underscored by adequate reporting standards (Section 6.3) and, ideally, openly accessible data in standardized data formats (Section 6.4).

5.4 | Artificial Intelligence (AI) Applications

Considerations:

- *The operational domain of AI models trained on synthetic data should be explicitly defined and characterized to identify performance boundaries, failure modes, and limitations.*
- *Synthetic training datasets should model clinically relevant metabolite distributions, nuisance signals, and acquisition artifacts to promote robustness under real-world conditions.*
- *Synthetic datasets should reflect the heterogeneity of* in vivo *acquisitions, including variability in hardware platforms, pulse sequences, acquisition protocols, physiological states, and demographic characteristics.*
- *AI models trained on synthetic data should be validated on independent* in vivo *datasets using clearly defined performance metrics and uncertainty quantification to assess clinical translatability.*
- *Benchmark synthetic datasets and standardized reporting protocols should be developed and adopted to improve reproducibility, transparency, and comparability across AI-driven MRS studies.*

Data synthesis and augmentation have increased in popularity due to limited access to in vivo data. A common strategy is to randomly select a partition of the number of signal averages or spectral transients [195–198]. Related bootstrap-based approaches have also been used, in which new spectra are constructed by randomly recombining existing spectra point-by-point, effectively resampling the empirical distribution to create multiple synthetic realizations from a limited number of acquisitions (e.g., [199]). While these techniques create new spectra, they do not increase variability in linewidth, noise, or metabolite concentrations and ignore the properties of single-shot spectra such as variations from phase cycling schemes or spectra editing schemes. Therefore, these are forms of augmentation that do not address generalizability or public availability [36]. Other augmentation strategies include multiplying and then corrupting in vivo spectra with noise, phase and frequency realignment, and linewidth broadening [200]. These approaches can bridge part of the gap and increase the robustness of AI models, but for broader applications, such as in clinical populations, they still do not diversify the data sufficiently and may risk overfitting to sparsely available in vivo data.

Alternatively, the use of purely synthetic data for training and testing AI methods for MRS applications is widely adopted (see Table S1). Simulated data offer several advantages, including the creation of large quantities of data, increased parameter diversity, and, critically, access to known ground truth values for accurate evaluation and benchmarking. Synthetic data also enhance accessibility due to their cost-effectiveness, allow the generation of disease-specific spectra, and enable class-balanced datasets.

As highlighted in Table S1, many past studies have employed simulation techniques, yet these often lack comprehensive modeling of background signals and nuisance artifacts. Many studies rely on basic simulations such as phase and frequency shifts, linewidth modulations, Gaussian noise, and simplified MM baselines. However, the inclusion of nuisance signals such as lipid contamination, residual water peaks, eddy-current effects, spurious echoes, and non-Gaussian noise is less common. Past works have largely focused on processing and quantification, with hardware-near approaches, realistic single-coil data, and individual transients with accurate correlations still lacking. Additionally, simulating nuisance signals such as water, fat, MM, and other baselines is intricate and therefore often omitted, hindering a realistic reflection of in vivo conditions.

The importance of training data in AI is fundamental, as models rely solely on the data to learn meaningful tasks. Synthetic data therefore offer a way to generate diverse and extensive datasets for training. Recent literature shows a trend toward synthetic data, particularly for accessing ground truth values in quantification tasks where accuracy and precision metrics can be uniquely defined. However, these papers also highlight limitations associated with current simulation methods, especially in accurately capturing in vivo conditions. While polynomial baselines may make spectra look more realistic, they are not well suited for AI models, as neural networks can easily learn and remove such structures without improving robustness. Incorporating smooth random walks or more realistic baseline components can help alleviate this limitation. To ensure that a model performs well in real-world settings, the training distribution should encapsulate or surpass the testing distribution [162], minimizing distribution-driven bias. The working regime of an AI model, that is, the range of inputs over which it performs reliably, must be understood to identify limitations, optimize training, and improve reliability. Benchmark synthetic datasets and standardized reporting protocols will be essential for improving reproducibility, comparability, and the development of robust AI solutions in MRS.

10991492, 2026, 12, Downloaded from https://analyticalsciencejournals.onlinelibrary.wiley.com/doi/10.1002/nbm.70427, Wiley Online Library on [17/11/2026]. See the Terms and Conditions (https://onlinelibrary.wiley.com/terms-and-conditions) on Wiley Online Library for rules of use; OA articles are governed by the applicable Creative Commons License

5.5 | Challenges and Next Steps

5.5.1 | Clinical Applications

A key challenge in generating synthetic MRS data for clinical populations is the limited prior knowledge of biological variability specific to each condition. Unlike healthy populations, where variability patterns are better characterized, clinical datasets often lack comprehensive phenotyping, which complicates the creation of realistic and representative synthetic models.

One primary hurdle is incorporating additional basis set components to reflect a broader range of metabolites. While standard basis sets cover common metabolites, expanding them to include rare or condition-specific metabolites is crucial for simulating pathological conditions and rare clinical scenarios. For instance, extending metabolite ranges as depicted in studies by Lee and Kim [201, 202] can provide more robust validation frameworks. But as shown by [40], caution remains necessary because machine learning and deep learning models may behave unpredictably when exposed to data distributions that differ from their training domain.

Beyond altered metabolite concentrations, structural pathology introduces additional complexity that is often not represented in synthetic datasets. Lesions, necrotic tissue, hemorrhage, and byproducts from surgical or other medical interventions can substantially alter water content, relaxation rates, and macromolecular background contributions. These factors may invalidate assumptions that are typically appropriate for healthy tissue and can introduce severe baseline distortions that exceed those commonly observed in normative data. If such effects are not modeled, synthetic data risk underestimating the spectral variability encountered in real clinical populations.

In certain pathological contexts, major metabolite peaks may be markedly reduced or effectively absent. This has direct implications for both simulation design and reporting conventions. For example, it may not be meaningful to report signal-to-noise ratio for NAA or linewidth for creatine if those metabolites are not present or fall below detectable levels in the simulated spectrum. Clinical synthetic data frameworks therefore require explicit consideration of scenarios in which canonical spectral features are altered, suppressed, or missing altogether.

Clinical variables substantially influence metabolite concentrations and relaxation values. As outlined in the preceding section on physiological metabolite ranges (Metabolite Ranges), factors such as brain region [64] and tissue composition [65] systematically shape spectral properties and baseline concentration distributions. In clinical contexts, however, these sources of variability are not merely descriptive but directly affect diagnostic thresholds, group comparisons, and biomarker interpretation. Age [66, 67], sex, and other demographic factors alter metabolite baselines and relaxation times in ways that may overlap with disease effects. Similarly, physiological state, medication status, psychiatric or neurological conditions, and psychological factors introduce structured variation that can mimic or mask pathology.

Synthetic datasets that do not explicitly model this multidimensional variability risk encoding overly narrow healthy reference assumptions, thereby limiting their translational validity. For clinical applications such as algorithm benchmarking, artificial intelligence training, or biomarker validation, synthetic data generation should therefore incorporate stratified biological and demographic parameters that reflect realworld patient heterogeneity. Doing so will improve external validity, reduce bias in downstream models, and enhance the clinical interpretability of methods developed using synthetic spectra.

5.5.2 | Preclinical

In the preclinical field, several challenges remain regarding the generation and application of synthetic data. One major limitation is the lack of standardized software tools for generating synthetic datasets tailored to species-specific characteristics and experimental paradigms. Unlike in human MRS, where spectral simulations and basis sets are generally well-characterized, preclinical studies must further account for additional physiological and anatomical variations between species, such as differences in metabolite relaxation properties and B_0 field inhomogeneities. Establishing standardized methodologies for synthetic data generation would improve reproducibility and comparability across studies.

Another critical future direction is a deeper integration of machine learning-based approaches for preclinical models, which have received less emphasis relative to human work. Emerging deep learning models have demonstrated the ability to create realistic MR spectra with varying noise characteristics and spectral distortions, providing a powerful resource for training robust quantification pipelines for highly specific preclinical models. These approaches could enhance preclinical MRS by generating more realistic datasets, especially in niche applications, some have already been explored in extracellular pH estimation and overlapping metabolite quantification [184, 203, 204].

Finally, collaboration between research groups and the establishment of open-access synthetic data repositories could accelerate progress in the field. Standardized synthetic datasets with well-characterized noise, artifact profiles, and metabolite dynamics would serve as valuable benchmarks for evaluating emerging acquisition protocols and quantification algorithms that are specific for preclinical applications. By fostering a more unified approach to synthetic data generation and application, preclinical MRS research can continue to refine and expand its methodological toolkit, ultimately improving the reliability and translational value of its findings.

5.5.3 | Software Validation

The challenges of using synthetic data to validate software can be broadly dichotomized into the challenge of data generation (i.e., the creation of data that reflect the variation and complexity of the in vivo environment) and the challenge of accessibility and replication (i.e., the ability of subsequent studies to utilize similar methods of validation for comparison and consistency).

5.5.3.1 | Data Generation. True validation of MRS methods using synthetic data is only valuable when the generated data sufficiently represent the intended application and the full

10991492, 2026, 12, Downloaded from https://analyticalsciencejournals.onlinelibrary.wiley.com/doi/10.1002/nbm.70427, Wiley Online Library on [17/11/2026]. See the Terms and Conditions (https://onlinelibrary.wiley.com/terms-and-conditions) on Wiley Online Library for rules of use; OA articles are governed by the applicable Creative Commons License

range of expected variability. In other words, if the simulation is too simplistic or idealized, or relies on experimental parameters from a single study or site, the utility of the resulting validation may be diminished. Methods validated on such data might perform adequately within the confines of the study, but then break down when confronted with real in vivo data. Bridging the gap between simulation and real data is one of the key challenges of using synthetic MRS data in this manner.

While it is difficult to lay out guidelines that apply across the broad spectrum of potential applications, researchers should carefully consider their choice of basis set simulation, signal model, parameter distributions, and representation of common artifacts. We recommend researchers include as much complexity in their validation data as they may reasonably expect from their application data, and should otherwise clearly report the limitations of their validation by reporting the full scope of parameters used (see Section 6.2). Furthermore, a robust sensitivity analysis is also important to determine the effects of variability or uncertainty of each parameter on the final synthetic data.

5.5.3.2 | Accessibility and Replication. Another challenge is in the replication of previous benchmarking and validation studies. Synthetic data are often not openly shared alongside publications. As data generation is often done as a small part of a larger study, it can often be underreported in the methods. This limits the possibility of replication studies and comparability of future studies working on similar methods. This is most directly addressed with open science practices and reporting standards. An important future goal is the development of a standardized synthetic dataset that can be used to evaluate new tools, i.e., all new fitting algorithms could be tested on the same synthetic dataset that includes known standards (e.g., known concentrations) to evaluate accuracy or precision and enable direct comparison with existing software tools.

5.5.4 | AI in MRS

AI methods require extensive and well-characterized training and validation data. Because in vivo datasets are limited and lack true ground truth, synthetic data often enable AI development in MRS [205]. A central challenge is that model performance depends on the quality of the synthetic training data and on how closely the training distribution matches the in vivo data encountered during deployment.

5.5.4.1 | Domain Shift. Machine learning (ML) and deep learning (DL) models learn patterns in the training data under the assumption that these generalize to new inputs. When simulated data are oversimplified or fail to capture real-world variability [206, 207], the training and testing distributions diverge, resulting in **domain shift** and degraded performance. This occurs, for example, when simulations lack realistic nuisance signals, spectral diversity, or acquisition-dependent variability [36]. Addressing domain shift requires improving the realism of synthetic data to better reflect in vivo scenarios, using ML architectures designed for stronger generalization, incorporating spectral priors for more robust feature learning, and detecting distribution shifts early in development [162].

Robust simulations are particularly important when training data are sparse, because AI performance is tightly coupled to how well the synthetic training distribution matches the target in vivo distribution. If the diversity of real data is not represented, models will fail to generalize [205] Hybrid models that combine data-driven and physics-informed components can enhance robustness, for example through DL-aided least squares optimization [208] that improves generalization to out-of-distribution metabolite levels or MRS-Sim which can analyze fitting parameters to create and sample from a multivariate distribution that complements an existing in vivo dataset [11]. Incorporating differentiable spectral-parameter layers [209] can further improve robustness across scanner vendor numbers, signal averages, and spectral resolutions, as demonstrated in recent work on multivendor harmonization.

5.5.4.2 | Increasing Realistic Representation. Representing realistic single-coil data, transient-level correlations, and nuisance signals such as water, fat, and MM remains challenging. Many simulations still omit these components due to their complexity. Generative models such as GANs and VAEs [40] can help by learning the underlying distribution of real spectra and producing synthetic data that better mimic in vivo behavior. However, these models cannot provide data with known ground truth metabolite concentrations unless conditional generative control is available. Future efforts should prioritize more realistic simulation methods and careful integration of generative models. Relevant approaches in related fields, such as Reyes et al. [210], may provide useful insights.

5.5.4.3 | Quality Metrics. Evaluating the quality of synthetic data is essential to ensure that it reflects real-world conditions and supports reliable AI model development. Beyond visual inspection, quantitative measures such as Kullback–Leibler divergence [211] or other distributional metrics commonly used in generative modeling can be applied. Performance comparisons between models trained on synthetic versus real data also provide practical indicators of how well the synthetic data approximate in vivo conditions.

Relevant work in spectral similarity assessment, such as the method introduced by Mostafapour et al. [212] or Bugler et al. [35], offers additional tools for evaluating how closely synthetic spectra match real acquisitions. Such approaches can help quantify deviations in spectral shape, noise structure, or artifact profiles and may guide future improvements in synthetic data generation.

5.5.4.4 | Reproducibility. Several AI methods directly modify spectral data, for example, by denoising or artifact removal. It is essential to evaluate how such methods affect the reproducibility of biologically relevant outcomes, such as metabolite concentrations or ratios, rather than relying on improved visual appearance alone.

DL–based denoising and artifact-removal approaches require particular scrutiny. Ghosting-removal and denoising methods have been proposed [77, 92], and while they can substantially improve the visual quality of spectra, their impact on quantitative accuracy must be carefully assessed. Similarly, methods designed to remove spurious echoes [36, 213], or motion artifacts must demonstrate

10991492, 2026, 12, Downloaded from https://analyticalsciencejournals.onlinelibrary.wiley.com/doi/10.1002/nbm.70427, Wiley Online Library on [17/11/2026]. See the Terms and Conditions (https://onlinelibrary.wiley.com/terms-and-conditions) on Wiley Online Library for rules of use; OA articles are governed by the applicable Creative Commons License

that they preserve or improve quantitative reproducibility in MRS and MRSI analyses. Ensuring that AI-based corrections enhance, not distort, the underlying biological signal is essential for their application in clinical research [77, 148, 169, 214]. Recent work by [204] used a DL model to decompose spectra into their constituent components, including a nuisance component, which can then be assessed individually for their quality prior to complete reconstruction. This ensures the integrity of the components is maintained, instead of relying on global visual improvement of the spectra. Care must also be taken to consider potentially altered noise characteristics when DL methods modify spectra, possibly invalidating subsequent methods that rely on the assumption of uncorrelated Gaussian noise.

5.5.4.5 | Additional Challenges and Next Steps. Remaining gaps include limited standardization of simulation parameters, insufficient realism of nuisance signals, and lack of shared benchmark datasets. Future developments should prioritize more diverse and realistic synthetic datasets, standardized reporting protocols, and community engagement. The accompanying master table of publications (Table S1) is intended as a living, openly accessible resource, and contributions from researchers will help maintain its completeness and relevance.

6 | Validation and Accessibility

6.1 | Synthetic Data Validation Methods

Considerations:

- *At least one representative synthetic dataset should be visually displayed when introduced in a publication to justify its structure and realism relative to the intended application.*
- *Visual inspection should be complemented by quantitative metrics that characterize similarity to* in vivo *or experimentally measured data. These may include* ***cross-correlation measures***, ***signal-to-noise ratio (SNR)***, ***full width at half maximum (FWHM)***, *or other post hoc quality indices. Such metrics are particularly important in applications sensitive to bias, including the generation of training data for AI models. When synthetic datasets extend beyond experimentally observed conditions, alternative validation strategies may be more appropriate.*
- *The selection of the empirical* ***reference dataset against which synthetic data are compared*** *should be carefully justified, as it may substantially influence perceived validity and generalizability.*
- *Future guidelines defining validation limits for synthetic spectra should remain adaptable to diverse and emerging applications. Both* ***qualitative and quantitative validation*** *approaches are associated with inherent biases, and no single validation strategy should be assumed to be universally sufficient.*

This section reviews current approaches used to assess whether synthetic datasets are appropriate for a given application in MRS. Here, the term "validation" is used to denote post hoc assessment of suitability for use. Features incorporated during dataset generation itself are not considered to constitute validation. For example, designing a synthetic spectrum to match the quality parameters and relative metabolite amplitudes of an in vivo measurement is not, in this context, a validation step. In contrast, quantitative comparison of the resulting synthetic data with the corresponding in vivo acquisition, such as by cross-correlation (Figure 6), represents post hoc validation. Once such agreement has been established, the framework may be used to generate larger datasets that extend beyond the available experimental observations. Furthermore, reproducing in vivo or phantom measurements is not necessarily the goal of every synthetic dataset, and alternative validation approaches may be required when synthetic data are intended to explore conditions outside experimentally observed parameter ranges.

To formulate this description, a nonsystematic review of MRS literature was conducted of representative publications (Table S5) that used synthetic data to investigate a question within in vivo MRS. In addition, each member of the Validation Methods focus group reported their current synthetic data use case(s) and associated validation protocols (data not shown).

The literature survey identified 39 publications documenting diverse applications of synthetic data. These included training ML models for various processing and analysis steps, providing ground-truth validation data for such models, providing ground-truth validation data for non-ML methods for processing and analysis (e.g., frequency registration, denoising, linear combination modeling), and providing context for making decisions about acquisition protocols (i.e., evaluating effects of variables like sequence timings or frequency drift on signals of interest). Similarly, this work considered 14 self-reported synthetic data application and validation protocols. Among them were applications for training, developing, and evaluating ML models; providing ground-truth metrics to evaluate diverse processing and quantification techniques, both ML-based and otherwise; and optimizing acquisition parameters like pulse sequences and timings for given signals of interest.

The most common form of post hoc synthetic data validation among the curated literature samples (37 of 39 publications) and self-reported synthetic data applications (9 of 14 publications) was visual inspection. Quantitative validation approaches, including but not limited to comparing specific signal intensities and direct cross-correlation between synthetic and in vivo acquisitions, were in the minority.

6.2 | Reporting Standards

Considerations:

- *Synthetic MRS datasets should be stored in a standardized format, such as NIfTI-MRS, to facilitate interoperability, reproducibility, and downstream analysis. A corresponding JSON sidecar file should be provided to document all relevant generation parameters, modeling assumptions, and simulation settings.*
- *A checklist summarizing the minimum recommended considerations, as defined by the respective subgroups, should accompany the dataset or publication to ensure transparency and completeness of reporting.*

10991492, 2026, 12, Downloaded from https://analyticalsciencejournals.onlinelibrary.wiley.com/doi/10.1002/nbm.70427, Wiley Online Library on [17/11/2026]. See the Terms and Conditions (https://onlinelibrary.wiley.com/terms-and-conditions) on Wiley Online Library for rules of use; OA articles are governed by the applicable Creative Commons License

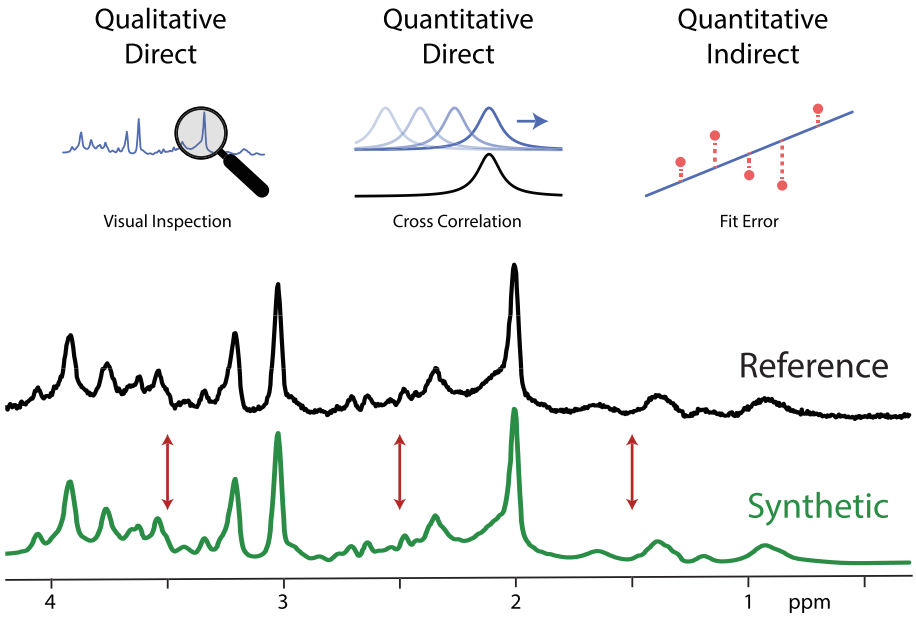


FIGURE 6 | Synthetic data validation framework. A candidate synthetic dataset (green) is validated by comparison with a reference (black), which may consist of in vivo or phantom measurements or predefined expected properties when no direct experimental reference is available. Validation approaches include qualitative assessment (e.g., visual inspection), quantitative similarity metrics (e.g., cross-correlation or feature comparison), and indirect evaluation via downstream model performance on measured data (e.g., fit error).

Experts' consensus recommendations in the MRS community have established minimum reporting standards for in vivo MRS data acquired (MRSinMRS, [4]). It should be no different for synthetic MRS datasets, where we need to establish reporting and data formatting standards. Synthetic datasets tailored for different studies can vary based on multiple factors, including simulated basis sets (see Section 2.1), optimal signal model settings chosen (see Section 2.2) and metabolite and parameter ranges applied (see Section 2.3).

Depending on the purpose of their study, researchers can either make use of downloadable, ready-made synthetic datasets or generate synthetic datasets using available software. Using downloadable datasets can enable straightforward comparison across literature, whereas generating new synthetic datasets using available software is necessary to investigate new topics. On the other hand, another key factor influencing reproducibility and user-friendliness is the data format of the existing datasets or possible export format options provided in the synthetic dataset generator software. To make informed decisions about a given synthetic dataset or generation software, it is essential to carefully document the data provenance with the corresponding parameters and to report them when presenting or making use of synthetic datasets.

A thorough literature search identified a list of previously used synthetic MRS datasets to investigate current reporting practices. Included within this list are downloadable, ready-made datasets, datasets that were not made publicly available, and software designed to create synthetic datasets. Table S1 provides a detailed overview of whether parameters used in generating the synthetic MRS datasets are reported or not in the respective literature. It also indicates the respective data format of the synthetic datasets.

The identified synthetic datasets were produced to be representative of in vivo human and rodent MRS data [36, 40, 200]. These datasets have been used primarily for validating linear combination modeling [23] and developing machine learning and deep learning algorithms [36, 40, 200].

6.3 | Data Format

As an initial step toward establishing reporting standards for synthetic MRS datasets, this section reviews current reporting practices and supported data formats across available software. We further provide recommendations for data standardization and propose minimum reporting standards for future studies presenting synthetic datasets.

Ready-made datasets have been created in various formats, including Python NumPy Archive (.npz) files [36], MATLAB (.dat) [40], LCModel (.RAW and .h2o) [23], jMRUI (.txt) [23], and standard text files (.txt) [23]. These datasets are hosted on Dryad [36], MRSHub [40], and the ISMRM website [23]. Several datasets have also been described within publications for demonstration but were not intended to serve as a publicly available dataset. For all of these datasets, nearly all report basic parameters, such as TE/TR, field strength, and the metabolites that were included, as can be seen from the Table S1 Master Table. Many have also detailed a more extensive list of parameter values.

10991492, 2026, 12, Downloaded from https://analyticalsciencejournals.onlinelibrary.wiley.com/doi/10.1002/nbm.70427, Wiley Online Library on [17/11/2026]. See the Terms and Conditions (https://onlinelibrary.wiley.com/terms-and-conditions) on Wiley Online Library for rules of use; OA articles are governed by the applicable Creative Commons License

6.4 | Challenges and Next Steps

6.4.1 | Synthetic Data Validation Methods

Objective, quantitative validation of synthetic MRS data is seldom reported in the literature, making it difficult to gauge the suitability of the generated data in numerous instances. To address this, it is key to first establish basic criteria to validate synthetic data. This may be achieved by evaluating fundamental signal properties and statistics, such as correlations or similarity coefficients to in vivo or phantom data when reproducing experimentally observed conditions is an intended objective, as well as by quantitative outcomes like the in vivo performance of models trained on synthetic data. Any such criteria might best be presented as broad guidelines, with sufficient flexibility to accommodate diverse and unforeseen applications. For example, suggesting that synthetic data be validated "by at least one quantitative comparison with similar in vivo data" may be a more functional guideline than "frequency-domain correlation of magnitude synthetic spectra with similar in vivo data". The former leaves open the potential for applications centered on time-domain FIDs, real-only spectral analysis, or synthetic data for which one-to-one signal correlations are not the most salient aspect of their utility. Similarly, corresponding guidelines for the systematic reporting of validation techniques, ideally integrated with the broader reporting of synthetic data generation (Section 6.3), would also be beneficial for clarifying the limits of a given synthetic dataset's generalizability.

6.4.2 | Reporting Standards

Publications that are focused on the generation or use of synthetic data for other applications in their studies tend to report some details and parameters of synthetic data, but not all that would be required to successfully reproduce the methods from these publications. Overall, parameters that are considered basic, such as field strength, TE, and sequence, tend to get reported more consistently across publications. However, more 'sophisticated' parameters related to scaling of the metabolite concentration ranges, adding noise, macromolecules, spline baselines, or artifacts seem very limited. Although these parameters tend to get overlooked, they are equally crucial to report since there are varied methods preferred by different studies to sample and add these other signal components.

With various methods for synthetic MRS data generation, it is critical to define a reporting standard and minimum documentation requirements, similar to the minimum reporting standards for in vivo MRS [4]. As a rule of thumb, all information regarding the simulated basis set, applied signal model parameters, metabolite ranges utilized, and other applied sophisticated parameters must be included. This is imperative as the dataset may be used for validating modeling software, informing supervised neural network training, and identifying areas for improvement. Furthermore, this documentation is needed to understand which dataset is best suited for a given task and to provide source documentation within publications where an extensive list of experimental details cannot be listed. As a guideline, we have created minimum reporting standards for synthetic MRS datasets (MRSsynMRS table as shown in Figure 7 and provided in Supplementary Table S4). This table is intended to be used as a template and can be modified to include/exclude experiment-specific details or different metabolites and nuclei as needed.

6.4.3 | Data Format

To create a library of downloadable synthetic datasets for the community, agreeing upon a standard data format as a community is necessary. In addition, this will ensure readability of the data using various modeling software, allowing us to test reproducibility or to compare performance. We recommend exporting and storing the synthetic MRS data in the NIfTI-MRS [215] format. To ensure full reproducibility, synthetic datasets should be accompanied by structured metadata stored in a JSON sidecar file alongside the NIfTI data. Field names and nomenclature should follow established standards where available, adopt existing community-defined metadata conventions, and remain aligned with the MRSsynMRS reporting structure wherever applicable. The metadata should be sufficiently detailed to satisfy current reporting standards, enabling complete reconstruction of the data generation process.

We further encourage alignment with existing community standards for data organization and metadata, such as the Brain Imaging Data Structure (BIDS) [216] and the MRS-BIDS extension [217]. While these standards were developed for experimentally acquired data, they provide a natural foundation for organizing, documenting, and sharing synthetic MRS datasets. Future synthetic MRS reporting standards should therefore seek compatibility with these established frameworks wherever appropriate.

A major goal for the future from this enormous effort is the creation of standardized tools for generating synthetic data that can be tailored to different research needs, including clinical, preclinical, and methodological studies. Such a tool could help ensure that synthetic data are used more effectively and consistently across the MRS community, ultimately improving the reproducibility and reliability of MRS research.

7 | Discussion

7.1 | Standardization and Accessibility

The increasing use of synthetic data in MRS highlights a growing need for shared datasets, common terminology, and transparent simulation practices. Current synthetic data generators differ substantially in how they model basis sets, nuisance signals, relaxation effects, spatial variability, and temporal dynamics. These differences complicate direct comparison of results across studies and limit reproducibility, particularly when synthetic datasets are used for software validation, benchmarking, or algorithm development. As with reporting standards established for experimental spectroscopy, community-driven guidance is needed to harmonize assumptions, parameter definitions, and output formats across simulation frameworks. Standardization efforts analogous to existing reporting initiatives would facilitate comparability while preserving the flexibility required to address diverse experimental questions.

10991492, 2026, 12, Downloaded from https://analyticalsciencejournals.onlinelibrary.wiley.com/doi/10.1002/nbm.70427, Wiley Online Library on [17/11/2026]. See the Terms and Conditions (https://onlinelibrary.wiley.com/terms-and-conditions) on Wiley Online Library for rules of use; OA articles are governed by the applicable Creative Commons License

Synthetic MRS Data Reporting Standard *(Abbreviated)*			
0. Experiment			
a. ID		1	
1. Software			
a. Basis Set Simulation			
i. Name		simulation_name	
ii. Repository (Link, DOI, or RRID)		github.com/simulation	
b. Signal Model			
• • •			
2. Pulse Sequence			
a. Field Strength	[T]	3.0	
b. Localization		PRESS	
• • •			
3. Metabolites			
a. Population			
i. Age Range	[yrs]	18.1	32.6
ii. Healthy Included		Yes	
iii. Clinical Included		Yes	
• • •			
e. Concentration Units		mM	
f. Concentration Ranges			
- N-acetylaspartate (NAA)	[mM]	9.75	18.43
• • •			
4. Components			
• • •			
e. Macromolecule			
i. Simulated, Modeled, Experimental, or Mixed		Simulated	
ii. Available in Isolation		Yes	
iii. Available as Combination		Yes	
• • •			
5. Quality			
a. Signal to Noise Ratio Range		5.72	90.39
b. Linewidths			
i. tCr Linewidth	[Hz]	6.85	17.22
ii. tNAA Linewidth	[Hz]	6.91	18.07
• • •			

FIGURE 7 | MRSsynMRS table. An **abbreviated** version of the Synthetic MRS Data Reporting Standards spreadsheet (Table S4) illustrating: overall structure including five major categories; organization layout and formatting to facilitate readability; demonstration of the ability to add values and ranges for a given line item. The full table is available as an Excel spreadsheet and includes Excel "notes" in value tabs providing guidance on inputting your own values. While the full table is meant to be inclusive to a variety of niches (e.g., MRSI, dMRS, and fMRS) with approximately 100 inputs and modality-specific (B_0 map, *b*-values, concentration percent changes, etc.) sections, users are encouraged to add rows as needed to ensure their methods are comprehensively provided for complete transparency and reproducibility. A downloadable version is available here: SyntheticMRS_Reporting_Standard.xlsx

Accessibility is equally important. Synthetic datasets that are publicly available, well documented, and accompanied by clear descriptions of underlying assumptions provide an essential resource for method development, education, and evaluation. Such resources lower barriers to entry, enable fair comparison of processing pipelines, and support reproducible research across institutions and application domains.

7.2 | Incorporation of Realistic Variability

A central challenge in synthetic spectroscopy is bridging the gap between idealized signal models and the complexity of experimental data. Variability and sparsity of spectral features remain areas of active development. Macromolecular, lipid, and baseline signal generation varies widely across simulators, despite

10991492, 2026, 12, Downloaded from https://analyticalsciencejournals.onlinelibrary.wiley.com/doi/10.1002/nbm.70427, Wiley Online Library on [17/11/2026]. See the Terms and Conditions (https://onlinelibrary.wiley.com/terms-and-conditions) on Wiley Online Library for rules of use; OA articles are governed by the applicable Creative Commons License

the well-documented influence of broad signal modeling on linear combination modeling outcomes. This raises the possibility that certain simulation strategies may preferentially favor specific quantification algorithms, an issue that warrants systematic investigation.

Beyond broad signals, the mathematical descriptions of eddy currents, spurious echoes, residual water, motion-related artifacts, and other nuisance contributions differ considerably between implementations. Even fundamental metrics such as signal-to-noise ratio are not defined consistently across generators, reflecting both historical conventions and differences in modeling complexity. Some simulators rely on weighted combinations of idealized functions, while others aim to reproduce the underlying physics and chemistry of pulse sequences with detailed timing and spatial information. This diversity reflects the inherent complexity of magnetic resonance experiments but also underscores the need for clearer characterization of model assumptions.

The inclusion of an unsuppressed water reference represents an important step toward improving realism and compatibility with in vivo quantification workflows. Generating paired water and metabolite spectra would address ongoing challenges in translating metabolite-specific and water-specific relaxation and diffusion properties into appropriate amplitude scaling. Such an approach would also allow direct inversion of water scaling procedures commonly applied in tissue-specific quantification, improving consistency between synthetic and experimental analyses.

Spatial variability remains another limitation. Region-specific metabolite concentrations and relaxation properties are still incompletely characterized, restricting their incorporation into simulation frameworks. Similarly, the integration of B_0 and B_1 inhomogeneities and coil sensitivity profiles would substantially improve the realism of spatially resolved synthetic data, particularly for spectroscopic imaging applications. Addressing these factors is especially relevant for studies that aim to evaluate spatial quantification accuracy or reconstruction performance.

Finally, there is a growing need for multi-spectrum synthetic datasets that capture temporal structure across acquisitions. Functional spectroscopy, diffusion-weighted spectroscopy, relaxometry, and fingerprinting approaches all require large numbers of temporally related spectra with controlled ground truth. Continued advances in computational resources, algorithmic efficiency, and prior knowledge of acquisition variability will enable more realistic multi-transient simulations that better reflect experimental conditions.

7.3 | Enhancing Interdisciplinary Collaboration

The development of realistic and reliable synthetic spectroscopy data inherently spans multiple disciplines. Progress depends on coordinated contributions from magnetic resonance physics, neuroscience, clinical research, artificial intelligence, and software engineering. High-fidelity synthetic data are particularly critical for artificial intelligence applications, where domain shift between simulated and experimental data can severely limit performance. Carefully designed benchmarks, uncertainty estimates, and standardized reporting are therefore essential components of future simulation frameworks.

Open-source tools, transparent documentation, and shared benchmark datasets provide a foundation for collaboration and collective progress. By aligning simulation strategies with modality-specific requirements and application contexts discussed throughout this work, synthetic data can support a broad range of clinical, preclinical, and methodological studies. Sustained interdisciplinary engagement will be essential to ensure that synthetic spectroscopy continues to evolve in parallel with experimental practice and emerging analytical approaches.

8 | Conclusion

Synthetic MRS data have become an essential resource for advancing acquisition strategies, processing methods, quantification techniques, and artificial intelligence-based applications. By outlining core, advanced, modality-specific, and application-driven components of simulation frameworks, this work highlights both the substantial progress achieved and the challenges that remain. Although current simulators capture many fundamental aspects of the spectroscopy signal, important sources of variability related to physiology, spatial heterogeneity, temporal dynamics, and hardware influences are still only partially represented.

Continued refinement of simulation models, improved characterization of biological and technical factors, and the integration of unsuppressed water references, voxel-specific field information, and dynamic processes will further enhance realism and applicability. Community-driven efforts toward standardization, transparency, and the sharing of benchmark synthetic datasets are critical for reproducibility and comparability across studies. As synthetic data play an increasingly central role in clinical and preclinical research and in artificial intelligence development, unified and well-validated simulation frameworks will become even more significant. Advancing synthetic spectroscopy therefore requires sustained interdisciplinary collaboration and long-term investment in open, well-documented resources to support robust, accessible, and impactful research across the field.

Author Contributions

John T. LaMaster: conceptualization, methodology, investigation, resources, data curation, writing – original draft preparation, writing – review and editing, visualization, supervision, project administration; **Aaron T. Gudmundson:** conceptualization, methodology, investigation, resources, data curation, writing – original draft preparation, writing – review and editing, visualization, supervision, project administration; **Alireza Abaei:** investigation, writing – review and editing; **Seyma Alcicek:** investigation, writing – review and editing; **Arturo Alvarado:** investigation, writing – review and editing; **Ovidiu Andronesi:** writing – review and editing; **Tiffany Bell:** investigation, data curation, writing – original draft preparation, writing – review and editing, visualization, project administration; **Wolfgang Bogner:** investigation, writing – review and editing, writing – original draft preparation, supervision; **Hanna Bugler:** investigation, data curation, writing – review and editing; **Alexander R. Craven:** investigation, data curation, writing – original draft preparation, writing – review and editing, project administration; **Cristina**

10991492, 2026, 12, Downloaded from https://analyticalsciencejournals.onlinelibrary.wiley.com/doi/10.1002/nbm.70427, Wiley Online Library on [17/11/2026]. See the Terms and Conditions (https://onlinelibrary.wiley.com/terms-and-conditions) on Wiley Online Library for rules of use; OA articles are governed by the applicable Creative Commons License

Cudalbu: investigation, writing – review and editing; **Alma Davidson:** investigation, writing – review and editing; **Christopher W. Davies-Jenkins:** investigation, writing – original draft, writing – review and editing, visualization; **Dinesh Deelchand:** investigation, writing – review and editing; **Richard Edden:** investigation, writing – review and editing; **Morteza Esmaeili:** investigation, writing – review and editing; **Candace C. Fleischer:** conceptualization, investigation, writing – original draft preparation, writing – review and editing, supervision; **Abdelrahman Gad:** investigation, writing – review and editing; **Guglielmo Genovese:** investigation, writing – review and editing; **Saumya Gurbani:** resources, writing – review and editing; **Ashley D. Harris:** investigation, writing – review and editing; **Pierre-Gilles Henry:** investigation, writing – review and editing; **Kay Chioma Igwe:** investigation, data curation, writing – original draft preparation, writing – review and editing, visualization, project administration; **Ajin Joy:** investigation, writing – review and editing; **Margarida Julià-Sapé:** investigation, writing – review and editing; **Hyeonjin Kim:** investigation, writing – review and editing; **Roland Kreis:** investigation, writing – review and editing; **Fan Lam:** investigation, data curation, writing – review and editing; **Karl Landheer:** investigation, writing – review and editing; **Bernard Lanz:** investigation, writing – review and editing; **Chu-Yu Lee:** investigation, writing – review and editing; **Clémence Ligneul:** investigation, writing – review and editing; **Julian P. Merkofer:** investigation, data curation, writing – original draft preparation, writing – review and editing, visualization, project administration; **Jack J. Miller:** investigation, data curation, writing – original draft preparation, writing – review and editing, visualization, project administration; **Jessie Mosso:** methodology, investigation, data curation, writing – original draft preparation, writing – review and editing, visualization, supervision, project administration; **Stanislav Motyka:** investigation, writing – review and editing; **Eloïse Mougel:** investigation, writing – review and editing; **Paul G. Mullins:** investigation, data curation, writing – original draft, writing – review and editing; **Saipavitra Murali-Manohar:** investigation, data curation, writing – original draft preparation, writing – review and editing, project administration; **Chloé Najac:** investigation, writing – review and editing; **Shinichiro Nakajima:** investigation, writing – review and editing; **Georg Oeltzschner:** conceptualization, methodology, investigation, resources, writing – original draft preparation, writing – review and editing, visualization, project administration, supervision; **İpek Özdemir:** investigation, writing – original draft preparation, writing – review and editing; **Esin Ozturk-Isik:** investigation, writing – review and editing; **Marco Palombo:** investigation, writing – review and editing; **Ulrich Pilatus:** investigation, writing – review and editing; **Justyna Platek:** investigation, writing – original draft preparation, writing – review and editing; **Esau Poblador Rodriguez:** investigation, writing – review and editing; **Xiaobo Qu:** investigation, writing – review and editing; **Rudy Rizzo:** investigation, writing – original draft preparation, writing – review and editing; **Christopher T. Rodgers:** conceptualization, investigation, writing – review and editing; **Yeison Rodriguez:** investigation, writing – review and editing; **Manoj K. Sammi:** investigation, writing – review and editing; **Manoj Kumar Sarma:** investigation, data curation, writing – review and editing; **Francesca Saviola:** investigation, writing – review and editing; **Anouk Schrantee:** investigation, writing – review and editing; **Amirmohammad Shamaei:** data curation, investigation, writing – review and editing; **Dunja Simicic:** investigation, writing – review and editing; **Brian J. Soher:** conceptualization, investigation, writing – review and editing; **Nico Sollmann:** investigation, writing – original draft preparation, writing – review and editing; **Yulu Song:** investigation, writing – review and editing; **Jeffrey A. Stanley:** investigation, writing – review and editing; **Bernhard Strasser:** investigation, writing – original draft preparation, writing – review and editing; **Antonia Susnjar:** investigation, data curation, writing – original draft, writing – review and editing, project administration; **Kelley M. Swanberg:** conceptualization, methodology, investigation, resources, data curation, writing – original draft preparation, writing – review and editing, project administration; **M. Albert Thomas:** investigation, writing – review and editing; **Ivan Tkáč:** conceptualization, investigation, resources, data curation, writing – review and editing; **Zhangren Tu:** investigation, writing – original draft preparation, writing – review and editing; **Dennis M. J. van de Sande:** investigation, data curation, writing – original draft preparation, writing – review and editing, visualization, project administration; **Emma Van Praagh:** data curation, investigation, writing – review and editing; **Paul J. Weiser:** investigation, writing – review and editing; **Mark Widmaier:** investigation, data curation, writing – original draft preparation, writing – review and editing, visualization, project administration; **Martin Wilson:** investigation, writing – original draft preparation, writing – review and editing, visualization, project administration; **Christopher J. Wu:** investigation, writing – review and editing; **Lijing Xin:** investigation, writing – review and editing; **Helge J. Zöllner:** investigation, writing – original draft preparation, writing – review and editing; **Antonia Kaiser:** conceptualization, methodology, investigation, resources, data curation, writing – original draft preparation, writing – review and editing, visualization, supervision, project administration.

Funding

This work was supported by the National Institutes of Health R01 EB035529, R21 EB033516, R00 AG02230, K99 AG080084, K99 EB034768, R01 EB016089, R01 EB023963, R01 EB032788, P41 EB031771, R01 EB031787; the Schweizerischer Nationalfonds zur Förderung der Wissenschaftlichen Forschung 225289; the UK Research and Innovation Future Leaders Fellowship MR/T020296/2, UKRI1073; the UK Research and Innovation Medical Research Council: MR/W031566/1; the Japan Society for the Promotion of Science 22H03002, 23K24263, 24K02541, 24K02387, 24K10740, 25K21813, 25K10856, 25K10823; the Japan Agency for Medical Research and Development JP24wm0625302, JP24wm0625307; the HORIZON EUROPE European Research Council 101088351; the Austrian Science Fund P34198, PAT4912324, I6037, P36328; and the Christian Doppler Society (BIOMAK).

Affiliations

[1]Munich Institute of Biomedical Engineering, Technical University of Munich, Munich, Germany | [2]School of Computation, Information, and Technology, Technical University of Munich, Munich, Germany | [3]The Malone Center for Engineering in Healthcare, Johns Hopkins University, Baltimore, Maryland, USA | [4]ULMTeC Core Facility Small Animal Imaging Medical Faculty, Ulm University, Ulm, Germany | [5]Institute of Neuroradiology, University Hospital Frankfurt, Goethe University, Frankfurt am Main, Germany | [6]University Cancer Center Frankfurt (UCT), Frankfurt am Main, Germany | [7]Frankfurt Cancer Institute (FCI), Frankfurt am Main, Germany | [8]Central University of Venezuela, Luis Razetti School of Medicine, Department of Pharmacology and Biochemistry, CDD Las Mercedes, Caracas, Venezuela | [9]Athinoula A. Martinos Center for Biomedical Imaging, Department of Radiology, Massachusetts General Hospital, Harvard Medical School, Boston, Massachusetts, USA | [10]Department of Radiology, University of Calgary, Calgary, Canada | [11]Hotchkiss Brain Institute, University of Calgary, Calgary, Canada | [12]Alberta Children's Hospital Research Institute, University of Calgary, Calgary, Canada | [13]High Field MR Center, Department of Biomedical Imaging and Image-Guided Therapy, Medical University of Vienna, Vienna, Austria | [14]Christian Doppler Laboratory for MR Imaging Biomarkers (BIOMAK), Vienna, Austria | [15]Comprehensive Center for AI in Medicine (CAIM), Medical University of Vienna, Vienna, Austria | [16]Department of Biomedical Engineering, University of Calgary, Calgary, Canada | [17]Department of Biological and Medical Psychology, University of Bergen, Bergen, Norway | [18]Department of Clinical Engineering, Haukeland University Hospital, Bergen, Norway | [19]CIBM Center for Biomedical Imaging, Lausanne, Switzerland | [20]École Polytechnique Fédérale de Lausanne (EPFL), Animal Imaging and Technology, Lausanne, Switzerland | [21]Department of Biomedical Engineering, Columbia

10991492, 2026, 12, Downloaded from https://analyticalsciencejournals.onlinelibrary.wiley.com/doi/10.1002/nbm.70427, Wiley Online Library on [17/11/2026]. See the Terms and Conditions (https://onlinelibrary.wiley.com/terms-and-conditions) on Wiley Online Library for rules of use; OA articles are governed by the applicable Creative Commons License

University, New York, New York, USA | [22]Russell H. Morgan Department of Radiology and Radiological Science, Johns Hopkins School of Medicine, Baltimore, Maryland, USA | [23]Center for Magnetic Resonance Research, University of Minnesota Medical School, Minneapolis, Minnesota, USA | [24]Department of Radiology, University of Minnesota Medical School, Minneapolis, Minnesota, USA | [25]Department of Electrical Engineering and Computer Science, Stavanger University, Stavanger, Norway | [26]Department of Radiology and Imaging Sciences, Emory University School of Medicine, Atlanta, Georgia, USA | [27]Department of Biomedical Engineering, Georgia Institute of Technology and Emory University, Atlanta, Georgia, USA | [28]Department of Neuromedicine and Movement Science, Faculty of Medicine and Health Sciences, Norwegian University of Science and Technology, Trondheim, Norway | [29]Department of Radiological Sciences, University of California, Los Angeles, Los Angeles, California, USA | [30]Departament de Bioquímica i Biologia Molecular, Universitat de Barcelona, Barcelona, Spain | [31]Institut de Biotecnologia i Biomedicina (IBB), Universitat Autònoma de Barcelona, Barcelona, Spain | [32]Centro de Investigación Biomédica en Red (CIBER), Barcelona, Spain | [33]Department of Medical Sciences, Seoul National University, Seoul, South Korea | [34]Department of Radiology, Seoul National University Hospital, Seoul, South Korea | [35]MR Methodology, Department for Diagnostic and Interventional Neuroradiology, University of Bern, Bern, Switzerland | [36]Translational Imaging Center (TIC), Swiss Institute for Translational and Entrepreneurial Medicine (Sitem-Insel), Bern, Switzerland | [37]Department of Bioengineering, University of Illinois Urbana-Champaign, Urbana-Champaign, Illinois, USA | [38]Beckman Institute of Advanced Science and Technology, University of Illinois Urbana-Champaign, Urbana-Champaign, Illinois, USA | [39]Regeneron Genetics Center, Tarrytown, New York, USA | [40]Department of Radiology, University of Iowa, Iowa City, Iowa, USA | [41]Wellcome Centre for Integrative Neuroimaging, FMRIB, Nuffield Department of Clinical Neurosciences, University of Oxford, Oxford, UK | [42]Department of Electrical Engineering, Eindhoven University of Technology, Eindhoven, the Netherlands | [43]The MR Research Centre, Aarhus University, Aarhus, Denmark | [44]Clarendon Laboratory, Department of Physics, University of Oxford, Oxford, UK | [45]CIBM Pre-Clinical Imaging EPFL Metabolic Imaging Section, École Polytechnique Fédérale de Lausanne, Lausanne, Switzerland | [46]Bernard and Irene Schwartz Center for Biomedical Imaging, Department of Radiology, New York University Grossman School of Medicine, New York, New York, USA | [47]Université Paris-Saclay, Commissariat à l'Energie Atomique et aux Energies Alternatives (CEA), Centre National de la Recherche Scientifique (CNRS), Molecular Imaging Research Center (MIRCen), Laboratoire des Maladies Neurodégénératives, Fontenay-aux-Roses, France | [48]School of Psychology and Sport Science, Bangor University, Bangor, UK | [49]C.J. Gorter MRI Center, Department of Radiology, Leiden University Medical Center, Leiden, the Netherlands | [50]Department of Neuropsychiatry, School of Medicine, Keio University, Tokyo, Tokyo, Japan | [51]Multimodal Imaging Group, Brain Health Imaging Centre, Centre for Addiction and Mental Health, Toronto, Canada | [52]Institute of Biomedical Engineering, Bogazici University, Istanbul, Türkiye | [53]Cardiff University Brain Research Imaging Centre (CUBRIC), School of Psychology, Cardiff University, Cardiff, UK | [54]School of Computer Science and Informatics, Cardiff University, Cardiff, UK | [55]Institute of Neuroradiology, Goethe-University Frankfurt, Frankfurt am Main, Germany | [56]Division of Medical Physics in Radiology, German Cancer Research Center (DKFZ), Heidelberg, Germany | [57]Faculty of Physics and Astronomy, Heidelberg University, Heidelberg, Germany | [58]International Max Planck Research School for Quantum Dynamics in Physics, Chemistry, and Biology, MPIK, Heidelberg, Germany | [59]Competence Center for Preclinical Imaging and Biomedical Engineering, Faculty of Health, University of Applied Sciences, Wiener Neustadt, Austria | [60]Department of Electronic Science, School of Electronic Science and Engineering, Xiamen University, Xiamen, China | [61]Fujian Provincial Key Laboratory of Plasma and Magnetic Resonance, Xiamen University, Xiamen, China | [62]Biomedical Intelligent Cloud Research and Development Center, National Institute for Data Science in Health and Medicine, Xiamen University, Xiamen, China | [63]Department of Radiology, University of Michigan, Ann Arbor, Michigan, USA | [64]Department of Clinical Neurosciences, University of Cambridge, Cambridge, UK | [65]Advanced Imaging Research Center, Department of Biomedical Engineering, University of Texas Southwestern Medical Center, Dallas, Texas, USA | [66]Advanced Imaging Research Center, Oregon Health & Science University, Portland, Oregon, USA | [67]Advanced Imaging Research Center, University of Texas Southwestern Medical Center, Dallas, Texas, USA | [68]Neuro-X Institute, École Polytechnique Fédérale de Lausanne (EPFL), Lausanne, Switzerland | [69]Department of Radiology and Nuclear Medicine, Amsterdam University Medical Center, University of Amsterdam, Amsterdam, the Netherlands | [70]Institute of Scientific Instruments of the Czech Academy of Sciences, Brno, Czech Republic | [71]Department of Electrical and Software Engineering, Schulich School of Engineering, University of Calgary, Calgary, Canada | [72]Center for Advanced MR Development, Department of Radiology, Duke University Medical Center, Durham, North Carolina, USA | [73]Department of Diagnostic and Interventional Radiology, University Hospital Ulm, Ulm, Germany | [74]Department of Nuclear Medicine, University Hospital Ulm, Ulm, Germany | [75]Department of Diagnostic and Interventional Neuroradiology, School of Medicine and Health, TUM Klinikum Rechts der Isar, Technical University of Munich, Munich, Germany | [76]TUM-Neuroimaging Center, TUM Klinikum Rechts der Isar, Technical University of Munich, Munich, Germany | [77]Psychiatry and Behavioral Neuroscience, Wayne State University School of Medicine, Detroit, Michigan, USA | [78]Athinoula A. Martinos Center for Biomedical Imaging, Institute for Innovation in Imaging, Department of Radiology, Massachusetts General Hospital, Harvard Medical School, Boston, Massachusetts, USA | [79]Institutionen för Experimentell Medicinsk Vetenskap, Medicinska Fakulteten, Lunds Universitet, Lund, Sweden | [80]Wallenberg Center for Molecular Medicine, Medicinska Fakulteten, Lunds Universitet, Lund, Sweden | [81]Department of Psychiatry, University of California, Los Angeles, Los Angeles, California, USA | [82]Medical Image Analysis Group, Department of Biomedical Engineering, Eindhoven University of Technology, Eindhoven, the Netherlands | [83]LIFMET, École Polytechnique Fédérale de Lausanne (EPFL), Lausanne, Switzerland | [84]Centre for Human Brain Health and School of Psychology, University of Birmingham, Birmingham, UK | [85]Taub Institute for Research on Alzheimer's Disease and the Aging Brain, Columbia University Irving Medical Center, New York, New York, USA | [86]CIBM Center for Biomedical Imaging, École Polytechnique Fédérale de Lausanne (EPFL), Lausanne, Switzerland

Acknowledgments

We thank the subgroup leaders for coordinating the thematic contributions and discussions that shaped this review: Kay Igwe, John LaMaster, and Julian Merkofer (AI in MRS); Sandeep Ganji, Margarida Julià-Sapé, and Ulrich Pilatus (Clinical); Jessie Mosso (Diffusion MRS); Alexander Craven, Paul Mullins, and Martin Wilson (Functional MRS); Tiffany Bell and Dennis van de Sande (Metabolite Ranges); Wolfgang Bogner and Bernhard Strasser (MRSI); Saipavitra Murali-Manohar and Georg Oeltzschner (Physics Model); Cristina Cudalbu and Dunja Simicic (Preclinical); Amirmohammad Shamaei and Antonia Susnjar (Reporting/Data Format); Kelley Swanberg (Validation Methods); and Andreas Korzowski and Mark Widmaier (X-Nuclei). We additionally thank Christopher Davies-Jenkins, Candace Fleischer, Roland Kreis, Jamie Near, Georg Oeltzschner, Anouk Schrantee, and Ivan Tkáč for their substantial contributions to reviewing and harmonizing the manuscript. We deeply appreciate every contribution to this initiative, which reflects the collective expertise, time, and dedication of a large community working together. Open access publishing facilitated by Ecole polytechnique federale de Lausanne, as part of the Wiley - Ecole polytechnique federale de Lausanne agreement via the Consortium Of Swiss Academic Libraries.

10991492, 2026, 12, Downloaded from https://analyticalsciencejournals.onlinelibrary.wiley.com/doi/10.1002/nbm.70427, Wiley Online Library on [17/11/2026]. See the Terms and Conditions (https://onlinelibrary.wiley.com/terms-and-conditions) on Wiley Online Library for rules of use; OA articles are governed by the applicable Creative Commons License

Conflicts of Interest

The authors declare no conflicts of interest.

Data Availability Statement

The data that supports the findings of this study are available in the Supporting Information of this article or are already publicly available.

References

1. K. Glunde, D. Artemov, M.-F. Penet, M. A. Jacobs, and Z. M. Bhujwalla, "Magnetic Resonance Spectroscopy in Metabolic and Molecular Imaging, and Diagnosis of Cancer," *Chemical Reviews* 110, no. 5 (2010): 3043–3059, https://doi.org/10.1021/cr9004007.

2. P. K. Mandal, "Magnetic Resonance Spectroscopy (MRS) and Its Application in Alzheimer's Disease," *Concepts in Magnetic Resonance Part A* 30A, no. 1 (2007): 40–64, https://doi.org/10.1002/cmr.a.20072.

3. G. Öz, J. R. Alger, P. B. Barker, et al., "Clinical Proton MR Spectroscopy in Central Nervous System Disorders," *Radiology* 270, no. 3 (2014): 658–679, https://doi.org/10.1148/radiol.13130531.

4. A. Lin, O. Andronesi, W. Bogner, et al., "Minimum Reporting Standards for In Vivo Magnetic Resonance Spectroscopy (MRSinMRS): Experts' Consensus Recommendations," *NMR in Biomedicine* 34, no. 5 (2021): e4484, https://doi.org/10.1002/nbm.4484.

5. J. Near, A. D. Harris, C. Juchem, et al., "Preprocessing, Analysis and Quantification in Single-Voxel Magnetic Resonance Spectroscopy: Experts' Consensus Recommendations," *NMR in Biomedicine* 34 (2021): e4257, https://doi.org/10.1002/nbm.4257.

6. S. W. Provencher, "Estimation of Metabolite Concentrations From Localized *In Vivo* Proton NMR Spectra," *Magnetic Resonance in Medicine* 30, no. 6 (1993): 672–679, https://doi.org/10.1002/mrm.1910300604.

7. C. W. Davies-Jenkins, H. J. Zöllner, S. Alcicek, R. A. E. Edden, and G. Oeltzschner, "A Data-Driven Algorithm to Determine ^{1}H-MRS Basis Set Composition," *Magnetic Resonance in Medicine* 95, no. 1 (2026): 20–37, https://doi.org/10.1002/mrm.70030.

8. P. Emeliyanova, L. M. Parkes, C. Lea-Carnall, and S. R. Williams, "Influence of Basis Set Composition on Metabolite MRS at 3 T: Combining In Silico, Quantification of ^{1}H- In Vivo and In Vitro Evidence," *NMR in Biomedicine* 39, no. 3 (2026): 1–22, https://doi.org/10.1002/nbm.70230.

9. L. Hofmann, J. Slotboom, B. Jung, P. Maloca, C. Boesch, and R. Kreis, "Quantitative 1 H-Magnetic Resonance Spectroscopy of Human Brain: Influence of Composition and Parameterization of the Basis Set in Linear Combination Model-Fitting," *Magnetic Resonance in Medicine* 48, no. 3 (2002): 440–453, https://doi.org/10.1002/mrm.10246.

10. A. Lazariev, A.-R. Allouche, M. Aubert-Frécon, et al., "Optimization of Metabolite Basis Sets Prior to Quantitation in Magnetic Resonance Spectroscopy: An Approach," *Measurement Science and Technology* 22 (2011): 114020, https://doi.org/10.1088/0957-0233/22/11/114020.

11. J. LaMaster, G. Oeltzschner, and Y. Li, "MRS-Sim: Open-Source Framework for Simulating In Vivo-Like Magnetic Resonance Spectra," *NMR in Biomedicine* 38, no. 10 (2025): e70130, https://doi.org/10.1002/nbm.70130.

12. T. Farrar, "Density Matrices in NMR Spectroscopy: Part I," *Concepts in Magnetic Resonance* 2 (1990): 1–12.

13. R. Simpson, G. A. Devenyi, P. Jezzard, T. J. Hennessy, and J. Near, "Advanced Processing and Simulation of MRS Data Using the FID Appliance (FID-A)—An Open Source, MATLAB-Based Toolkit," *Magnetic Resonance in Medicine* 77, no. 1 (2017): 23–33, https://doi.org/10.1002/mrm.26091.

14. S. A. Smith, T. O. Levante, B. H. Meier, and R. R. Ernst, "Computer Simulations in Magnetic Resonance. An Object-Oriented Programming Approach," *Journal of Magnetic Resonance, Series A* 106, no. 1 (1994): 75–105, https://doi.org/10.1006/jmra.1994.1008.

15. K. Landheer, K. M. Swanberg, and C. Juchem, "Magnetic Resonance Spectrum Simulator (MARSS), a Novel Software Package for Fast and Computationally Efficient Basis Set Simulation," *NMR in Biomedicine* 34, no. 5 (2021): e4129, https://doi.org/10.1002/nbm.4129.

16. S. C. N. Hui, M. G. Saleh, H. J. Zöllner, et al., "MRSCloud: A Cloud-Based MRS Tool for Basis Set Simulation," *Magnetic Resonance in Medicine* 88, no. 5 (2022): 1994–2004, https://doi.org/10.1002/mrm.29370.

17. Z. Starčuk and J. Starčuková, "Quantum-Mechanical Simulations for *In Vivo* MR Spectroscopy: Principles and Possibilities Demonstrated With the Program NMRScopeB," *Analytical Biochemistry* 529 (2017): 79–97, https://doi.org/10.1016/j.ab.2016.10.007.

18. B. J. Soher, P. Semanchuk, D. Todd, et al., "Vespa: Integrated Applications for RF Pulse Design, Spectral Simulation and MRS Data Analysis," *Magnetic Resonance in Medicine* 90, no. 3 (2023): 823–838, https://doi.org/10.1002/mrm.29686.

19. C. Cudalbu, K. L. Behar, P. K. Bhattacharyya, et al., "Contribution of Macromolecules to Brain ^{1}H MR Spectra: Experts' Consensus Recommendations," *NMR in Biomedicine* 34, no. 5 (2021): 1–24, https://doi.org/10.1002/nbm.4393.

20. G. Oeltzschner, H. J. Zöllner, S. C. N. Hui, et al., "Osprey: Open-Source Processing, Reconstruction & Estimation of Magnetic Resonance Spectroscopy Data," *Journal of Neuroscience Methods* 343, no. June (2020): 108827, https://doi.org/10.1016/j.jneumeth.2020.108827.

21. Y. Xiao, B. Lanz, S.-I. Lim, I. Tkáč, and L. Xin, "Improved Reproducibility of γ-Aminobutyric Acid Measurement From Short-Echo-Time Proton MR Spectroscopy by Linewidth-Matched Basis Sets in LCModel," *NMR in Biomedicine* 37, no. 2 (2024): e5056, https://doi.org/10.1002/nbm.5056.

22. H. J. Zöllner, C. Davies-Jenkins, D. Simicic, A. Tal, J. Sulam, and G. Oeltzschner, "Simultaneous Multi-Transient Linear-Combination Modeling of MRS Data Improves Uncertainty Estimation," *Magnetic Resonance in Medicine* 92, no. 3 (2024): 916–925, https://doi.org/10.1002/mrm.30110.

23. M. Marjańska, D. K. Deelchand, R. Kreis, et al., "Results and Interpretation of a Fitting Challenge for MR Spectroscopy Set Up by the MRS Study Group of ISMRM," *Magnetic Resonance in Medicine* 87, no. 1 (2022): 11–32, https://doi.org/10.1002/mrm.28942.

24. L. Vanhamme, A. van den Boogaart, and S. Van Huffel, "Improved Method for Accurate and Efficient Quantification of MRS Data With Use of Prior Knowledge," *Journal of Magnetic Resonance* 129, no. 1 (1997): 35–43, https://doi.org/10.1006/jmre.1997.1244.

25. J. Xu, M. Vaeggemose, R. F. Schulte, et al., "PyAMARES, an Open-Source Python Library for Fitting Magnetic Resonance Spectroscopy Data," *Diagnostics* 14, no. 23 (2024): 23, https://doi.org/10.3390/diagnostics14232668.

26. L. A. B. Purvis, W. T. Clarke, L. Biasiolli, L. Valkovič, M. D. Robson, and C. T. Rodgers, "OXSA: An Open-Source Magnetic Resonance Spectroscopy Analysis Toolbox in MATLAB," *PLoS ONE* 12, no. 9 (2017): e0185356, https://doi.org/10.1371/journal.pone.0185356.

27. D. Stefan, F. D. Cesare, A. Andrasescu, et al., "Quantitation of Magnetic Resonance Spectroscopy Signals: The jMRUI Software Package," *Measurement Science and Technology* 20, no. 10 (2009): 104035, https://doi.org/10.1088/0957-0233/20/10/104035.

28. S. W. Provencher, "Automatic Quantitation of Localized *In Vivo* ^{1}H Spectra With LCModel," *NMR in Biomedicine* 14, no. 4 (2001): 260–264, https://doi.org/10.1002/nbm.698.

10991492, 2026, 12, Downloaded from https://analyticalsciencejournals.onlinelibrary.wiley.com/doi/10.1002/nbm.70427, Wiley Online Library on [17/11/2026]. See the Terms and Conditions (https://onlinelibrary.wiley.com/terms-and-conditions) on Wiley Online Library for rules of use; OA articles are governed by the applicable Creative Commons License

29. W. T. Clarke, C. J. Stagg, and S. Jbabdi, "FSL-MRS: An End-to-End Spectroscopy Analysis Package," *Magnetic Resonance in Medicine* 85, no. 6 (2021): 2950–2964, https://doi.org/10.1002/MRM.28630.

30. K. Landheer, M. Treacy, R. Instrella, et al., "synMARSS—An End-to-End Platform for the Parametric Generation of Synthetic In Vivo Magnetic Resonance Spectra," *NMR in Biomedicine* 38, no. 3 (2025): e70013, https://doi.org/10.1002/nbm.70013.

31. D. K. Deelchand, T.-M. Nguyen, X.-H. Zhu, F. Mochel, and P.-G. Henry, "Quantification of *In Vivo* ^{31}P NMR Brain Spectra Using LCModel," *NMR in Biomedicine* 28, no. 6 (2015a): 633–641, https://doi.org/10.1002/nbm.3291.

32. M. Lu, X. H. Zhu, Y. Zhang, and W. Chen, "Intracellular Redox State Revealed by In Vivo ^{31}P MRS Measurement of NAD(+) and NADH Contents in Brains," *Magnetic Resonance in Medicine* 71, no. 6 (2014): 1959–1972, https://doi.org/10.1002/mrm.24859.

33. P. Sedivy, T. Dusilova, M. Hajek, M. Burian, M. Krššák, and M. Dezortova, "In Vitro ^{31}P MR Chemical Shifts of In Vivo-Detectable Metabolites at 3T as a Basis Set for a Pilot Evaluation of Skeletal Muscle and Liver ^{31}P Spectra With LCModel Software," *Molecules (Basel, Switzerland)* 26, no. 24 (2021): 7571, https://doi.org/10.3390/molecules26247571.

34. K. Bingol, F. Zhang, L. Bruschweiler-Li, and R. Brüschweiler, "TOCCATA: A Customized Carbon Total Correlation Spectroscopy NMR Metabolomics Database," *Analytical Chemistry* 84, no. 21 (2012): 9395–9401, https://doi.org/10.1021/ac302197e.

35. H. Bugler, A. Shamaei, R. Souza, and A. D. Harris, "SMART MRS: A Simulated MEGA-PRESS ARTifacts Toolbox for GABA-Edited MRS," *Magnetic Resonance in Medicine* 94, no. 5 (2025): 1826–1839, https://doi.org/10.1002/mrm.30597.

36. A. T. Gudmundson, C. W. Davies-Jenkins, İ. Özdemir, et al., "Application of a ^{1}H Brain MRS Benchmark Dataset to Deep Learning for Out-of-Voxel Artifacts," *Imaging Neuroscience* no.1 (2023): 00025, https://doi.org/10.1162/imag_a_00025.

37. A. T. Gudmundson, A. Koo, A. Virovka, et al., "Meta-Analysis and Open-Source Database for In Vivo Brain Magnetic Resonance Spectroscopy in Health and Disease," *Analytical Biochemistry* 676 (2023a): 115227, https://doi.org/10.1016/j.ab.2023.115227.

38. A. R. Craven, T. K. Bell, L. Ersland, A. D. Harris, K. Hugdahl, and G. Oeltzschner, "Linewidth-Related Bias in Modelled Concentration Estimates From GABA-Edited ^{1}H-MRS," *bioRxiv* (2024), https://doi.org/10.1101/2024.02.27.582249.

39. T. Borbath, S. Murali-Manohar, J. Dorst, A. M. Wright, and A. Henning, "ProFit-1D—A 1D Fitting Software and Open-Source Validation Data Sets," *Magnetic Resonance in Medicine* 86, no. 6 (2021): 2910–2929, https://doi.org/10.1002/mrm.28941.

40. R. Rizzo, M. Dziadosz, S. P. Kyathanahally, A. Shamaei, and R. Kreis, "Quantification of MR Spectra by Deep Learning in an Idealized Setting: Investigation of Forms of Input, Network Architectures, Optimization by Ensembles of Networks, and Training Bias," *Magnetic Resonance in Medicine* 89, no. 5 (2023): 1707–1727, https://doi.org/10.1002/mrm.29561.

41. D. Simicic, H. J. Zöllner, C. W. Davies-Jenkins, K. E. Hupfeld, R. A. E. Edden, and G. Oeltzschner, "Model-Based Frequency-and-Phase Correction of ^{1}H MRS Data With 2D Linear-Combination Modeling," *Magnetic Resonance in Medicine* 92, no. 5 (2024): 2222–2236, https://doi.org/10.1002/mrm.30209.

42. S. Motyka, P. Moser, L. Hingerl, et al., "The Influence of Spatial Resolution on the Spectral Quality and Quantification Accuracy of Whole-Brain MRSI at 1.5T, 3T, 7T, and 9.4T," *Magnetic Resonance in Medicine* 82, no. 2 (2019): 551–565, https://doi.org/10.1002/mrm.27746.

43. J. Slotboom, C. Boesch, and R. Kreis, "Versatile Frequency Domain Fitting Using Time Domain Models and Prior Knowledge," *Magnetic Resonance in Medicine* 39, no. 6 (1998): 899–911, https://doi.org/10.1002/mrm.1910390607.

44. T. Borbath, S. Murali-Manohar, A. M. Wright, and A. Henning, "In Vivo Characterization of Downfield Peaks at 9.4 T: T(2)Relaxation Times, Quantification, pH Estimation, and Assignments," *Magnetic Resonance in Medicine* 85, no. 2 (2021): 587–600, https://doi.org/10.1002/mrm.28442.

45. I. Marshall, J. Higinbotham, S. Bruce, and A. Freise, "Use of Voigt Lineshape for Quantification of *In Vivo* ^{1}H Spectra," *Magnetic Resonance in Medicine* 37, no. 5 (1997): 651–657, https://doi.org/10.1002/mrm.1910370504.

46. S. L. Whittenburg, "Bayesian Analysis of Time-Domain Voigt Functions," *Spectrochimica Acta Part A: Molecular and Biomolecular Spectroscopy* 52, no. 10 (1996): 1169–1174, https://doi.org/10.1016/0584-8539(96)01685-6.

47. J. Mosso, D. Simicic, K. Şimşek, R. Kreis, C. Cudalbu, and I. O. Jelescu, "MP-PCA Denoising for Diffusion MRS Data: Promises and Pitfalls," *NeuroImage* 263 (2022): 119634, https://doi.org/10.1016/j.neuroimage.2022.119634.

48. D. Simicic, V. Rackayova, L. Xin, et al., "In Vivo Macromolecule Signals in Rat Brain ^{1}H-MR Spectra at 9.4T: Parametrization, Spline Baseline Estimation, and T_2 Relaxation Times," *NMR in Biomedicine* 85, no. 5 (2021): 2384–2401, https://doi.org/10.1002/mrm.28910.

49. J. E. Jensen, D. J. Drost, R. S. Menon, and P. C. Williamson, "*In Vivo* Brain ^{31}P-MRS: Measuring the Phospholipid Resonances at 4 Tesla From Small Voxels," *NMR in Biomedicine* 15, no. 5 (2002): 338–347, https://doi.org/10.1002/nbm.776.

50. J. J. Potwarka, D. J. Drost, and P. C. Williamson, "Quantifying ^{1}H Decoupled *In Vivo* ^{31}P Brain Spectra," *NMR in Biomedicine* 12, no. 1 (1999): 8–14.

51. J. A. Stanley, J. W. Pettegrew, and M. S. Keshavan, "Magnetic Resonance Spectroscopy in Schizophrenia: Methodological Issues and Findings–Part I," *Biological Psychiatry* 48, no. 5 (2000): 357–368, https://doi.org/10.1016/S0006-3223(00)00949-5.

52. V. L. Franke, J. Breitling, P. S. Boyd, et al., "A Versatile Look-Up Algorithm for Mapping pH Values and Magnesium Ion Content Using ^{31}P MRSI," *NMR in Biomedicine* 37, no. 6 (2024): e5113, https://doi.org/10.1002/nbm.5113.

53. A. Korzowski, N. Weinfurtner, S. Mueller, et al., "Volumetric Mapping of Intra- and Extracellular pH in the Human Brain Using ^{31}P MRSI at 7T," *Magnetic Resonance in Medicine* 84, no. 4 (2020): 1707–1723, https://doi.org/10.1002/mrm.28255.

54. M. Lu, X.-H. Zhu, and W. Chen, "*In vivo* ^{31}P MRS Assessment of Intracellular NAD Metabolites and NAD^+/NADH Redox State in Human Brain at 4 T," *NMR in Biomedicine* 29, no. 7 (2016): 1010–1017, https://doi.org/10.1002/nbm.3559.

55. F. Du, X.-H. Zhu, H. Qiao, X. Zhang, and W. Chen, "Efficient In Vivo 31P Magnetization Transfer Approach for Noninvasively Determining Multiple Kinetic Parameters and Metabolic Fluxes of ATP Metabolism in the Human Brain," *Magnetic Resonance in Medicine* 57, no. 1 (2007): 103–114, https://doi.org/10.1002/mrm.21107.

56. J. Ren, A. D. Sherry, and C. R. Malloy, "Efficient ^{31}P Band Inversion Transfer Approach for Measuring Creatine Kinase Activity, ATP Synthesis, and Molecular Dynamics in the Human Brain at 7 T," *Magnetic Resonance in Medicine* 78, no. 5 (2017): 1657–1666, https://doi.org/10.1002/mrm.26560.

57. M. Widmaier, A. Kaiser, P. Pandurevic, et al., "Creatine Kinase Imaging (CKI) for In Vivo Whole-Brain Mapping of Creatine Kinase Reaction Kinetics," *Proceedings of the National Academy of Sciences of*

10991492, 2026, 12, Downloaded from https://analyticalsciencejournals.onlinelibrary.wiley.com/doi/10.1002/nbm.70427, Wiley Online Library on [17/11/2026]. See the Terms and Conditions (https://onlinelibrary.wiley.com/terms-and-conditions) on Wiley Online Library for rules of use; OA articles are governed by the applicable Creative Commons License

the United States of America 122, no. 47 (2025): e2505323122, https://doi.org/10.1073/pnas.2505323122.

58. A. Duguid, F. Niess, W. Bogner, et al., "Comparison of Low-Rank Denoising Methods for Dynamic Deuterium MRSI at 7 T," *NMR in Biomedicine* 38, no. 10 (2025): e70125, https://doi.org/10.1002/nbm.70125.

59. A. P. Osburg, A. Shamaei, B. Strasser, et al., "A Deep Autoencoder for Fast Spectral–Temporal Fitting of Dynamic Deuterium Metabolic Imaging Data at 7T," *NeuroImage* 324 (2025): 121632, https://doi.org/10.1016/j.neuroimage.2025.121632.

60. J. A. García, M. D. Noseworthy, and A. Santos-Díaz, "Assessment of Reconstruction Accuracy for Under-Sampled 31P-MRS Data Using Compressed Sensing and a Low Rank Hankel Matrix Completion Approach," *Frontiers in Endocrinology* 16 (2025): 1581328, https://doi.org/10.3389/fendo.2025.1581328.

61. J. Songeon, S. Courvoisier, L. Xin, et al., "In Vivo Magnetic Resonance 31P-Spectral Analysis With Neural Networks: 31P-SPAWNN," *Magnetic Resonance in Medicine* 89, no. 1 (2023): 40–53.

62. K. M. Brindle, S. E. Bohndiek, F. A. Gallagher, and M. I. Kettunen, "Tumor Imaging Using Hyperpolarized Resonance Spectroscopy ^{13}C Magnetic Resonance Spectroscopy," *Magnetic Resonance in Medicine* 66, no. 2 (2011): 505–519, https://doi.org/10.1002/mrm.22999.

63. Y. Li, D. B. Vigneron, and D. Xu, "Current Human Brain Applications and Challenges of Dynamic Hyperpolarized Carbon-13 Labeled Pyruvate MR Metabolic Imaging," *European Journal of Nuclear Medicine and Molecular Imaging* 48 (2021): 4225–4235, https://doi.org/10.1007/s00259-021-05508-8.

64. P. J. W. Pouwels and J. Frahm, "Regional Metabolite Concentrations in Human Brain as Determined by Quantitative Localized Proton MRS," *Magnetic Resonance in Medicine* 39, no. 1 (1998): 53–60, https://doi.org/10.1002/mrm.1910390110.

65. A. D. Harris, N. A. J. Puts, and R. A. E. Edden, "Tissue Correction for GABA-Edited MRS: Considerations of Voxel Composition, Tissue Segmentation, and Tissue Relaxations," *Journal of Magnetic Resonance Imaging* 42, no. 5 (2015): 1431–1440, https://doi.org/10.1002/jmri.24903.

66. E. Angelie, A. Bonmartin, A. Boudraa, P.-M. Gonnaud, J.-J. Mallet, and D. Sappey-Marinier, "Regional Differences and Metabolic Changes in Normal Aging of the Human Brain: Proton MR Spectroscopic Imaging Study," *AJNR. American Journal of Neuroradiology* 22, no. 1 (2001): 119–127.

67. T. Gong, S. C. N. Hui, H. J. Zöllner, et al., "Neurometabolic Timecourse of Healthy Aging," *NeuroImage* 264 (2022): 119740, https://doi.org/10.1016/j.neuroimage.2022.119740.

68. L. Chang, C. S. Jiang, and T. Ernst, "Effects of Age and Sex on Brain Glutamate and Other Metabolites," *Magnetic Resonance Imaging* 27, no. 1 (2009): 142–145, https://doi.org/10.1016/j.mri.2008.06.002.

69. M. Cichocka, J. Kozub, P. Karcz, and A. Urbanik, "Sex Differences in Brain Metabolite Concentrations in Healthy Children—Proton Magnetic Resonance Spectroscopy Study (^{1}HMRS)," *Polish Journal of Radiology* 83 (2018): e24–e31, https://doi.org/10.5114/pjr.2018.74536.

70. R. J. Maddock, M. H. Buonocore, S. P. Lavoie, et al., "Brain Lactate Responses During Visual Stimulation in Fasting and Hyperglycemic Subjects: A 1.5 Tesla ^{1}H-MRS Study," *Psychiatry Research* 148, no. 1 (2006): 47–54, https://doi.org/10.1016/j.pscychresns.2006.02.004.

71. Y. Song, J. J. Prisciandaro, D. Apšvalka, et al., "Magnetic Resonance Spectroscopy and the Menstrual Cycle: A Multi-Centre Assessment of Menstrual Cycle Effects on GABA & GSH," *Journal of Neuroscience Methods* 418 (2025): 110430, https://doi.org/10.1016/j.jneumeth.2025.110430.

72. T. K. Bell, K. J. Godfrey, A. L. Ware, K. O. Yeates, and A. D. Harris, "Harmonization of Multi-Site MRS Data With ComBat," *NeuroImage* 257 (2022): 119330, https://doi.org/10.1016/j.neuroimage.2022.119330.

73. M. Považan, M. Mikkelsen, A. Berrington, et al., "Comparison of Multivendor Single-Voxel MR Spectroscopy Data Acquired in Healthy Brain at 26 Sites," *Radiology* 295, no. 1 (2020): 171–180, https://doi.org/10.1148/radiol.2020191037.

74. T. K. Bell, D. Goerzen, J. Near, and A. D. Harris, "Examination of Methods to Separate Overlapping Metabolites at 7T," *Magnetic Resonance in Medicine* 93, no. 2 (2025a): 470–480, https://doi.org/10.1002/mrm.302930.

75. T. K. Bell, D. Goerzen, J. Near, and A. D. Harris, "Comparison of MRS Acquisition Methods for Separation of Overlapping Signals at 3 T," *Journal of Neuroscience Methods* 423 (2025b): 110523, https://doi.org/10.1016/j.jneumeth.2025.110523.

76. I. Hancu, "Optimized Glutamate Detection at 3T," *Journal of Magnetic Resonance Imaging* 30, no. 5 (2009): 1155–1162, https://doi.org/10.1002/jmri.21936.

77. M. Dziadosz, R. Rizzo, S. P. Kyathanahally, and R. Kreis, "Denoising Single MR Spectra by Deep Learning: Miracle or Mirage?," *Magnetic Resonance in Medicine* 90, no. 5 (2023): 1749–1761, https://doi.org/10.1002/mrm.29762.

78. R. A. de Graaf, "In Vivo NMR Spectroscopy," in *Basic life sciences*, vol. 55 (John Wiley & Sons, Ltd, 2019a), https://doi.org/10.1002/9781119382461.

79. V. Govindaraju, K. Young, and A. A. Maudsley, "Proton NMR Chemical Shifts and Coupling Constants for Brain Metabolites," *NMR in Biomedicine* 13, no. 3 (2000): 129–153.

80. R. A. de Graaf, *In Vivo NMR Spectroscopy: Principles and Techniques* (John Wiley & Sons, 2019b).

81. LCModel User's Manual, (n.d.). Retrieved 6 December 2025, from https://www.lcmodel.ca/lcm-manual.shtml.

82. R. Kaptein, K. Dijkstra, and C. E. Tarr, "A Single-Scan Fourier Transform Method for Measuring Spin-Lattice Relaxation Times," *Journal of Magnetic Resonance* 24, no. 2 (1976): 295–300, https://doi.org/10.1016/0022-2364(76)90039-1.

83. A. J. Taylor, M. Salerno, R. Dharmakumar, and M. Jerosch-Herold, "T1 Mapping: Basic Techniques and Clinical Applications," *JACC: Cardiovascular Imaging* 9, no. 1 (2016): 67–81, https://doi.org/10.1016/j.jcmg.2015.11.005.

84. V. Mlynárik, S. Gruber, and E. Moser, "Proton T_1 and T_2 Relaxation Times of Human Brain Metabolites at 3 Tesla," *NMR in Biomedicine* 14, no. 5 (2001): 325–331, https://doi.org/10.1002/nbm.713.

85. R. Rizzo and R. Kreis, "Multi-Echo Single-Shot Spectroscopy Combined with Simultaneous 2D Model Fitting for Fast and Accurate Measurement of Metabolite-Specific Concentrations and T_2 Relaxation Times Measurement Setup," *NMR in Biomedicine* 36, no. 12 (2023): 1–20, https://doi.org/10.1002/nbm.5016.

86. D. K. Deelchand, P.-F. V. de Moortele, G. Adriany, et al., "In Vivo 1H NMR Spectroscopy of the Human Brain at 9.4 T: Initial Results," *Journal of Magnetic Resonance* 206, no. 1 (2010): 74–80.

87. M. Marjańska, E. J. Auerbach, R. Valabrègue, P. Van De Moortele, G. Adriany, and M. Garwood, "Localized ^{1}H NMR Spectroscopy in Different Regions of Human Brain *In Vivo* at 7T: T_2 Relaxation Times and Concentrations of Cerebral Metabolites," *NMR in Biomedicine* 25, no. 2 (2012): 332–339, https://doi.org/10.1002/nbm.1754.

88. J. A. Stanley, D. J. Drost, P. C. Williamson, and R. T. Thompson, "The Use of a Priori Knowledge to Quantify Short Echo in Vivo1h Mr Spectra," *Magnetic Resonance in Medicine* 34, no. 1 (1995): 17–24.

10991492, 2026, 12, Downloaded from https://analyticalsciencejournals.onlinelibrary.wiley.com/doi/10.1002/nbm.70427, Wiley Online Library on [17/11/2026]. See the Terms and Conditions (https://onlinelibrary.wiley.com/terms-and-conditions) on Wiley Online Library for rules of use; OA articles are governed by the applicable Creative Commons License

89. J. P. Wansapura, S. K. Holland, R. S. Dunn, and W. S. Ball, "NMR Relaxation Times in the Human Brain at 3.0 Tesla†," *Journal of Magnetic Resonance Imaging* 9, no. 4 (1999): 531–538.

90. R. Kreis, "The Trouble With Quality Filtering Based on Relative Cramér-Rao Lower Bounds," *Magnetic Resonance in Medicine* 75, no. 1 (2016): 15–18, https://doi.org/10.1002/mrm.25568.

91. R. Kreis, V. Boer, I.-Y. Choi, et al., "Terminology and Concepts for the Characterization of In Vivo MR Spectroscopy Methods and MR Spectra: Background and Experts' Consensus Recommendations," *NMR in Biomedicine* 34, no. 5 (2021): e4347, https://doi.org/10.1002/nbm.4347.

92. S. P. Kyathanahally and R. Kreis, "Forecasting the Quality of Water-Suppressed ^{1}H MR Spectra Based on a Single-Shot Water Scan," *Magnetic Resonance in Medicine* 78, no. 2 (2017): 441–451, https://doi.org/10.1002/mrm.26389.

93. M. Wilson, "Adaptive Baseline Fitting for MR Spectroscopy Analysis," *Magnetic Resonance in Medicine* 85, no. 1 (2021): 13–29, https://doi.org/10.1002/mrm.28385.

94. P. J. Weiser, G. Langs, S. Motyka, et al., "WALINET: A Water and Lipid Identification Convolutional Neural Network for Nuisance Signal Removal in ^{1}H MR Spectroscopic Imaging," *Magnetic Resonance in Medicine* 93, no. 4 (2025): 1430–1442.

95. S. J. Nelson, "Analysis of Volume MRI and MR Spectroscopic Imaging Data for the Evaluation of Patients With Brain Tumors," *Magnetic Resonance in Medicine* 46, no. 2 (2001): 228–239, https://doi.org/10.1002/mrm.1183.

96. C. T. Rodgers and M. D. Robson, "Coil Combination for Receive Array Spectroscopy: Are Data-Driven Methods Superior to Methods Using Computed Field Maps?," *Magnetic Resonance in Medicine* 75, no. 2 (2016): 473–487, https://doi.org/10.1002/mrm.25618.

97. R. A. de Graaf, Y. Liu, Z. A. Corbin, and H. M. De Feyter, "Lipid Removal in Deuterium Metabolic Imaging (DMI) Using Spatial Prior Knowledge," *Magnetic Resonance* 5, no. 1 (2024): 21–31, https://doi.org/10.5194/mr-5-21-2024.

98. P. Lazen, "Creating an Radio Frequency Pulse Simulation Model for Whole-Brain Magnetic Resonance Spectroscopic Imaging at 7 Tesla [Thesis, Technische Universität Wien]," [Thesis, Technische Universität Wien]. (2020), https://repositum.tuwien.at/handle/20.500.12708/16202.

99. Z. Iqbal, N. E. Wilson, and M. A. Thomas, "Prior-Knowledge Fitting of Accelerated Five-Dimensional Echo Planar J-Resolved Spectroscopic Imaging: Effect of Nonlinear Reconstruction on Quantitation," *Scientific Reports* 7, no. 1 (2017): 6262, https://doi.org/10.1038/s41598-017-04065-1.

100. B. Kadota, "Brendo-k/MRSI_Simulation [MATLAB]," (2025), https://github.com/brendo-k/MRSI_Simulation (Original work published 2021).

101. Z. Iqbal, D. Nguyen, G. Hangel, S. Motyka, W. Bogner, and S. Jiang, "Super-Resolution ^{1}H Magnetic Resonance Spectroscopic Imaging Utilizing Deep Learning," *Frontiers in Oncology* 9 (2019): 1010, https://doi.org/10.3389/fonc.2019.01010.

102. J. Kasten, F. Lazeyras, and D. Van De Ville, "Data-Driven MRSI Spectral Localization via Low-Rank Component Analysis," *IEEE Transactions on Medical Imaging* 32, no. 10 (2013): 1853–1863, https://doi.org/10.1109/TMI.2013.2266259.

103. M. L. Maguire, S. Geethanath, C. A. Lygate, V. D. Kodibagkar, and J. E. Schneider, "Compressed Sensing to Accelerate Magnetic Resonance Spectroscopic Imaging: Evaluation and Application to 23Na-Imaging of Mouse Hearts," *Journal of Cardiovascular Magnetic Resonance* 17, no. 1 (2015): 45, https://doi.org/10.1186/s12968-015-0149-6.

104. X.-P. Zhu, A.-T. Du, G.-H. Jahng, et al., "Magnetic Resonance Spectroscopic Imaging Reconstruction With Deformable Shape-Intensity Models," *Magnetic Resonance in Medicine* 50, no. 3 (2003): 474–482, https://doi.org/10.1002/mrm.10572.

105. AlvBrayan, "AlvBrayan/MC_MRSI_datasetgenerator [MATLAB]," https://github.com/AlvBrayan/MC_MRSI_datasetgenerator (Original work published 2023). (2024).

106. B. Strasser, "Bernhard-strasser/SpiceSimForPEMRSI [MATLAB]," https://github.com/bernhard-strasser/SpiceSimForPEMRSI (Original work published 2020), (2024).

107. MRSI Data Processing Challenge 2024, (n.d.). Retrieved 6 December 2025, from https://bsoher.github.io/FittingChallenge2024/.

108. MRSI-HFMR-Group-Vienna, "MRSI-HFMR-Group-Vienna/Synthetic_MRSI [Python]," (2025), https://github.com/MRSI-HFMR-Group-Vienna/Synthetic_MRSI (Original work published 2024).

109. J. T. LaMaster, J. P. Merkofer, D. M. J. van de Sande, et al., "The 2024 MRSI Data Processing and Quantification Challenge Synthetic Dataset," arXiv, (2026), https://doi.org/10.48550/arXiv.2609.02637.

110. G. Genovese and M. Marjańska, "Effects of Denoising on Diffusion-Weighted MRS Data," ISMRM 2024. (2024), https://archive.ismrm.org/2023/3697.html.

111. D. Apšvalka, A. Gadie, M. Clemence, and P. G. Mullins, "Event-Related Dynamics of Glutamate and BOLD Effects Measured Using Functional Magnetic Resonance Spectroscopy (fMRS) at 3T in a Repetition Suppression Paradigm," *NeuroImage* 118 (2015): 292–300, https://doi.org/10.1016/j.neuroimage.2015.06.015.

112. P. Bednařík, I. Tkáč, F. Giove, et al., "Neurochemical and BOLD Responses During Neuronal Activation Measured in the Human Visual Cortex at 7 Tesla," *Journal of Cerebral Blood Flow & Metabolism* 35, no. 4 (2015): 601–610, https://doi.org/10.1038/jcbfm.2014.233.

113. N. D. Fichtner, I.-A. Giapitzakis, N. Avdievich, et al., "In Vivo Characterization of the Downfield Part of ^{1}H MR Spectra of Human Brain at 9.4 T: Magnetization Exchange With Water and Relation to Conventionally Determined Metabolite Content," *Magnetic Resonance in Medicine* 79, no. 6 (2018): 2863–2873, https://doi.org/10.1002/mrm.26968.

114. B. Lanz, J. M. N. Duarte, N. Kunz, V. Mlynárik, R. Gruetter, and C. Cudalbu, "Quantification of In Vivo Brain ^{13}C MR Spectra Following ^{13}C Glucose Infusion Using AMARES," *Magnetic Resonance in Medicine* 69, no. 6 (2013): 1512–1522, https://doi.org/10.1002/mrm.24406.

115. S. Mangia, I. Tkáč, N. K. Logothetis, R. Gruetter, P.-F. Van de Moortele, and K. Uğurbil, "Dynamics of Lactate Concentration and Blood Oxygen Level-Dependent Effect in the Human Visual Cortex During Repeated Identical Stimuli," *Journal of Neuroscience Research* 85, no. 15 (2007): 3340–3346, https://doi.org/10.1002/jnr.21371.

116. S. Mangia, I. Tkáč, R. Gruetter, P.-F. Van De Moortele, B. Maraviglia, and K. Uğurbil, "Sustained Neuronal Activation Raises Oxidative Metabolism to a New Steady-State Level: Evidence From ^{1}H NMR Spectroscopy in the Human Visual Cortex," *Journal of Cerebral Blood Flow & Metabolism* 27, no. 5 (2007a): 1055–1063, https://doi.org/10.1038/sj.jcbfm.9600401.

117. P. G. Mullins, "Towards a Theory of Functional Magnetic Resonance Spectroscopy (fMRS): A Meta-Analysis and Discussion of Using MRS to Measure Changes in Neurotransmitters in Real Time," *Scandinavian Journal of Psychology* 59, no. 1 (2018): 91–103, https://doi.org/10.1111/sjop.12411.

118. B. Alves, D. Simicic, J. Mosso, et al., "Noise-Reduction Techniques for ^{1}H-FID-MRSI at 14.1 T: Monte Carlo Validation and in Vivo Application," *NMR in Biomedicine* 37, no. 11 (2024): e5211, https://doi.org/10.1002/nbm.5211.

119. J. Felblinger, R. Kreis, and C. Boesch, "Effects of Physiologic Motion of the Human Brain Upon Quantitative ^{1}H-MRS: Analysis and Correction by Retro-Gating," *NMR in Biomedicine* 11, no. 3 (1998): 107–114, https://doi.org/10.1002/(SICI)1099-1492(199805)11:3%253C107::AID-NBM525%253E3.0.CO;2-I.

10991492, 2026, 12, Downloaded from https://analyticalsciencejournals.onlinelibrary.wiley.com/doi/10.1002/nbm.70427, Wiley Online Library on [17/11/2026]. See the Terms and Conditions (https://onlinelibrary.wiley.com/terms-and-conditions) on Wiley Online Library for rules of use; OA articles are governed by the applicable Creative Commons License

120. W. T. Clarke, C. Ligneul, M. Cottaar, I. B. Ip, and S. Jbabdi, "Universal Dynamic Fitting of Magnetic Resonance Spectroscopy," *Magnetic Resonance in Medicine* 91 (2024): 2229–2246, https://doi.org/10.1002/mrm.30001.

121. L. A. Jelen, S. King, P. G. Mullins, and J. M. Stone, "Beyond Static Measures: A Review of Functional Magnetic Resonance Spectroscopy and Its Potential to Investigate Dynamic Glutamatergic Abnormalities in Schizophrenia," *Journal of Psychopharmacology* 32, no. 5 (2018): 497–508, https://doi.org/10.1177/0269881117747579.

122. Y. Koush, D. L. Rothman, K. L. Behar, R. A. de Graaf, and F. Hyder, "Human Brain Functional MRS Reveals Interplay of Metabolites Implicated in Neurotransmission and Neuroenergetics," *Journal of Cerebral Blood Flow & Metabolism* 42, no. 6 (2022): 911–934, https://doi.org/10.1177/0271678X221076570.

123. J. A. Stanley and N. Raz, "Functional Magnetic Resonance Spectroscopy: The 'New' MRS for Cognitive Neuroscience and Psychiatry Research," *Frontiers in Psychiatry* 9 (2018): 76, https://doi.org/10.3389/fpsyt.2018.00076.

124. P. G. Mullins, L. M. Rowland, R. E. Jung, and W. L. Sibbitt, "A Novel Technique to Study the Brain's Response to Pain: Proton Magnetic Resonance Spectroscopy," *NeuroImage* 26, no. 2 (2005): 642–646, https://doi.org/10.1016/j.neuroimage.2005.02.001.

125. J. Prichard, D. Rothman, E. Novotny, et al., "Lactate Rise Detected by ^{1}H NMR in Human Visual Cortex During Physiologic Stimulation," *Proceedings of the National Academy of Sciences* 88, no. 13 (1991): 5829–5831, https://doi.org/10.1073/pnas.88.13.5829.

126. S. Hu, A. P. Chen, M. L. Zierhut, et al., "In Vivo Carbon-13 Dynamic MRS and MRSI of Normal and Fasted Rat Liver," *Molecular Imaging and Biology* 11 (2009): 399–407, https://doi.org/10.1007/s11307-009-0218-z.

127. J. Ma, M. C. Pinho, C. E. Harrison, et al., "Dynamic ^{13}C MR Spectroscopy as an Alternative to Imaging for Assessing Cerebral Metabolism Using Hyperpolarized Pyruvate in Humans," *Magnetic Resonance in Medicine* 87, no. 3 (2022): 1136–1149, https://doi.org/10.1002/mrm.29049.

128. A. R. Craven, L. Ersland, K. Hugdahl, and R. Grüner, "Modeling Intershot Variability for Robust Temporal Subsampling of Dynamic, GABA-Edited MR Spectroscopy Data," *NMR in Biomedicine* 38, no. 9 (2025): e70097, https://doi.org/10.1002/nbm.70097.

129. F. T. van Vugt, J. Near, T. Hennessy, J. Doyon, and D. J. Ostry, "Early Stages of Sensorimotor Map Acquisition: Neurochemical Signature in Primary Motor Cortex and Its Relation to Functional Connectivity," *Journal of Neurophysiology* 124, no. 6 (2020): 1615–1624, https://doi.org/10.1152/jn.00285.2020.

130. D. Pasanta, J. L. He, T. Ford, G. Oeltzschner, D. J. Lythgoe, and N. A. Puts, "Functional MRS Studies of GABA and Glutamate/Glx—A Systematic Review and Meta-Analysis," *Neuroscience & Biobehavioral Reviews* 144 (2023): 104940, https://doi.org/10.1016/j.neubiorev.2022.104940.

131. J. Near, J. Andersson, E. Maron, et al., "Unedited In Vivo Detection and Quantification of γ-Aminobutyric Acid in the Occipital Cortex Using Short-TE MRS at 3 T," *NMR in Biomedicine* 26, no. 11 (2013): 1353–1362, https://doi.org/10.1002/nbm.2960.

132. B. Schaller, L. Xin, K. O'Brien, A. W. Magill, and R. Gruetter, "Are Glutamate and Lactate Increases Ubiquitous to Physiological Activation? A ^{1}H Functional MR Spectroscopy Study During Motor Activation in Human Brain at 7Tesla," *NeuroImage* 93 (2014): 138–145, https://doi.org/10.1016/j.neuroimage.2014.02.016.

133. A. Schrantee, A. Berrington, P. J. W. Pouwels, B. F. Coolen, O. Gurney-Champion, and C. Najac, "The Effect of the Glutamate Response Function on Detection Sensitivity for Functional MRS: A Simulation Study," ISMRM. (2020), https://archive.ismrm.org/2022/1077.html.

134. D. G. Q. Chong, R. Kreis, C. S. Bolliger, C. Boesch, and J. Slotboom, "Two-Dimensional Linear-Combination Model Fitting of Magnetic Resonance Spectra to Define the Macromolecule Baseline Using FiTAID, a Fitting Tool for Arrays of Interrelated Datasets," *Magnetic Resonance Materials in Physics, Biology and Medicine* 24, no. 3 (2011): 147–164, https://doi.org/10.1007/s10334-011-0246-y.

135. R. Kreis, J. Slotboom, L. Hofmann, and C. Boesch, "Integrated Data Acquisition and Processing to Determine Metabolite Contents, Relaxation Times, and Macromolecule Baseline in Single Examinations of Individual Subjects," *Magnetic Resonance in Medicine* 54, no. 4 (2005): 761–768, https://doi.org/10.1002/mrm.20673.

136. A. Tal, "The Future Is 2D: Spectral-Temporal Fitting of Dynamic MRS Data Provides Exponential Gains in Precision Over Conventional Approaches," *Magnetic Resonance in Medicine* 89, no. 2 (2023): 499–507, https://doi.org/10.1002/mrm.29456.

137. M. Morelli, K. Dudzikowska, and D. K. Deelchand, "Functional Magnetic Resonance Spectroscopy of Prolonged Motor Activation Using Conventional and Spectral GLM Analyses," bioRxiv: The Preprint Server for Biology, 2024.05.15.594270. (2024), https://doi.org/10.1101/2024.05.15.594270.

138. M. Wilson, "Chemical Shift and Relaxation Regularization Improve the Accuracy of ^{1}H MR Spectroscopy Analysis," *Magnetic Resonance in Medicine* 93, no. 6 (2025): 2287–2296, https://doi.org/10.1002/mrm.30462.

139. C. Ligneul, C. Najac, A. Döring, et al., "Diffusion-Weighted MR Spectroscopy: Consensus, Recommendations, and Resources From Acquisition to Modeling," *Magnetic Resonance in Medicine* 91, no. 3 (2024): 860–885, https://doi.org/10.1002/mrm.29877.

140. M. Palombo, N. Shemesh, I. Ronen, and J. Valette, "Insights Into Brain Microstructure From *In Vivo* DW-MRS," *NeuroImage* 182 (2018): 97–116, https://doi.org/10.1016/j.neuroimage.2017.11.028.

141. I. Ronen and J. Valette, "Diffusion-Weighted Magnetic Resonance Spectroscopy," in *eMagRes* (John Wiley & Sons, Ltd, 2015), 733–750, https://doi.org/10.1002/9780470034590.emrstm1471.

142. V. Adalid, A. Döring, S. P. Kyathanahally, C. S. Bolliger, C. Boesch, and R. Kreis, "Fitting Interrelated Datasets: Metabolite Diffusion and General Lineshapes," *Magma (New York, N.Y.)* 30, no. 5 (2017): 429–448, https://doi.org/10.1007/s10334-017-0618-z.

143. C. W. Jenkins, "The Influence of Spectral Registration on Diffusion-Weighted Magnetic Resonance Spectroscopy ADC Estimates," ISMRM 2021. (2021), https://archive.ismrm.org/2021/2022.html.

144. C. Najac, A. Döring, W. T. Clarke, et al., "Differences in Diffusion-Weighted MRS Processing and Fitting Pipelines, and Their Effect on Tissue Modeling: Results From a Workshop Challenge," ISMRM 2022. (2022), https://archive.ismrm.org/2022/2616.html.

145. M. Palombo, D. C. Alexander, and H. Zhang, "A Generative Model of Realistic Brain Cells With Application to Numerical Simulation of the Diffusion-Weighted MR Signal," *NeuroImage* 188 (2019): 391–402, https://doi.org/10.1016/j.neuroimage.2018.12.025.

146. M. Palombo, C. Ligneul, C. Najac, et al., "New Paradigm to Assess Brain Cell Morphology by Diffusion-Weighted MR Spectroscopy In Vivo," *Proceedings of the National Academy of Sciences of the United States of America* 113, no. 24 (2016): 6671–6676, https://doi.org/10.1073/pnas.1504327113.

147. E. B. Bjørkeli, J. T. Geitung, and M. Esmaeili, "Artificial Intelligence-Powered Four-Fold Upscaling of Human Brain Synthetic Metabolite Maps," *Journal of International Medical Research* 53, no. 4 (2025): 03000605251330578, https://doi.org/10.1177/03000605251330578.

148. W. T. Clarke and M. Chiew, "Uncertainty in Denoising of MRSI Using Low-Rank Methods," *Magnetic Resonance in Medicine* 87, no. 2 (2022): 574–588, https://doi.org/10.1002/mrm.29018.

10991492, 2026, 12, Downloaded from https://analyticalsciencejournals.onlinelibrary.wiley.com/doi/10.1002/nbm.70427, Wiley Online Library on [17/11/2026]. See the Terms and Conditions (https://onlinelibrary.wiley.com/terms-and-conditions) on Wiley Online Library for rules of use; OA articles are governed by the applicable Creative Commons License

149. F. Lam, Y. Li, and X. Peng, "Constrained Magnetic Resonance Spectroscopic Imaging by Learning Nonlinear Low-Dimensional Models," *IEEE Transactions on Medical Imaging* 39, no. 3 (2020): 545–555, https://doi.org/10.1109/TMI.2019.2930586.

150. S. Maruyama and H. Takeshima, "Generating Synthetic MR Spectroscopic Imaging Data With Generative Adversarial Networks to Train Machine Learning Models," *Magnetic Resonance in Medical Sciences: MRMS: An Official Journal of Japan Society of Magnetic Resonance in Medicine* 24, no. 4 (2025): 2023-0125, https://doi.org/10.2463/mrms.mp.2023-0125.

151. C. I. Haupt, N. Schuff, M. W. Weiner, and A. A. Maudsley, "Removal of Lipid Artifacts in ^{1}H Spectroscopic Imaging by Data Extrapolation," *Magnetic Resonance in Medicine* 35, no. 5 (1996): 678–687, https://doi.org/10.1002/mrm.1910350509.

152. C. T. Rodgers and M. D. Robson, "Receive Array Magnetic Resonance Spectroscopy: Whitened Singular Value Decomposition (WSVD) Gives Optimal Bayesian Solution," *Magnetic Resonance in Medicine* 63, no. 4 (2010): 881–891, https://doi.org/10.1002/mrm.22230.

153. S. Motyka, E. Niess, B. Strasser, et al., "Towards Prediction of Motion Affected Spectra for MRSI at 7T,". ISMRM 2024. (2024), https://archive.ismrm.org/2024/4702.html.

154. O. C. Andronesi, P. K. Bhattacharyya, W. Bogner, et al., "Motion Correction Methods for MRS: Experts' Consensus Recommendations," *NMR in Biomedicine* 34, no. 5 (2021): e4364, https://doi.org/10.1002/nbm.4364.

155. X. H. Zhu and W. Chen, "Observed BOLD Effects on Cerebral Metabolite Resonances in Human Visual Cortex During Visual Stimulation: A Functional ^{1}H MRS Study at 4 T," *Magnetic Resonance in Medicine* 46, no. 5 (2001): 841–847, https://doi.org/10.1002/mrm.1267.

156. K. Uludağ, B. Müller-Bierl, and K. Uğurbil, "An Integrative Model for Neuronal Activity-Induced Signal Changes for Gradient and Spin Echo Functional Imaging," *NeuroImage* 48, no. 1 (2009): 150–165, https://doi.org/10.1016/j.neuroimage.2009.05.051.

157. G. Genovese, M. Marjańska, E. J. Auerbach, et al., "In Vivo Diffusion-Weighted MRS Using Semi-LASER in the Human Brain at 3 T: Methodological Aspects and Clinical Feasibility," *NMR in Biomedicine* 34, no. 5 (2021): e4206, https://doi.org/10.1002/nbm.4206.

158. A. Loktyushin, K. Herz, N. Dang, et al., "MRzero - Automated Discovery of MRI Sequences Using Supervised Learning," *Magnetic Resonance in Medicine* 86, no. 2 (2021): 709–724, https://doi.org/10.1002/mrm.28727.

159. L. Kerkelä, F. Nery, M. G. Hall, and C. A. Clark, "Disimpy: A Massively Parallel Monte Carlo Simulator for Generating Diffusion-Weighted MRI Data in Python," *Journal of Open Source Software* 5, no. 52 (2020): 2527, https://doi.org/10.21105/joss.02527.

160. Cottaar Michiel MCMRSimulator.jl GitLab, GitLab. (2025), https://git.fmrib.ox.ac.uk/ndcn0236/mcmrsimulator.jl.

161. N. Olliverre, G. Yang, G. Slabaugh, C. C. Reyes-Aldasoro, and E. Alonso, "Generating Magnetic Resonance Spectroscopy Imaging Data of Brain Tumours From Linear, Non-Linear and Deep Learning Models," in *Simulation and Synthesis in Medical Imaging*, vol. 11037, eds. A. Gooya, O. Goksel, I. Oguz, and N. Burgos (Springer International Publishing, 2018), 130–138, https://doi.org/10.1007/978-3-030-00536-8_14.

162. A. R. Tate, J. R. Griffiths, I. Martínez-Pérez, et al., "Towards a Method for Automated Classification of ^{1}H MRS Spectra From Brain Tumours," *NMR in Biomedicine* 11, no. 4-5 (1998): 177–191, https://doi.org/10.1002/(sici)1099-1492(199806/08)11:4/5<177::aid-nbm534>3.0.co;2-u.

163. A. R. Tate, J. Underwood, D. M. Acosta, et al., "Development of a Decision Support System for Diagnosis and Grading of Brain Tumours Using *In Vivo* Magnetic Resonance Single Voxel Spectra," *NMR in Biomedicine* 19, no. 4 (2006): 411–434, https://doi.org/10.1002/nbm.1016.

164. N. Dikaios, "Deep Learning Magnetic Resonance Spectroscopy Fingerprints of Brain Tumours Using Quantum Mechanically Synthesised Data," *NMR in Biomedicine* 34, no. 4 (2021): e4479, https://doi.org/10.1002/nbm.4479.

165. S. Ortega-Martorell, I. Olier, M. Julià-Sapé, C. Arús, and P. Lisboa, "Automatic Relevance Source Determination in Human Brain Tumors Using Bayesian NMF," 2014 IEEE Symposium on Computational Intelligence and Data Mining (CIDM), (2014). 99–104, https://doi.org/10.1109/CIDM.2014.7008654.

166. S. Ortega-Martorell, I. Olier, O. Hernandez, P. D. Restrepo-Galvis, R. A. A. Bellfield, and A. P. Candiota, "Tracking Therapy Response in Glioblastoma Using 1D Convolutional Neural Networks," *Cancers* 15, no. 15 (2023): 15, https://doi.org/10.3390/cancers15154002.

167. M. A. York and M. Terpstra, "A Study of Effectiveness of Simulated Data in Classifying Alzheimer's Disease Status Using MRS Parameters [University of Missouri-Columbia]," [University of Missouri-Columbia]. (2023), https://mospace.umsystem.edu/items/45b4ccb6-cc16-4be9-a6f8-031d7ecf391e.

168. C. Cudalbu, S. Cavassila, H. Rabeson, D. van Ormondt, and D. Graveron-Demilly, "Influence of Measured and Simulated Basis Sets on Metabolite Concentration Estimates," *NMR in Biomedicine* 21, no. 6 (2008): 627–636, https://doi.org/10.1002/nbm.1234.

169. H. H. Lee and H. Kim, "Deep Learning-Based Target Metabolite Isolation and Big Data-Driven Measurement Uncertainty Estimation in Proton Magnetic Resonance Spectroscopy of the Brain," *Magnetic Resonance in Medicine* 84, no. 4 (2020): 1689–1706, https://doi.org/10.1002/mrm.28234.

170. R. E. Hurd, M. Gu, K. Okamura, et al., "Detection of Elevated Succinate in Brain During Circulatory Arrest in a Piglet Model: A 3T ^{1}H MR Spectroscopy Study," *Magnetic Resonance in Medicine* 93, no. 5 (2025): 1874–1885, https://doi.org/10.1002/mrm.30414.

171. D. K. Deelchand, P. G. Henry, and M. Marjańska, "Effect of Carr-Purcell Refocusing Pulse Trains on Transverse Relaxation Times of Metabolites in Rat Brain at 9.4 Tesla," *Magnetic Resonance in Medicine* 73, no. 1 (2015): 13–20, https://doi.org/10.1002/mrm.25088.

172. D. K. Deelchand, J. D. Walls, and M. Marjańska, "In Vivo ^{1}H MR Spectroscopy With *J*-Refocusing," *Magnetic Resonance in Medicine* 86, no. 6 (2021): 2957–2965, https://doi.org/10.1002/mrm.28936.

173. A. Abaei, D. K. Deelchand, J. Kassubek, F. Roselli, and V. Rasche, "Sub-Microliter ^{1}H Magnetic Resonance Spectroscopy for In Vivo High-Spatial Resolution Metabolite Quantification in the Mouse Brain," *Journal of Neurochemistry* 169 (2025): e16303, https://doi.org/10.1111/jnc.16303.

174. I. Tkáč, R. Rao, M. K. Georgieff, and R. Gruetter, "Developmental and Regional Changes in the Neurochemical Profile of the Rat Brain Determined by In Vivo ^{1}H NMR Spectroscopy," *Magnetic Resonance in Medicine* 50, no. 1 (2003): 24–32, https://doi.org/10.1002/mrm.10497.

175. I. Tkáč, T. Xie, N. Shah, et al., "Regional Sex Differences in Neurochemical Profiles of Healthy Mice Measured by Magnetic Resonance Spectroscopy at 9.4 Tesla," *Frontiers in Neuroscience* 17 (2023): 1278828, https://doi.org/10.3389/fnins.2023.1278828.

176. R. Kreis, T. Ernst, and B. D. Ross, "Absolute Quantitation of Water and Metabolites in the Human Brain. II. Metabolite Concentrations," *Journal of Magnetic Resonance* 102 (1993): 9–19, https://doi.org/10.1006/jmrb.1993.1056.

177. C. Cudalbu, A. Bucur, D. Graveron-Demilly, O. Beuf, and S. Cavassila, "Comparison of Two Strategies of Background-Accommodation: Influence on the Metabolite Concentration Estimation From In Vivo Magnetic Resonance Spectroscopy Data," 2007 29th Annual International Conference of the IEEE Engineering in Medicine

10991492, 2026, 12, Downloaded from https://analyticalsciencejournals.onlinelibrary.wiley.com/doi/10.1002/nbm.70427, Wiley Online Library on [17/11/2026]. See the Terms and Conditions (https://onlinelibrary.wiley.com/terms-and-conditions) on Wiley Online Library for rules of use; OA articles are governed by the applicable Creative Commons License

and Biology Society, 2077–2080. (2007), https://doi.org/10.1109/IEMBS.2007.4352730.

178. S. Hu, M. Lustig, A. Balakrishnan, et al., "3D Compressed Sensing for Highly Accelerated Hyperpolarized ^{13}C MRSI With In Vivo Applications to Transgenic Mouse Models of Cancer," *Magnetic Resonance in Medicine* 63, no. 2 (2010): 312–321, https://doi.org/10.1002/mrm.22233.

179. J. J. Miller, A. Z. Lau, and D. J. Tyler, "Susceptibility-Induced Distortion Correction in Hyperpolarized Echo Planar Imaging," *Magnetic Resonance in Medicine* 79, no. 4 (2018): 2135–2141, https://doi.org/10.1002/mrm.26839.

180. M. A. Ohliger, P. E. Z. Larson, R. A. Bok, et al., "Combined Parallel and Partial Fourier MR Reconstruction for Accelerated 8-Channel Hyperpolarized Carbon-13 In Vivo Magnetic Resonance Spectroscopic Imaging (MRSI)," *Journal of Magnetic Resonance Imaging* 38, no. 3 (2013): 701-13, https://doi.org/10.1002/jmri.23989.

181. P.-G. Henry, M. Marjanska, J. D. Walls, J. Valette, R. Gruetter, and K. Uğurbil, "Proton-Observed Carbon-Edited NMR Spectroscopy in Strongly Coupled Second-Order Spin Systems," *Magnetic Resonance in Medicine* 55, no. 2 (2006): 250–257, https://doi.org/10.1002/mrm.20764.

182. L. Xin, V. Mlynárik, B. Lanz, H. Frenkel, and R. Gruetter, "1H-[^{13}C] NMR Spectroscopy of the Rat Brain During Infusion of [2-^{13}C] Acetate at 14.1 T," *Magnetic Resonance in Medicine* 64, no. 2 (2010): 334–340, https://doi.org/10.1002/mrm.22359.

183. D. K. Deelchand, K. Uğurbil, and P.-G. Henry, "Investigating Brain Metabolism at High Fields Using Localized ^{13}C NMR Spectroscopy Without ^{1}H Decoupling," *Magnetic Resonance in Medicine* 55, no. 2 (2006): 279–286, https://doi.org/10.1002/mrm.20756.

184. W.-Y. R. Fok, M. Grashei, J. G. Skinner, B. H. Menze, and F. Schilling, "Prediction of Multiple pH Compartments by Deep Learning in Magnetic Resonance Spectroscopy With Hyperpolarized 13C-Labelled Zymonic Acid," *EJNMMI Research* 12, no. 1 (2022): 24, https://doi.org/10.1186/s13550-022-00894-y.

185. B. Lanz, A. Abaei, O. Braissant, et al., "Magnetic Resonance Spectroscopy in the Rodent Brain: Experts' Consensus Recommendations," *NMR in Biomedicine* 34, no. 5 (2021): e4325, https://doi.org/10.1002/nbm.4325.

186. J. Near, R. Edden, C. J. Evans, R. Paquin, A. Harris, and P. Jezzard, "Frequency and Phase Drift Correction of Magnetic Resonance Spectroscopy Data by Spectral Registration in the Time Domain," *Magnetic Resonance in Medicine* 73, no. 1 (2015): 44–50, https://doi.org/10.1002/mrm.25094.

187. M. Wilson, "Robust Retrospective Frequency and Phase Correction for Single-Voxel MR Spectroscopy," *Magnetic Resonance in Medicine* 81, no. 5 (2019): 2878–2886, https://doi.org/10.1002/mrm.27605.

188. L. Lin, M. Považan, A. Berrington, Z. Chen, and P. B. Barker, "Water Removal in MR Spectroscopic Imaging With L2 Regularization," *Magnetic Resonance in Medicine* 82, no. 4 (2019): 1278–1287, https://doi.org/10.1002/mrm.27824.

189. M. Wilson, G. Reynolds, R. A. Kauppinen, T. N. Arvanitis, and A. C. Peet, "A Constrained Least-Squares Approach to the Automated Quantitation of In Vivo ^{1}H Magnetic Resonance Spectroscopy Data," *Magnetic Resonance in Medicine* 65, no. 1 (2011): 1–12, https://doi.org/10.1002/mrm.22579.

190. H. J. Zöllner, M. Považan, S. C. N. Hui, S. Tapper, R. A. E. Edden, and G. Oeltzschner, "Comparison of Different Linear-Combination Modeling Algorithms for Short-TE Proton Spectra," *NMR in Biomedicine* 34, no. 4 (2021): e4482, https://doi.org/10.1002/nbm.4482.

191. M. Lindner, T. Bell, S. Iqbal, P. G. Mullins, and A. Christakou, "In Vivo Functional Neurochemistry of Human Cortical Cholinergic Function During Visuospatial Attention," *PLoS ONE* 12, no. 2 (2017): e0171338, https://doi.org/10.1371/journal.pone.0171338.

192. Program - ISMRM 2024 Workshop on MR Spectroscopy: Frontiers in Molecular & Metabolic Imaging, "Ismrm.Org," (n.d.). Retrieved 26 December 2025, from https://www.ismrm.org/workshops/2024/MRS/program.php.

193. P. E. Anderson, M. L. Raymer, B. J. Kelly, N. V. Reo, N. J. DelRaso, and T. E. Doom, "Characterization of ^{1}H NMR Spectroscopic Data and the Generation of Synthetic Validation Sets," *Bioinformatics* 25, no. 22 (2009): 2992–3000, https://doi.org/10.1093/bioinformatics/btp540.

194. D. M. J. van de Sande, A. T. Gudmundson, S. Murali-Manohar, et al., "A Digital Phantom for MR Spectroscopy Data Simulation," *Magnetic Resonance in Medicine* 95, no. 3 (2026): 1345–1359, https://doi.org/10.1002/mrm.70138.

195. R. P. Berto, H. Bugler, G. Dias, et al., "Results of the 2023 ISBI Challenge to Reduce GABA-Edited MRS Acquisition Time," *Magnetic Resonance Materials in Physics, Biology and Medicine* 37, no. 3 (2024): 449–463, https://doi.org/10.1007/s10334-024-01156-9.

196. D. Chen, W. Hu, H. Liu, et al., "Magnetic Resonance Spectroscopy Deep Learning Denoising Using Few In Vivo Data," *IEEE Transactions on Computational Imaging* 9 (2023): 1–12, https://doi.org/10.1109/TCI.2023.3267623.

197. G. Dias, R. P. Berto, M. Oliveira, et al., "Spectro-ViT: A Vision Transformer Model for GABA-Edited MEGA-PRESS Reconstruction Using Spectrograms," *Magnetic Resonance Imaging* 113 (2024): 110219, https://doi.org/10.1016/j.mri.2024.110219.

198. H. Lee, H. H. Lee, and H. Kim, "Reconstruction of Spectra From Truncated Free Induction Decays by Deep Learning in Proton Magnetic Resonance Spectroscopy," *Magnetic Resonance in Medicine* 84, no. 2 (2020): 559–568, https://doi.org/10.1002/mrm.28164.

199. C. S. Bolliger, C. Boesch, and R. Kreis, "On the Use of Cramér–Rao Minimum Variance Bounds for the Design of Magnetic Resonance Spectroscopy Experiments," *NeuroImage* 83 (2013): 1031–1040, https://doi.org/10.1016/j.neuroimage.2013.07.062.

200. A. Shamaei, J. Starcukova, and Z. Starcuk, "Physics-Informed Deep Learning Approach to Quantification of Human Brain Metabolites from Magnetic Resonance Spectroscopy Data," *Computers in Biology and Medicine* 158 (2023): 106837, https://doi.org/10.1016/j.compbiomed.2023.106837.

201. H. H. Lee and H. Kim, "Bayesian Deep Learning–Based ^{1}H-MRS of the Brain: Metabolite Quantification With Uncertainty Estimation Using Monte Carlo Dropout," *Magnetic Resonance in Medicine* 88, no. 1 (2022): 38–52.

202. H. Lee and H. Kim, "Noninvasive Identification of IDH-Mutational Status From ^{1}H-MRS Spectra by Deep Learning," Proceedings of ISMRM, abstract 2718, (2018).

203. G. Fischetti, N. Schmid, S. Bruderer, et al., "Automatic Classification of Signal Regions in ^{1}H Nuclear Magnetic Resonance Spectra," *Frontiers in Artificial Intelligence* 5 (2023): 1116416, https://doi.org/10.3389/frai.2022.1116416.

204. J. P. Merkofer, D. M. J. van de Sande, S. Amirrajab, K. M. Nam, R. J. G. van Sloun, and A. A. Bhogal, "WAND: Wavelet Analysis-Based Neural Decomposition of MRS Signals for Artifact Removal," *NMR in Biomedicine* 38, no. 6 (2025): e70038, https://doi.org/10.1002/nbm.70038.

205. D. M. J. van de Sande, J. P. Merkofer, S. Amirrajab, et al., "A Review of Machine Learning Applications for the Proton MR Spectroscopy Workflow," *Magnetic Resonance in Medicine* 90, no. 4 (2023): 1253–1270.

206. E. Kondrateva, S. Barg, A. Z. Mohamed, and F. Kofler, "Benchmarking the Reproducibility of Brain MRI Segmentation Across Scanners and Time," in *Proceedings of the 9th International Conference on Medical Imaging With Deep Learning* (PMLR, 2026), 1–4.

207. W. Yan, L. Huang, L. Xia, et al., "MRI Manufacturer Shift and Adaptation: Increasing the Generalizability of Deep Learning

10991492, 2026, 12, Downloaded from https://analyticalsciencejournals.onlinelibrary.wiley.com/doi/10.1002/nbm.70427, Wiley Online Library on [17/11/2026]. See the Terms and Conditions (https://onlinelibrary.wiley.com/terms-and-conditions) on Wiley Online Library for rules of use; OA articles are governed by the applicable Creative Commons License

Segmentation for MR Images Acquired With Different Scanners," *Radiology: Artificial Intelligence* 2, no. 4 (2020): e190195, https://doi.org/10.1148/ryai.2020190195.

208. D. Chen, M. Lin, H. Liu, et al., "Magnetic Resonance Spectroscopy Quantification Aided by Deep Estimations of Imperfection Factors and Overall Macromolecular Signal," *IEEE Transactions on Biomedical Engineering* 71, no. 6 (2024): 1841–1852, https://doi.org/10.1109/TBME.2024.3354123.

209. Z. Tu, J. Zhang, Y. H. Chu, et al., "Multi-Vendor Physical Intelligent Network for Accurate Quantification of Magnetic Resonance Spectroscopy Metabolites. Proceedings of the International Society for Magnetic Resonance in Medicine 33rd Scientific Meeting-ISMRM'25, Honolulu, Hawaii, USA, May 10–15, 2025," Abstract # 4016. (2025).

210. M. Reyes, R. Meier, S. Pereira, et al., "On the Interpretability of Artificial Intelligence in Radiology: Challenges and Opportunities," *Radiology. Artificial Intelligence* 2, no. 3 (2020): e190043, https://doi.org/10.1148/ryai.2020190043.

211. S. Kullback and R. A. Leibler, "On Information and Sufficiency," *Annals of Mathematical Statistics* 22, no. 1 (1951): 79–86, http://www.jstor.org/stable/2236703.

212. S. Mostafapour, A. Mokari, S. Guo, J. Popp, and T. Bocklitz, "Raman Spectra Comparison: Cautions and Pitfalls of Similarity Metrics," *Spectrochimica Acta Part A, Molecular and Biomolecular Spectroscopy* 344 (2026): 126702, https://doi.org/10.1016/j.saa.2025.126702.

213. Y. Song, H. J. Zöllner, S. C. N. Hui, et al., "Impact of Gradient Scheme and Non-Linear Shimming on Out-of-Voxel Echo Artifacts in Edited MRS," *NMR in Biomedicine* 36, no. 2 (2023): e4839.

214. S. P. Kyathanahally, A. Döring, and R. Kreis, "Deep Learning Approaches for Detection and Removal of Ghosting Artifacts in MR Spectroscopy," *Magnetic Resonance in Medicine* 80, no. 3 (2018): 851–863, https://doi.org/10.1002/mrm.27096.

215. W. T. Clarke, T. K. Bell, U. E. Emir, et al., "NIfTI-MRS: A Standard Data Format for Magnetic Resonance Spectroscopy," *Magnetic Resonance in Medicine* 88, no. 6 (2022): 2358–2370, https://doi.org/10.1002/mrm.29418.

216. K. J. Gorgolewski, T. Auer, V. D. Calhoun, et al., "The Brain Imaging Data Structure, a Format for Organizing and Describing Outputs of Neuroimaging Experiments," *Scientific Data* 3, no. 160044 (2016): 208–217, https://doi.org/10.1038/sdata.2016.44.

217. A. E. Bouchard, D. Wong, W. Bogner, et al., "MRS-BIDS, an Extension to the Brain Imaging Data Structure for Magnetic Resonance Spectroscopy," *Scientific Data* 12, no. 1384 (2025): 1–2, https://doi.org/10.1038/s41597-025-05543-2.

Supporting Information

Additional supporting information can be found online in the Supporting Information section. **Table S1:** Live Document showing publications in synthetic MRS. **Table S2:** Basis set simulation tools. **Table S3:** The full dataset used to create the Metabolite Ranges Figure. **Table S4:** Reporting Standards Checklist. **Table S5:** Sample of reported synthetic data applications and associated data validation methods in the MRS literature.

10991492, 2026, 12, Downloaded from https://analyticalsciencejournals.onlinelibrary.wiley.com/doi/10.1002/nbm.70427, Wiley Online Library on [17/11/2026]. See the Terms and Conditions (https://onlinelibrary.wiley.com/terms-and-conditions) on Wiley Online Library for rules of use; OA articles are governed by the applicable Creative Commons License